ALFVÉN WAVE STUDIES ON A TOKAMAK

by

DAVID KORTBAWI

A thesis submitted in partial fulfillment of the
requirements for the degree of

Doctor of Philosophy
(Physics)

at the
UNIVERSITY OF WISCONSIN-MADISON
1987

ALFVÉN WAVE STUDIES ON A TOKAMAK

David Kortbawi

Under the supervision of Professor Julien Clinton Sprott

The continuum modes of the shear Alfvén resonance are studied on the Tokapole II device, a small tokamak operated in a four node poloidal divertor configuration. (R=50cm, a=8-10cm, $B_t \simeq 0.5T$, $I_p \simeq 40kA$, $<n_e> < 10^{13} cm^{-3}$, $T_e \simeq 100$ eV, $T_i \simeq 20$ eV). A variety of antenna designs and the efficiency with which they deliver energy to the resonant layer are discussed. The spatial structure of the driven waves is studied by means of magnetic probes inserted into the current channel.

In an attempt to optimize the coupling of energy in to the resonant layer, the angle of antenna currents with respect to the equilibrium field, antenna size, and plasma-to-antenna distance are varied. The usefulness of Faraday shields, particle shields, and local limiters are investigated. Driving antenna currents parallel to the equilibrium field (which would directly drive the shear Alfvén wave) leads to large parasitic loading, due to the wave electric field being heavily attenuated in the edge of the plasma. Antenna currents perpendicular to the equilibrium field (which drive the fast wave which couples to the shear Alfvén wave at the resonant surface) more efficiently delivers energy to the resonant surface. Antennas should be well shielded, either a dense Faraday shield or particle shield being satisfactory. The antenna should be

large and very near to the plasma.

The wave magnetic fields measured show a spatial resonance, the position of which varies with the value of the equilibrium field and mass density. They are polarized perpendicular to the equilibrium field. A wave propagates radially in to the resonant surface where it is converted to the shear Alfvén wave. The signal has a short risetime and does not propagate far toroidally. These points are all consistent with a strongly damped shear Alfvén wave.
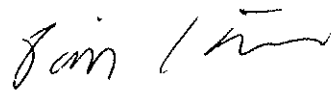
Comparisons of this work to theoretical predictions and results from other tokamaks are made.

Acknowledgements

Firstly I would like to acknowledge the support and guidance of my advisor Professor J.C. Sprott, and Professor S.C. Prager. Their continued interest in this project over the years and assistance in the interpretation of results and suggestions for further work has been invaluable. I would also like to thank Professor R.N. Dexter for his assistance with various diagnostics used throughout this work. I have also had useful conversations with Professor J.A. Tataronis, and Dr. C.K. Phillips concerning the rather complex nature of waves in plasmas. A special debt of gratitude is due to Dr. F.D. Witherspoon who began these studies on the Tokapole, and helped me get started on my research. Most of the experimental apparatus used for this work was designed by Tom Lovell, our chief engineer. He has spent many long hours at the drawing board and lab bench with me and has taught me most of what I know about the lore and voodoo associated with rf circuitry, a great deal of which can only be learned the hard way. His assistance has also been essential to keeping the Tokapole running through the many abuses it has suffered through the years. Jim Morin has also been of great help in the practical aspects of keeping much of the equipment in useful condition and in my continuing education in the technique and technology of rf work. He has also managed the ever changing crew of student hourly workers who have rendered a great deal of assistance with the day to day maintennance of Tokapole and

construction of the large array of electronics used in this work. I would also like to thank our crew of computer hackers who have made it as painless as possible to collect the seemingly endless stream of data that went to this thesis. I must also thank the many graduate students who have gone before me, they built the Tokapole and made it work, and those who have been here with me, for their assistance in keeping Tokapole operating, and their friendship. I have many happy memories of my years in graduate school due to them. Special thanks are due to Mike LaPointe and Dr. Shi-yao Zhu who assisted in acquiring some of the data presented here. On a more personal note, I want to thank my parents for all they have given me in the past and the love and support they continue to give, I can never repay them. Lastly, I would like to acknowledge the enormous contribution of my wife, Fran, and children, Geoffrey and Jennifer. Their patience and understanding through the many late nights and long weekends has been deeply appreciated. Their love and support has been unfailing through it all.

CHAPTER 1
Introduction

Waves in plasmas have been the subject of theoretical and experimental research for many years. This research has been carried out over an enormous range of plasma parameters, from extremely tenuous space plasmas to the temperatures and densities expected for fusion reactor plasmas. It has covered a wide range of frequencies and power levels. The applications of waves in plasmas have included diagnostics, control, and heating.

Plasmas are a very complex medium for the propagation of waves. They can support many different types of waves, have cutoffs and resonances, non-linear effects, and many forms of damping[1]. In a uniform, magnetized plasma, the shear Alfvén wave propagates along the equilibrium field nondispersively at the Alfvén speed, $V_A = B/(\mu_0 \rho)^{\frac{1}{2}}$. In a spatially non-uniform plasma, the variation in the magnetic field and density produces a singularity in the MHD equations describing its propagation at the place where the phase velocity of the wave equals the local Alfvén speed[2]. This is the shear Alfvén resonance which is the subject of this thesis.

The Alfvén spectrum is a rich one exhibiting many complex phenomenon. An understanding of this spectrum would lend significantly to an understanding of plasma behavior, in particular to the response of a plasma to perturbations, either external or from spontaneous fluctuations. It is also important to understand how to

couple energy to these waves from external sources, a subject of some debate.

Alfvén waves have been suggested and applied for many uses in tokamaks; as a diagnostic for the central mass and current density[3,4], for current drive[5,6,7], and heating[8,9,10]. Heating is perhaps the most important application since it is generally conceded that some form of auxiliary (i.e. non-ohmic) heating will be needed to bring a tokamak fusion reactor to operating temperature. Many other forms of auxiliary heating have been studied, and have met with varying degrees of success. Neutral beam injection[11], ion cyclotron resonance heating[12], electron cyclotron resonance heating[13], and lower hybrid heating[14] are some of the best studied ones. Shear Alfvén resonance heating has several advantages. The relatively low frequency (~1-2 MHz for most tokamaks) means that large amounts of power can be generated with existing technology. The energy deposition is also predicted to be on a magnetic surface. This would allow some profile control and give uniform heating over the core of the plasma if the frequency is swept. One significant disadvantage may be the large physical size and number of antennas required. Since a global mode structure is to be set up, several antennas must be located around the machine fairly close to the plasma. Constructing antennas which can survive in the edge plasma of a fusion plasma is a formidable engineering task.

There are presently only two other groups doing research on Alfvén waves in tokamaks. The largest effort is at the TCA tokamak

in Lausanne, Switzerland. They have demonstrated efficient heating of both ions and electrons and have studied the spectrum of the Alfvén wave in great detail[10,15]. The other is a smaller effort on the TORTUS tokamak at the University of Sydney, Australia. They have made measurements of the wave magnetic fields in the plasma over a range of plasma conditions and frequencies and for several different antennas[16]. Their results are quite similar to those presented in this thesis. There was a program at the University of Texas at Austin on the PRETEXT tokamak. They used a CO_2 laser interferometer to measure the structure of the global Alfvén eigenmode[17]. (These global modes are discrete eigenmodes which extend over a large fraction of the plasma radius and are distinct from the continuum modes, the subject of this thesis, which are localized radially.) Alfvén waves have also been studied on linear devices and stellarators. Much of this work is summarized in reference 2.

The goal when this work began was to do Alfvén wave heating of a tokamak, and to study the structure of the driven waves by means of direct measurement of the internal wave magnetic fields with probes. As is often the case in science, the initial goals proved to be less trivial than initially supposed.

The correct design of an antenna to couple energy efficiently in to the shear Alfvén resonance position became one of the main concerns of this research. The parameters varied include: the angle of the antenna currents with respect to the equilibrium

magnetic field; the use of local limiters, Faraday shields, and particle shields; the physical size of the driving loop; (all antennas used were loop antennas and should perhaps more correctly be referred to as coupling loops, see chapter 5); and the spacing of the plasma to antenna. No bulk heating of the plasma is observed. The results are significant, however, in that such a wide variety of antenna structures has not been tested elsewhere.

Initially, it was expected a global eigenmode structure would be established in the machine, having distinct poloidal and toroidal mode numbers determined by the launching structure. This too turned out to be an apparent oversimplification of the problem. This thesis presents data which constitute a fairly clear identification of the shear Alfvén resonance in a tokamak, driven by mode coupling to an inward propagating wave which mode converts at the resonant surface. There is no clear evidence for a global eigenmode structure, and the observed signal appears to be damped in a relatively short distance.

Chapter 2 presents a review of some of the theoretical work done on Alfvén waves in tokamaks and summarizes the key results and their implications for heating. Chapter 3 describes the Tokapole II device on which the experiments were performed. Chapter 4 describes the antennas used in the experiment, and describes the probes and electronics used to make the internal magnetic field measurements. Chapter 5 presents the experimental results and makes comparisons to theory. Chapter 6 is a summary of the

conclusions and contains suggestions for the direction of future work on Alfvén waves in the Tokapole II.

Plasma physics is a field rich in jargon. Attempts have been made to avoid the use of jargon or at least define the terms that are used. Many terms that are specific to the Tokapole are defined in Chapter 3 including the coordinates used for locations of diagnostics and antennas. Chapter 4 defines some of the terms used for the rf apparatus specific to the experiment. Attempts have also been made to be consistent in notation throughout. This is difficult when trying to reconcile the work of many different people. The following notations are used throughout:

Subscripts: $i\rightarrow$ion, $e\rightarrow$electron, $\|\rightarrow$parallel to the equilibrium magnetic field, $r\rightarrow$radial, $\perp\rightarrow$perpendicular to both the equilibrium magnetic field and minor radius, $t\rightarrow$toroidal, $p\rightarrow$poloidal or plasma depending on context

Lower case letters are used to represent perturbed (wave) quantities and upper case for equilibrium quantities (B = equilibrium magnetic field, b = wave magnetic field). Most symbols are defined as they arise or are obvious from context and standard usage.

Throughout this thesis, references are made to PLP reports. These are internal reports of the University of Wisconsin, Madison Plasma Physics Group. Copies of these and detailed drawings of circuits and apparatus discussed in this thesis are available upon request from:

Plasma Physics Department

University of Wisconsin, Madison

1150 University Avenue

Madison, WI 53706

References

1. T.H. Stix, _The Theory of Plasma Waves_ (McGraw-Hill, New York, 1962)

2. A. Hasegawa and C. Uberoi, _The Alfvén Wave_ Technical Information Center, USDOE (1982)

3. LRP 196 (Internal Report of the TCA Group), B. Joye, A. Lietti, J.B. Lister, A. Pochelon (1981)

4. G.A. Collins, J.B. Lister, Ph. Marmillod, _13th European Conference on Controlled Fusion and Plasma Physics_ (Schliersee, Germany, 1986)

5. A. Hasegawa, Nucl. Fusion $\underline{20}$, 1158 (1980)

6. N. Fisch and C. Karney, Phys. Fluids $\underline{24}$, 27 (1981)

7. J. Gahl, O. Ishihara, M. Hagler, and M. Kristiansen, Bulletin of the American Physical Society $\underline{31}$, 1605 (1986)

8. W. Grossman and J. Tataronis, Z. Physik $\underline{261}$, 203 and 217 (1983)

9. A. Hasegawa and L. Chen, Phus. Rev. Lett. $\underline{32}$, 454 (1974) and Phys. Fluids $\underline{19}$, 1399 (1974)

10. G. Besson, A. deChambrier, G.A. Collins, B. Joye, A. Lietti, J.B. Lister, J.M. Moret, S. Nowak, C. Simm, H. Weisen, $\underline{13}^{th}$ _European Conference on Controlled Fusion and Plasma Physics_ (Schliersee, Germany, 1986)

11. M.M. Menon, Proc. IEEE $\underline{69}$, 1012 (1981)

12. P.L. Colestock, C. Barnes, M. Bitter, D. Boyd, N. Bretz, et al, _Proceedings of the Fifth Topical Conference on Radio Frequency Plasma Heating_ (Madison, WI 1983)

13. C.P. Moeller, _Proceedings of the Fifth Topical Conference on Radio Frequency Plasma Heating_ (Madison, WI 1983)

14. T. Imai, T. Yamamoto, N. Suzuki, K. Uehara, et al, _Proceedings of the Fifth Topical Conference on Radio Frequency Plasma Heating_ (Madison, WI 1983)

15. G.A. Collins, F. Hofman, B. Joye, R. Keller, A. Lietti, J.B. Lister, and A. Pochelon, Phys. Fluids 29, 2260 (1986)

16. G.G. Borg, M.H. Brennan, R.C. Cross, J.A. Lehane, and A.B. Murphy, 13th European Conference on Controlled Fusion and Plasma Physics (Schliersee, Germany, 1986)

17. T.E. Evans, P.M. Valanju, J.F. Benesch, Roger D. Bengtson, Y.-M. Li, S.M. Mahajan, M.E. Oakes, D.W. Ross, X.-Z. Wang, and J.G. Watkins, and C.M. Surko, Phys. Rev. Lett. 53, 1743 (1984)

Chapter 2
Theory

2-A Overview

There has been a great deal of theoretical work done on Alfvén waves in many geometries and plasma parameter ranges.[1] In the simplest case of uniform, magnetized plasma the linearized-ideal-MHD equations lead to the dispersion relation[2]

$$\omega^2 = k_\parallel^2 V_A^2 = \frac{k_\parallel^2 B^2}{\mu_0 \rho}$$

where $k_\parallel$ is the parallel component of the wave vector, V_A is the Alfvén speed, B is the magnetic field, and ρ is the plasma mass density.

In laboratory plasmas, the field and mass density are usually nonuniform in at least one direction. This means that V_A will be a function of position in the plasma. There is then a resonance condition and the wave quantities can tend to infinity. Energy will build up at the location in the plasma where the frequency and the parallel wave number match the local Alfvén speed, $\omega_0 = k_\parallel V_A(x_0)$. Here ω_0 and $k_\parallel$ are determined by the external launching structure. There is a continuum of such modes corresponding to the range of V_A in the plasma.

The application of this to the heating of a plasma was first suggested by Tataronis and Grossman[3] and Hasegawa and Chen[4]. They showed that energy would be deposited locally at the resonant

layer. Later work by Hasegawa and Chen[5], Ross et al.[6], and Donelly et al.[7] showed that at the resonant layer, the wave is mode converted to the "kinetic Alfvén wave". This wave can propagate either further into the plasma or be reflected out, depending on the plasma parameters at the resonance location. In the latter two of these papers[6,7] and in other work by Appert et al.[8] the global Alfvén eigenmode is described. This occurs just below the continuum threshold and arises from finite frequency effects or consideration of a plasma carrying an equilibrium current. Kieras and Tataronis[9,10] have considered the MHD resonance problem in full toroidal geometry and have shown that, in this case, gaps appear in the continuum of modes arising in the cylindrical or slab case, and there is a coupling of modes of different azimuthal mode numbers at certain locations in the plasma. In this chapter the key results of these and other papers will be summarized, and their relation to Alfvén wave heating will be discussed.

2-B The Simple Model

Hasegawa and Chen[4] calculate the functional form of the fluid-displacement vector, ξ, near the resonance in a fairly simple geometry. All equilibrium quantities are either constant or vary only in the direction orthogonal to the equilibrium field ($\hat{e}_r$ in cylindrical or toroidal geometry, $\hat{e}_x$ in slab geometry). The equilibrium magnetic field is straight but sheared. They also assume that $\beta = \mu_0 P/B^2$ (the ratio of plasma pressure to magnetic pressure) is

low. They derive from the MHD equations a second-order wave equation for ξ_x of the form

$$\frac{d}{dx}\left(\frac{\epsilon\alpha B^2}{\alpha k_\perp^2 B^2 - \epsilon}\ \frac{d\xi_x}{dx}\right)\ -\epsilon\xi_x = 0 \qquad (1)$$

Here $\epsilon = \omega^2\mu_0\rho - k_\parallel^2 B^2$, $\alpha = 1 + \gamma\beta + \gamma^2\beta^2 k_\parallel B^2/(\omega^2\mu_0\rho - \gamma\beta k_\parallel B^2) \sim 1$ for low β, and $k_\perp$ is the component of the wave vector perpendicular to the equilibrium field. (A set of local orthogonal coordinates will be frequently employed where $\hat{e}_\parallel = \mathbf{B}/B$, $\hat{e}_x = x$, $\hat{e}_\perp = \hat{e}_r \times \hat{e}_\parallel$.)

The singularity at x_0 where $\epsilon(x) = 0$ is the Alfvén resonance. By expanding $\epsilon(x)$ to first order about x_0, equation (1) can be simplified to

$$\frac{d^2\xi_x}{dx^2} + \frac{1}{x - x_0}\ \frac{d\xi_x}{dx}\ -k_\perp^2\xi_x = 0 \qquad (2)$$

Equation (2) has a logarithmic singularity at $x = x_0$, and so $\xi_x = C\ln(x - x_0)$.

The other components can be calculated from this and the linearized MHD equations, as displayed by Witherspoon[11]. The results are summarized below for the fluid displacement $\boldsymbol{\xi}$ and the wave magnetic field $\mathbf{b}$.

$$\xi_\parallel = 0$$
$$\xi_\perp \sim 1/(x - x_0(\omega))$$
$$\xi_x \sim \ln(x - x_0(\omega))$$
$$b_\parallel = \text{constant}$$
$$b_\perp \sim 1/(x - x_0(\omega))$$
$$b_x \sim \ln(x - x_0(\omega))$$

It should be pointed out again that the x component would correspond to the radial component in toroidal geometry and the perpendicular direction is very nearly the poloidal direction in a normal tokamak. In chapter 5, experimental measurements of $b_\parallel$ and $b_\perp$ will be discussed.

Tataronis[12] calculates the time dependence of the fields in the ideal MHD limit (no dissipation) and finds that $b_\parallel$ oscillates at a constant amplitude, the amplitude of $b_\perp$ grows linearly in time, and that of b_r grows logarithmically. Tataronis also calculates the rate of energy absorption for the ideal MHD case by integrating the wave kinetic and potential energy over the plasma volume. Since the perpendicular components of the wave energy are non-square integrable, the energy accumulates at the resonance location, and grows without bound, being concentrated into a vanishingly thin layer as time proceeds.

2-B 1 Resistive Effects in MHD

Kapraff and Tataronis[13] have calculated the effects of small but finite plasma resistivity, η, on the time dependence of the fields. They show that early in time, ($t < \tau_{rise}$), the resistivity has little effect. This is easily understood since the rate of dissipation $(\sim\eta(d\xi/dt)^2)$ when the wave amplitude is small is low compared with rate of energy accumulation at the resonant surface. They calculate this rise time as

$$\tau_{rise} = \left(\frac{24\mu_0}{\omega_0^2 \eta}\right)^{1/3} \left(\frac{2B'(x_0)}{B} - \frac{\rho'(x_0)}{\rho}\right)^{-4/3} \tag{3}$$

The time dependence of the fields is given by

$$\xi \sim \exp(i\omega_0 t) \int_0^t \tau \exp\{-(\tau/\tau_{rise})^3\} \, d\tau \ .$$

This function will grow approximately as t^2 up to τ_{rise} and saturate thereafter. This is plotted in figure 2-1.
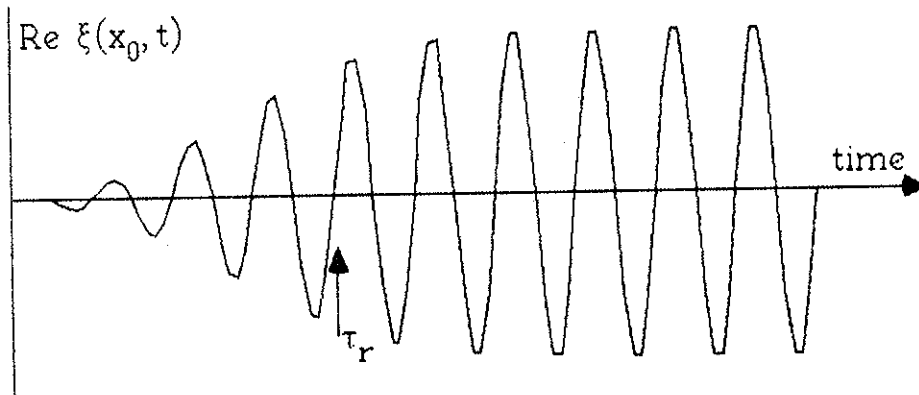

Figure 2-1
The fluid displacement grows as the square
of time initially and saturates after τ_r.

They also calculate the width, Δ, of the layer about the resonance position in which nearly all of the energy will be deposited

$$\Delta = 8\pi \left(\frac{\eta}{\mu_0 \omega_0}\right)^{1/3} \left(\frac{2B'(x_0)}{B} - \frac{\rho'(x_0)}{\rho}\right)^{-1/3} . \tag{4}$$

These can be compared to experimentally measured values .

2-C The Kinetic Alfven Wave

When the perpendicular wavelength, $2\pi/k_\perp$, becomes comparable to the ion gyroradius, ρ_i, the ions can no longer follow the field lines, whereas the electrons, being lighter, still can[1]. There are two cases of interest, $\beta > m_e/m_i$, and $\beta < m_e/m_i$ at the resonant surface.

For $\beta > m_e/m_i$, the wave is mode converted to the kinetic Alfvén wave and propagates further into the plasma. If $k_x\rho_i \ll 1$ the dispersion relation is given by

$$\omega^2 = k_\parallel^2 V_A^2 \left[1 + k_x^2\rho_i^2 \left(\tfrac{3}{4} + T_e/T_i \right) \right] \ .$$

Since the ions no longer follow the field lines, there can now be charge separation and an electric field component parallel to the equilibrium field. This can give rise to Landau damping of the wave energy by both the ions and electrons. If the damping is relatively weak, this wave could be reflected from the origin, and a resonance may occur. If the damping is moderately strong, then the core of the plasma may be uniformly heated as the wave propagates toward the center. This is the best scenario for heating.

For $\beta < m_e/m_i$ the wave is reflected out of the plasma, and a surface electrostatic wave is created. The dispersion relation is

$$\omega^2 = k_\parallel^2 V_A^2 (1 + k_x^2\rho_i^2) \left[1 + \frac{k_x^2 c^2}{\omega_{pe}^2} \right] \ .$$

Again, this wave could be reflected from the plasma edge, and a resonance may occur.

Hasegawa and Chen[5] calculate the heating rates for various damping mechanisms and show that they are the same as the energy absorption rate for the MHD limit. They are summarized below.

Collisional Regime:　　Ion Viscous Damping

$$n_0 \frac{dT_i}{dt} = 0.7 \upsilon_{ii} (k_x \rho_i)^2 \frac{b_\perp^2}{2\mu_0} \qquad (5)$$

(υ_{ii} is the ion-ion collision frequency)

Ohmic Dissipation (electron heating)

$$n_0 \frac{dT_e}{dt} = \upsilon_{ei} \frac{T_e}{T_i} (k_x \rho_i)^2 \frac{b_\perp^2}{2\mu_0} \frac{\omega_0^2}{k_\parallel^2 V_{Te}^2} \qquad (6)$$

(υ_{ei} is the electron-ion collision frequency, V_{Te} is the electron thermal velocity)

Collisionless Regime:　　Ion Landau Damping

$$n_0 \frac{dT_i}{dt} = \omega_0 \frac{\delta_i}{2} \beta_i (T_e/T_i)^2 (k_x \rho_i)^2 \frac{b_\perp^2}{2\mu_0} \qquad (7)$$

$$\delta_i = 2\pi^{1/2} \beta_i^{-3/2} \exp(1/\beta_i) \qquad \beta_i = 2V_{Ti}^2/V_A^2$$

Electron Landau Damping

$$n_0 \frac{dT_e}{dt} = \omega_0 \delta_e \frac{T_e}{T_i} (k_x \rho_i)^2 \frac{b_\perp^2}{2\mu_0} \qquad (8)$$

$$\delta_e = \pi^{1/2} \beta_i^{-1/2} (T_i/T_e)^{1/2} (m_e/m_i)^{1/2}$$

In the above equations, some approximations relevant to the plasma parameters usually encountered on Tokapole II have been made.

They also calculate the resonant enhancement of the field in the plasma over the vacuum field of the external source.

$$|b_\perp| \simeq (\kappa\rho_i)^{-2/3}[1 + (T_e/T_i)k_x^2\rho_i^2]|b_{\perp vac}| \quad (9)$$

Here, $1/\kappa$ is the inhomogeneity scale length.

The work of Ross et al.[6] concentrates on numerical solution of the equations of kinetic theory for the perturbed fields including the effects of electron inertia, Landau damping, finite ion gyroradius, equilibrium plasma current, magnetic shear, and finite frequency. They calculate the fields and antenna loading assuming an idealized-sheet antenna encircling the plasma carrying helical currents to match the modes to be driven. They find significant loading in the continuum (providing that finite equilibrium current terms are kept in the equations), and show that the kinetic Alfvén wave is damped within a few ion gyroradii of the resonant layer. They find, especially on a small tokamak, that finite frequency effects can be very significant, giving significantly enhanced or reduced loading depending on the mode numbers driven. They also see surface modes which are standing waves generated when $\beta < m_e/m_i$ and the wave is reflected out from the resonant layer. Standing waves are then set up between the resonant layer and the edge plasma. Another effect observed is the "stable kink mode" or global Alfvén eigenmode occurring just below the threshold of the
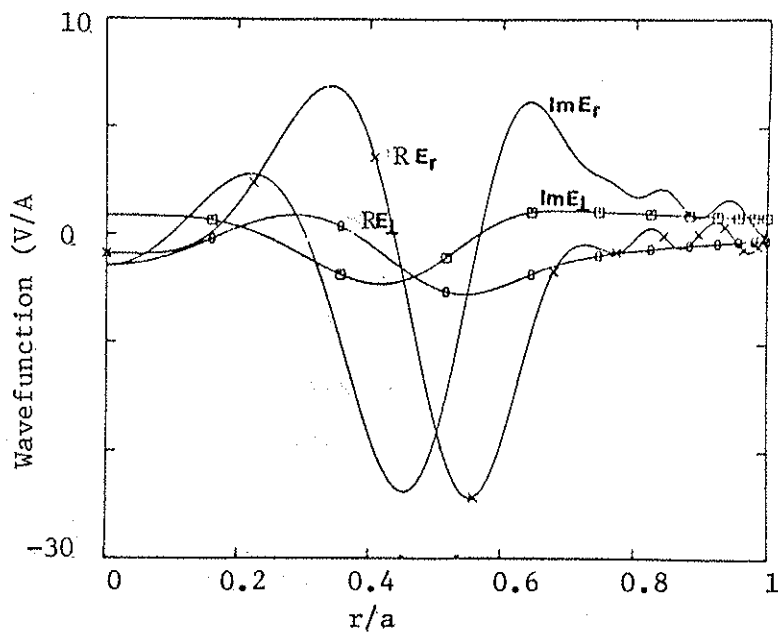
figure 2-2a
E_r and $E_\perp$ vs. normalized radius for
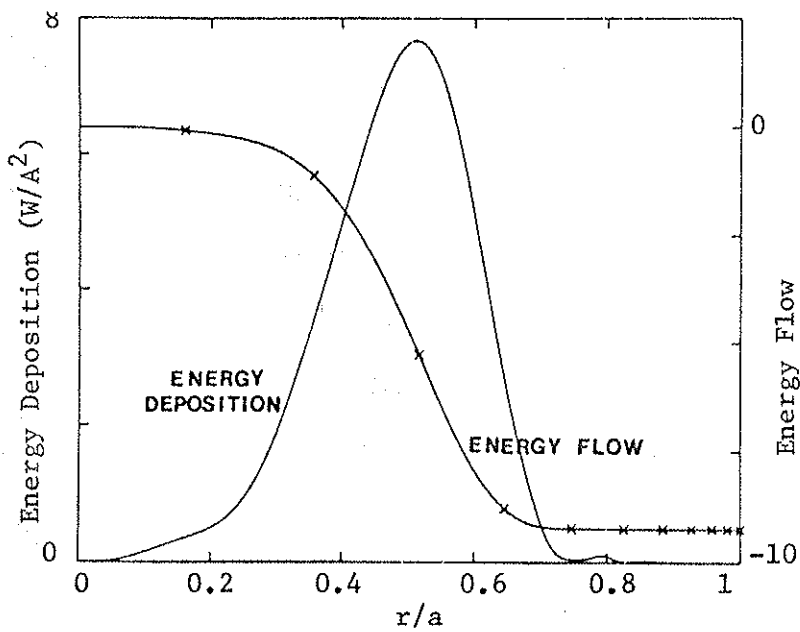PRETEXT (at the resonant surface, $\beta \geq m_e/m_i$)

figure 2-2b
Energy flow and deposition profiles for PRETEXT

continuum. These will be discussed further in the next section. Figure 2-2a is a plot of the wave electric fields for a kinetic Alfvén wave, and 2-2b is the energy deposition and flow profiles calculated for the Pretext tokamak.

2-D Global Alfvén Eigenmodes

By taking into account the effects of equilibrium current and finite frequency[6,7,8], global eigenmodes occurring at frequencies below the threshold for the continuum, defined as the minimum frequency where

$$k_\parallel(r)V_A(r)(1-\omega^2/\omega_{ci}^2)=\omega \qquad (10)$$

is satisfied, are found. These modes distinguish themselves by a large, sharp spike on the real part of the antenna loading, and a global profile of the perturbed fields showing a radial eigenmode.

Appert et al.[8] show that their presence can be attributed to the equilibrium current in the ideal MHD limit ($\omega/\omega_{ci}\sim 0$). This is clearly shown by Ross et al.[6] (figure 2-3.). Appert et al.[14] have shown that curvature of the field in cylindrical geometry can significantly change the radial profiles of these eigenmodes. In particular, they show that the energy can be more efficiently absorbed in the core of the plasma and not in the edge as was initially suspected. Appert and Vaclavik[15] and Ross et al.[6] have also shown that finite frequency effects are quite important in correctly modeling these modes.
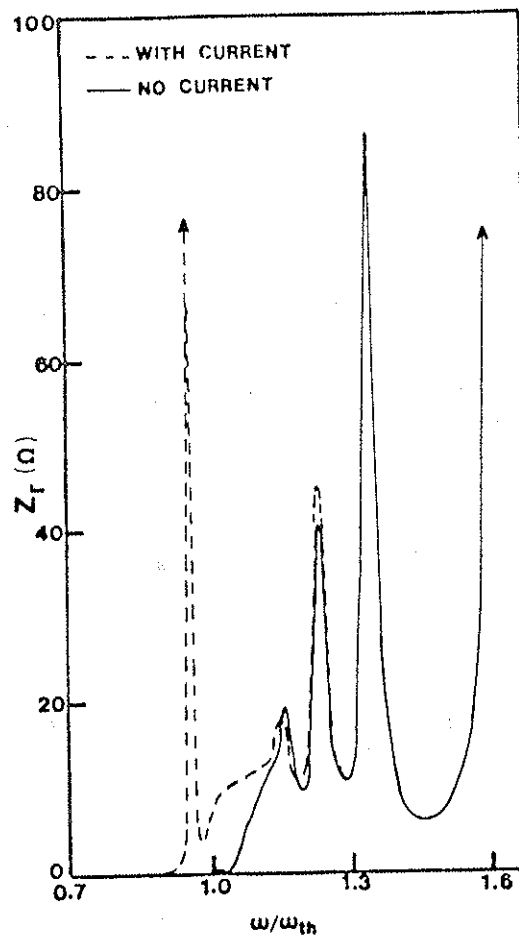
Figure 2-3
The real part of the antenna impedance is
plotted vs. normalized frequency. The peaks in the
continuum correspond to surface modes. (from Ross
et al.[6] used with permission from D.W. Ross)

Under all circumstances considered, the loading spikes of these
modes are quite narrow, and this could be a problem for heating,
since the frequency of the driving system would have to track the
evolution of the plasma.

2-E Toroidal Effects

In cylindrical geometry, all equilibrium quantities are assumed to vary only with the radial coordinate. This gives rise to two symmetry directions. A resonant surface is thus circular and coincides with a magnetic surface. If periodic boundary conditions are assumed along the axial direction(to approximate a toroidal system), the resonant condition for the shear Alfvén wave becomes,

$$\omega^2(r) = \frac{1}{R} \left(n + \frac{m}{q(r)}\right)^2 V_A^2 = k_\parallel^2 V_A^2 \qquad (11)$$

$$q(r) = \frac{B_t r}{B_p R}$$

where n is the toroidal (axial) mode number, m is the poloidal (azimuthal) mode number, q is the safety factor, r is the minor radius, R is the major radius, B_t is the toroidal field, and B_p is the poloidal field. In a tokamak, the equations of cylindrical geometry are not always a good approximation. The toroidal field has a 1/R dependence which will give the total equilibrium field a poloidal dependence. The surfaces of constant $k_\parallel V_A$ do not necessarily fall on magnetic surfaces, and thus it is not obvious that calculations based on a screw pinch (a straight cylindrical plasma with a strong axial field carrying axial plasma current) are applicable. To make corrections for toroidicity, it is customary to make an inverse aspect ratio ($\epsilon = r_p/R$) expansion.

Pao[16] and Goedbloed[17] were the first to treat the toroidal problem. They showed that, even though V_A is not a constant on a

magnetic surface, there is a single eigenvalue on a given magnetic surface. They will thus form a continuum which can be mapped from these flux coordinates to actual space. The radial eigenfunction is still singular on these surfaces. The problem has also been treated by Tataronis et al.[18], Tataronis and Salat[19], Hameiri[20], and Hameiri and Hammer[21] for more general equilibria such as stellerators.

Kieras[9,10] calculates the location and structures of various modes of the Alfvén wave for an axisymmetric toroidal equilibrium in the linearized MHD limit. In particular, a numerical code[22] is used for the equilibrium of Tokapole II and the resonant frequencies of low-numbered modes are calculated, again numerically, as a function of radius. It is found that the continuum is broken up into gaps due to coupling of modes of different poloidal mode number near the rational q surfaces. Far from these rational surfaces, the continua is described by the appropriate generalization of the equations for a periodic screw pinch. On the rational surface it is possible for different modes to be degenerate. (For example from eqn. (11) for $m,n=(3,-2)$ $Rk_{\parallel} = 2/5$ at $q=5/4$ and for $m,n=(2,-2)$ $Rk_{\parallel} = -2/5$.) This coupling is indicated in figure 2-5a,b. The poloidal structure of these modes is shown at two different radii in figures 2-6a-d. (all from ref 9)

Only modes of $\Delta m = \pm 1$ couple. In the numerical calculations, the values near the separatrix are also strongly affected by the non-circular flux surfaces. (see figure 2-5)

Appert et al.[23] have also observed a toroidal coupling of

modes, but only when finite ω/ω_{ci} effects are included. They calculate, for example, the loading for a single helicity, $(2,-1)$, idealized antenna and observe a peak in the antenna resistance vs density just below the $(2,0)$ threshold, corresponding to the global Alfvén eigenmode, and the continuum loading.

Cheng and Chance[24] have also predicted that more discrete modes will appear in these gaps in the continuum.
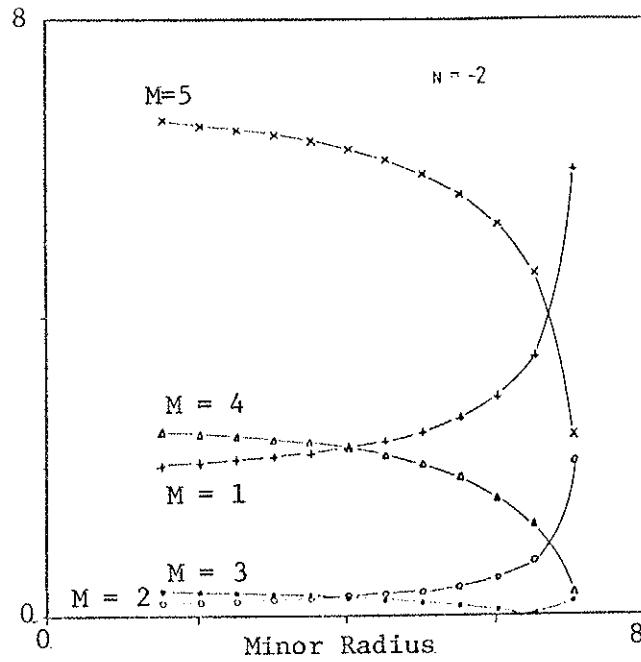
figure 2-5a
The shear Alfvén eigenvalues as calculated for the screw pinch model as a function of minor radius for n=-2, m=1-5
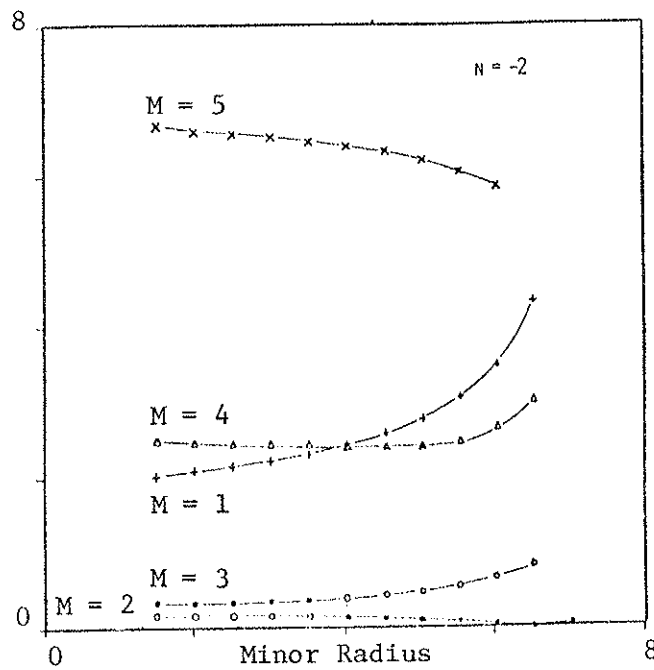
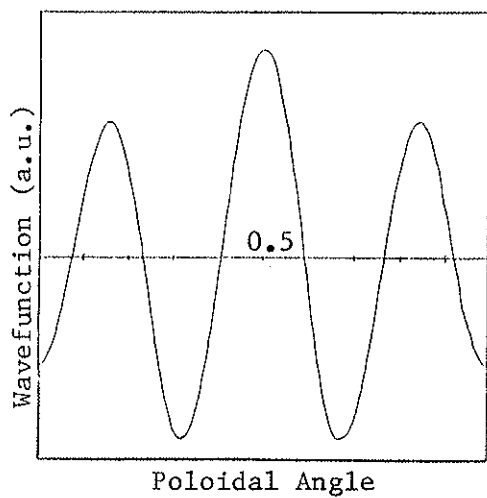
figure 2-5b
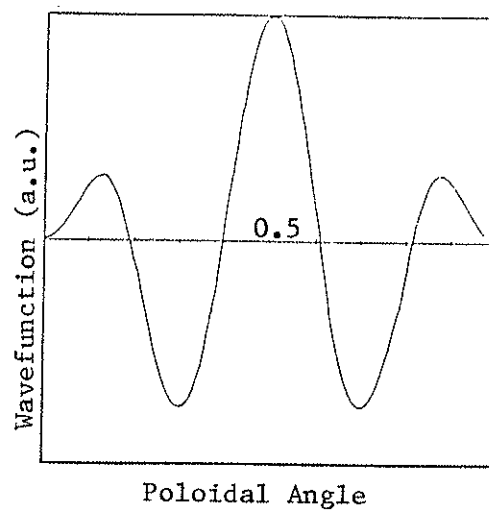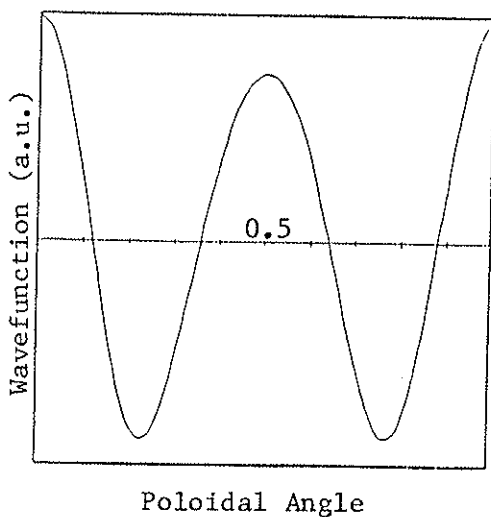The same eigenvalues as calculated numerically
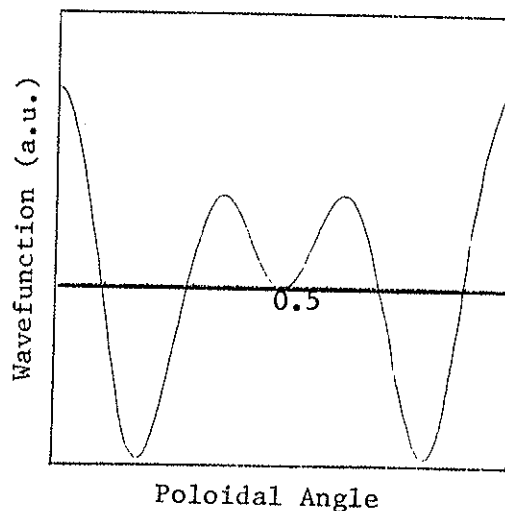
figure 2-6 a

figure 2-6b

figure 2-6c

figure 2-6c

a; The poloidal structure for the 3,−2 mode at r=1.53 cm.
b; 3,−2 mode at r=4.03 cm (the coupling surface)
c; 2,−2 mode at r=1.53 cm
d; 2,−2 mode at r=4.03 cm

References

1. A. Hasegawa and C. Uberoi, The Alfvén Wave, Technichal Information Center, USDOE (1982)

2. J.D. Jackson, Classical Electrodynamics, (Wiley, New York 1975) Chapter 10

3. W. Grossman and J. Tataronis, Z. Physik, 261, 203 and 217 (1973)

4. A. Hasegawa and L. Chen, Phys Rev. Lett. 32, 454 (1974) and Phys. Fluids 17, 1399 (1974)

5. A. Hasegawa and L. Chen, Phys. Rev. Lett. 35, 370 (1975) and Phys. Fluids 19, 1924 (1976)

6. D.W. Ross, G.L. Chen, and S.M. Mahajan, Phys. Fluids 25, 652 (1982)

7. I.J. Donnelly, B.E. Clancy, and N.F. Cramer, J. Plasma Phys. 35, 75 (1986)

8. K. Appert, R. Gruber, F. Troyon, and J. Vaclavik, Plasma Phys. 24, 1147 (1982)

9. C.E. Kieras, Ph.D. Thesis, University of Wisconsin (1982)

10. C.E. Kieras and J.A. Tataronis, J. Plasma Phys. 28, 395 (1982)

11. F.D. Witherspoon, Ph.D. Thesis, University of Wisconsin (1984)

12. J.A. Tataronis, J. Plasma Phys. 13, 87 (1975)

13. J.M. Kapraff and J.A. Tataronis, J. Plasma Phys. 18, 209 (1975)

14. K. Appert, B. Balet, and J. Vaclavik, Phys. Lett. 87A, 233 (1982)

15. K. Appert and J. Vaclavik, Plasma Phys. 25, 551 (1983)

16. Y.P.Pao, Nucl. Fusion 15, 631 (1975)

17. J.P. Goedbloed, Phys. Fluids 18, 1258 (1975)

18. J.A. Tataronis, J.N. Talmadge, and J.L. Shohet, Comments Plasma Phys. Controlled Fusion 7, 29, (1982)

19. J.A. Tataronis and A. Salat, Proc. 2nd Joint Grenoble-Varenna

<u>Int. Symp. on Heating in Toroidal Plasmas</u>, (Como, Italy, 1980)

20. E. Hameiri, Phys. Fluids 24, 562 (1981)

21. E. Hameiri and J.H. Hammer, Phys. Fluids 22, 1700 (1979)

22. M.W. Phillips, University of Wisconsin PLP 765 (1978)

23. K. Appert, G.A. Collins, F. Hoffman, R. Keller, A. Lietti, J.B. Lister, A. Pochelon, and L. Villard, Phys. Rev. Lett. 54, 1671 (1985)

24. C.Z. Cheng and M.S. Chance, Phys. Fluids 29, 3695 (1986)

Chapter 3
Tokapole II

3-A Machine description

The experiments described in this thesis were conducted on the Tokapole II tokamak at the University of Wisconsin-Madison.[1] Tokapole II (shown in figure 3-1) is a small tokamak operated in a four node poloidal divertor configuration. A complete description of the device can be found elsewhere.[2,3]

The vacuum vessel is a 44 cm square cross section aluminum torus with a major radius of 50 cm. Since the walls are 3 cm thick, there are insulated gaps in both the poloidal and toroidal directions to allow the externally driven magnetic fields in. The divertor configuration is formed by four, inductively driven, solid copper rings located inside the vacuum vessel (figure 3-2). These divertor rings are supported at three locations by insulated beryllium copper rods. The position of the divertor rings can be adjusted ± 5 mm, without venting the vacuum vessel, to position and shape the plasma.

The pumping for the vacuum is by a 1500 l/sec turbomolecular pump which typically maintains the base pressure in the low 10^{-7} torr range. There is a quadrupole residual gas analyzer to monitor vacuum quality.

The toroidal field is generated by 96 turns of 4/0 wire wound poloidally around the machine in 4 sections. This was driven directly by a 52 mF, 5 kV capacitor bank switched by a class E
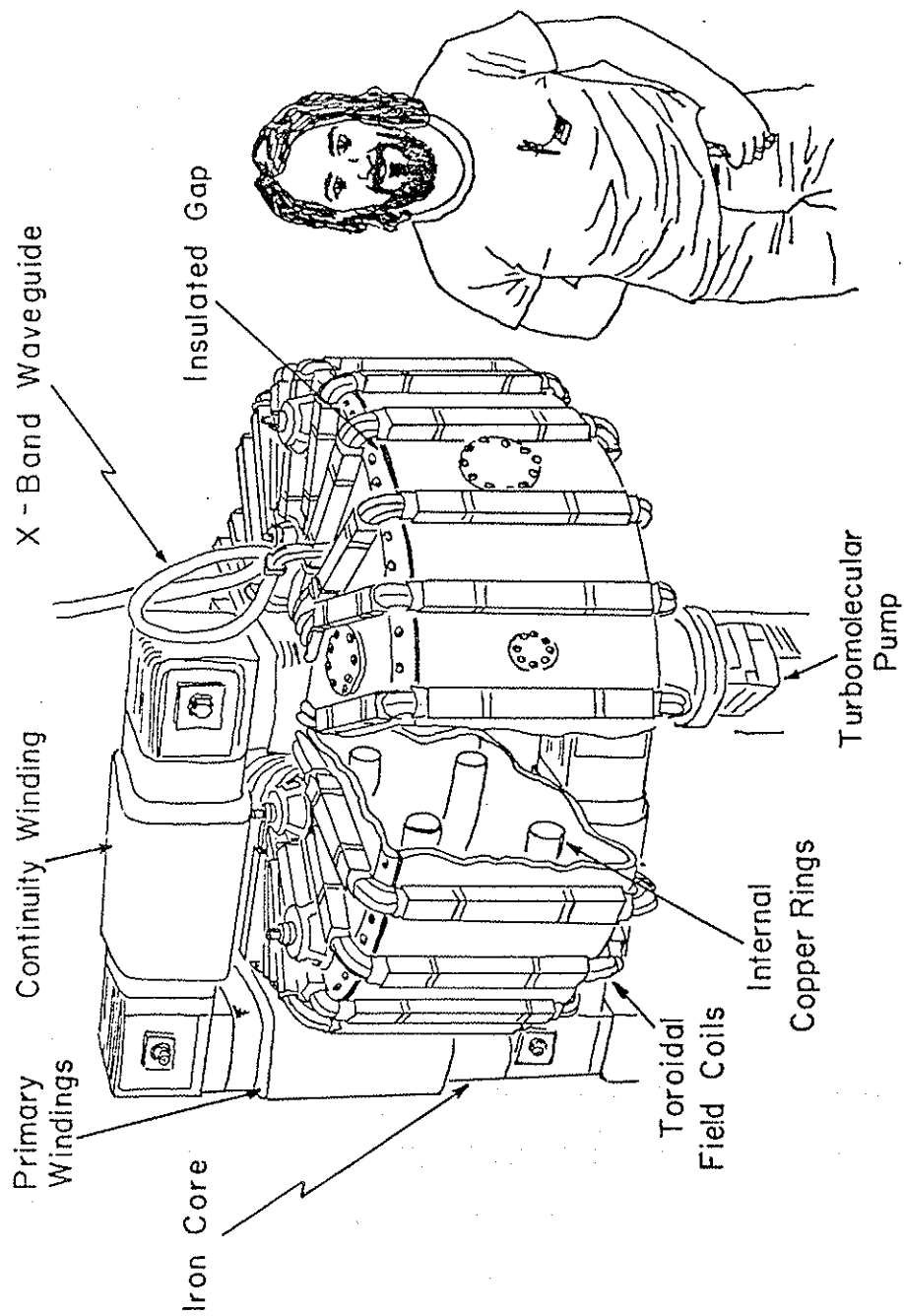
figure 3-1
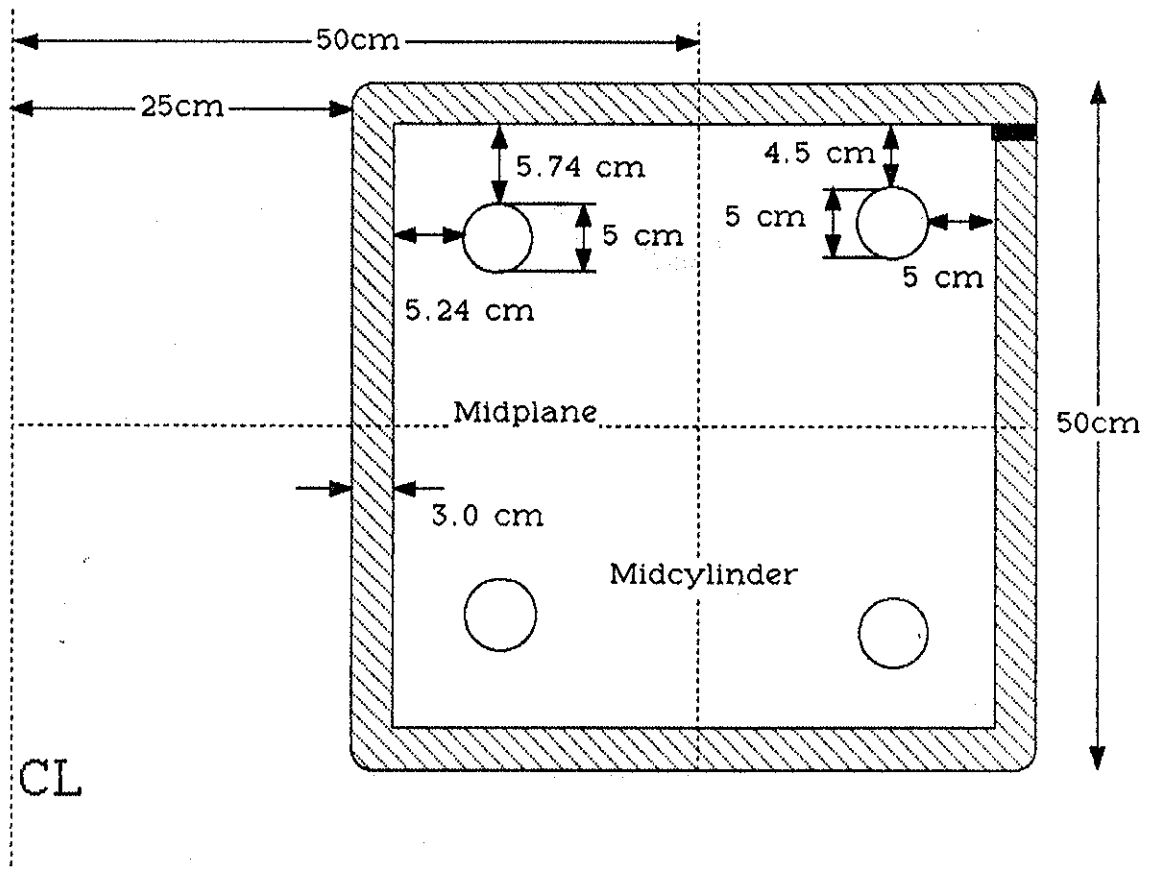Tokapole II device with a typical experimenter

figure 3-2
Tokapole II cross section

ignitron. This bank was passively crowbarred by another class E ignitron wired to automatically trigger at the peak field. This arrangement would give a field which was reasonably flat for ~10 msec which is the longest discharges typically lasted. Fully charging the banks would give a bit more than 7 kgauss of field. However, due to mechanical and voltage standoff limitations, the peak field was usually held to under 5.5 kgauss. The toroidal field can be reversed in direction by a knife switch.

The toroidal current in the divertor rings and the plasma is driven by a 40:1 turns ratio iron core transformer with a total flux swing of 0.17 V-sec when reverse biased. The primary of the transformer is driven by a 7.2 mF, 5kV capacitor bank switched through a class E ignitron. The half period of the current waveform is ~5.6 msec. There is also a 0.96 F, 450 V bank of electrolytic capacitors connected by a diode stack as a power crowbar to clamp the poloidal gap voltage at the peak of the current waveform. There is a removeable damping resistor in the circuit. Greater peak currents can be achieved without the damping resistor, but longer discharges are more easily obtained with it in.

The poloidal field is a combination of the vacuum octupole field of the divertor rings and the field generated by the toroidal plasma current. Since these currents are in the same direction, there will be nulls (x-points) in the region between the plasma current and the divertor rings. There will also be a surface (the separatrix) which separates the field lines which enclose a single conductor (private flux) and those which enclose all 5 conductors (common flux). The vacuum flux plot is shown in figure 3-3a, and one with plasma is shown in 3-3b. The exact location of the x-points and separatrix depends on the ratio of current in the divertor rings to that in the plasma, and the exact positioning of the divertor rings.

Figure 3-4 shows the device in cross section with a flux plot, the antennas used in this work, and a probe. Some of the other terms used to describe locations on the machine are also indicated.
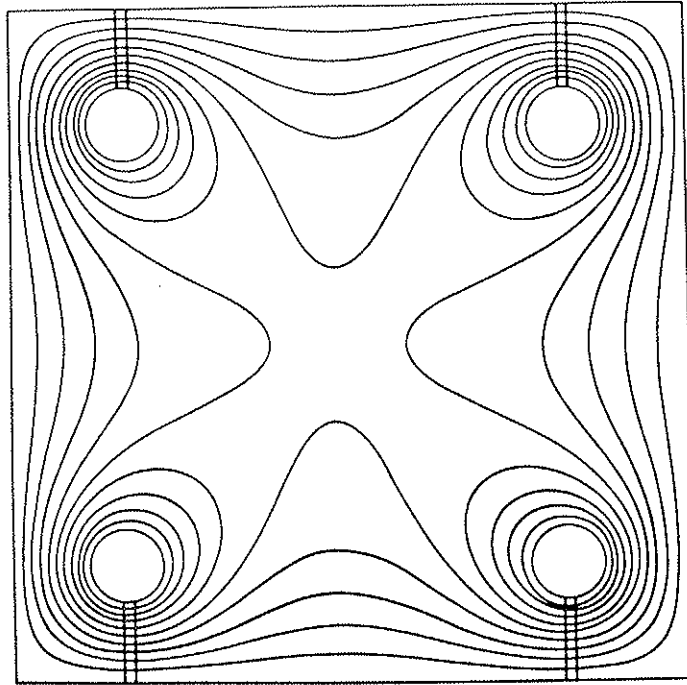
figure 3-3a
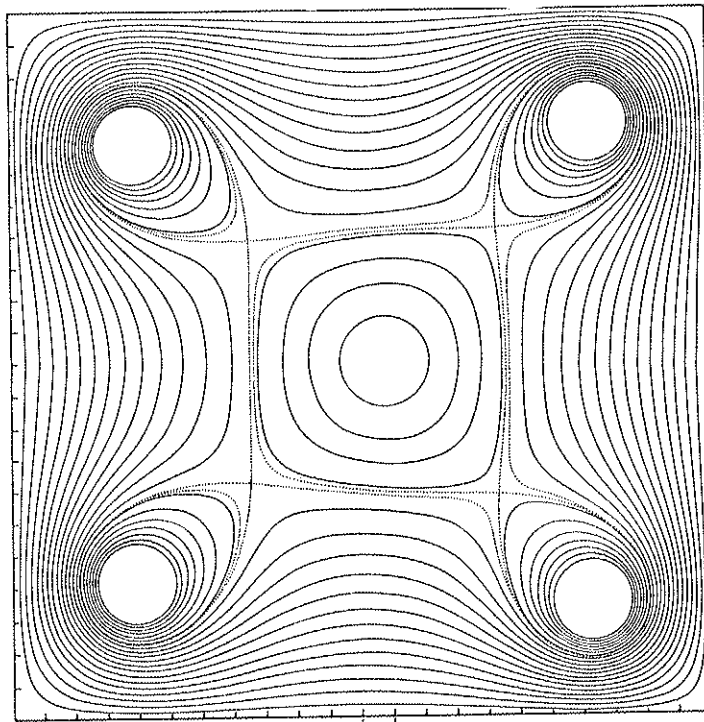Vacuum flux plot showing octupole fields

figure 3-3b
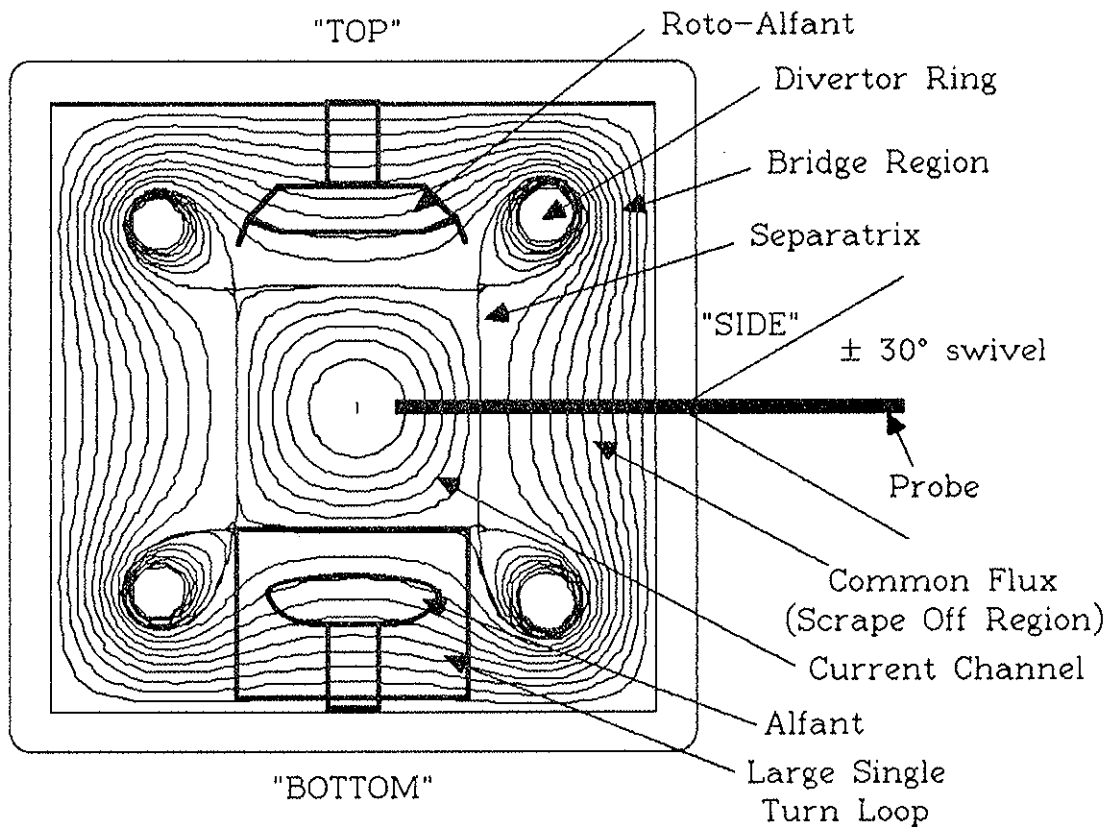Flux plot with plasma showing separatrix and x-points

figure 3-4
Tokapole II cross section and flux plot showing projections of the
various antennas and a typical probe

The central region, inside the separatrix, is where the majority of
the plasma current flows and contains the hottest and most dense
plasma. The region outside of this current channel, the scrape off
region, can carry some current unless something is there to inhibit
it. There are stainless steel plates which can be inserted into this
region for this purpose, and of course the antennas themselves will

act as limiters. Probes can be inserted at various places around the machine without breaking vacuum from the outside along the midplane and from the top and bottom along the midcylinder through valves. Many of these probe ports can swivel up to 30° away from radial in all directions allowing access to a large
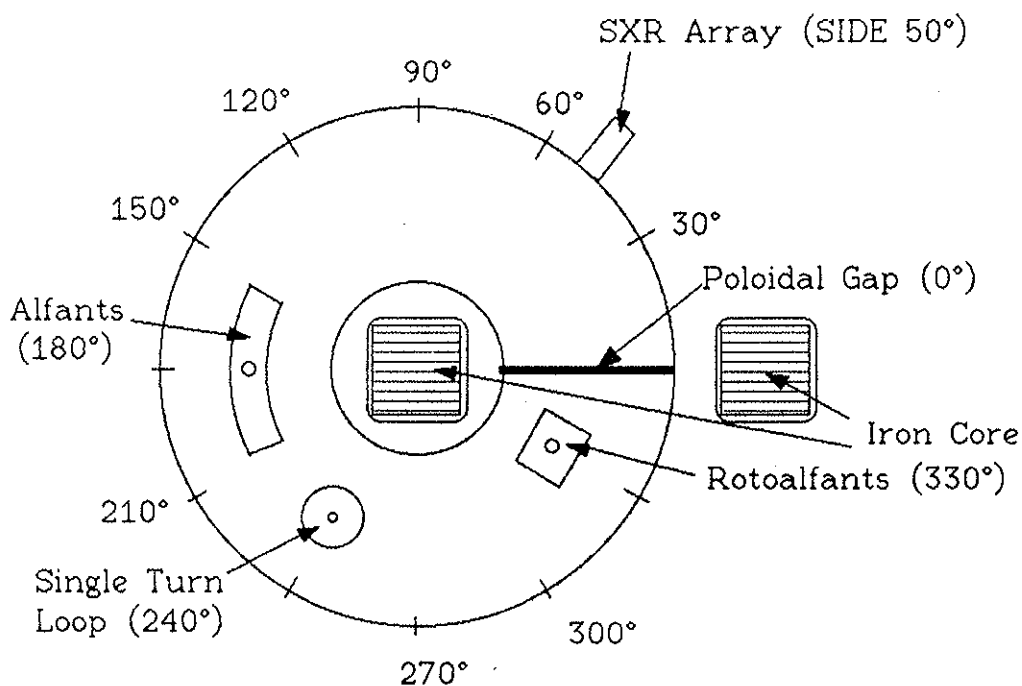

figure 3-5
Tokapole II top view showing locations of antennas and diagnostics

fraction of the volume of the vessel. Figure 3-5 shows a top view indicating the locations of the various antennas and defines the coordinates used for toroidal locations on the device. An x-y coordinate system is used to describe the locations of probes and antennas in a poloidal cross section. The origin is located at the

geometric center of the machine, and y is positive going up, x is positive going radially out, units are in cm.

3-B Plasma Characteristics

Plasma formation in Tokapole is essentially like that of most other tokamaks and has been described in detail by Groebner[3]. There are several review articles[4,5,6] on tokamaks.

Tokapole operates with hydrogen, puffed by a fast piezoelectric "puff" valve 16.66 msec before the firing of the poloidal field. Additional gas can also be let in during the discharge. This can be controlled by a feedback circuit which tries to hold the line-averaged saturation current, drawn by a Langmuir probe in the "bridge" region, constant.(The "bridge" region is the space between a divertor ring and the wall.) Filling pressure is typically in the range of 100 to 300 mtorr. The toroidal field is fired 10.66 msec before the poloidal field is fired and crowbarred at peak field. There are ten kW of pulsed X-band (9.0 GHz) or K-band (16.5 GHz) as well as 100 W of cw S-band (2.45 GHz) for use as preionization depending on the field settings used. This is not necessary, but is useful for consistency of the discharges at startup. The digitizers are triggered at 0.5 msec before the poloidal gap voltage to allow subtracting off any DC offset in the diagnostics. RF is operated in two modes, long pulse at low power or short pulse at high power (see chapter 4). In long pulse mode, the RF is switched on at 0.25 msec before the firing

of the poloidal field to allow subtracting off dc offsets and vacuum signal on the probes. The short pulse RF can be switched on at any time during the discharge. The timing of the fields in shown in figure 3-6.
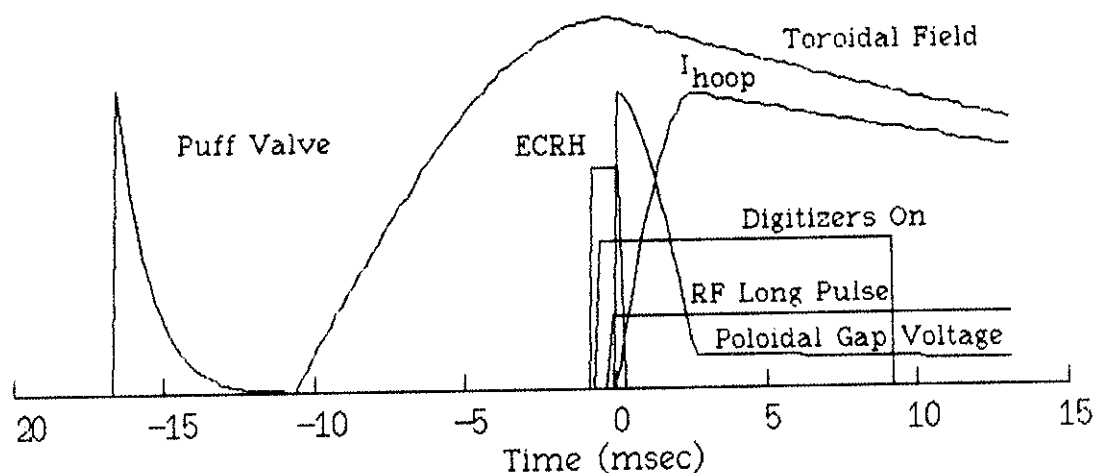

figure 3-6
Timing diagram for a typical Tokapole II pulse

There are two types of discharge usually run on Tokapole, relatively short discharges with high peak current and density, and longer lived discharges with a plateau region on the current and density (providing there are no probes into the current channel). The high-current discharges are much less sensitive to having probes inserted as can be seen in figures 3-7a and 3-7b. The dashed line indicates the effect of insertion of a probe into the current channel. The details of the physics of the discharges in Tokapole are discussed in significantly more detail by Brickhouse[7] and Osborne[8]. Table 3-1 lists a summary of typical Tokapole parameters.
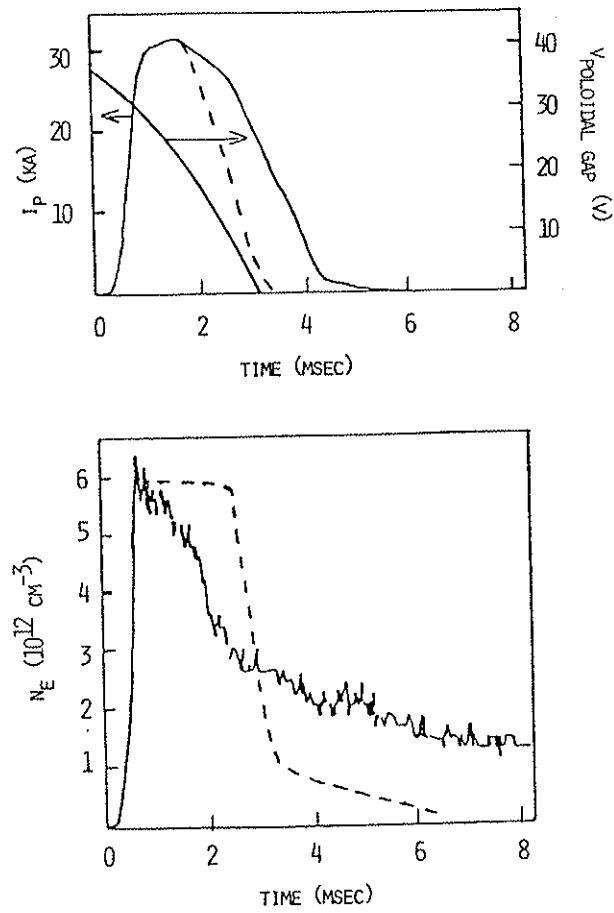
figure 3-7a
Plasma current and line-averaged density for a
typical high-current shot
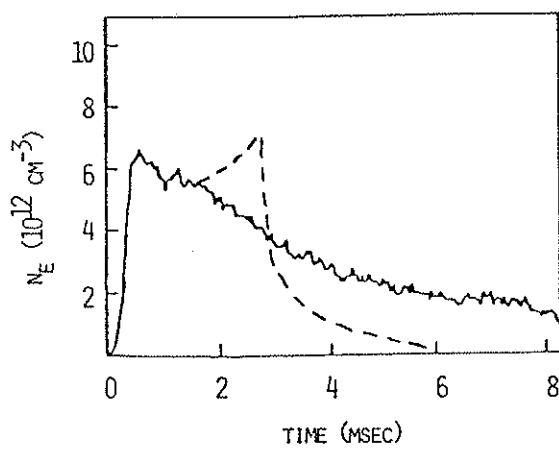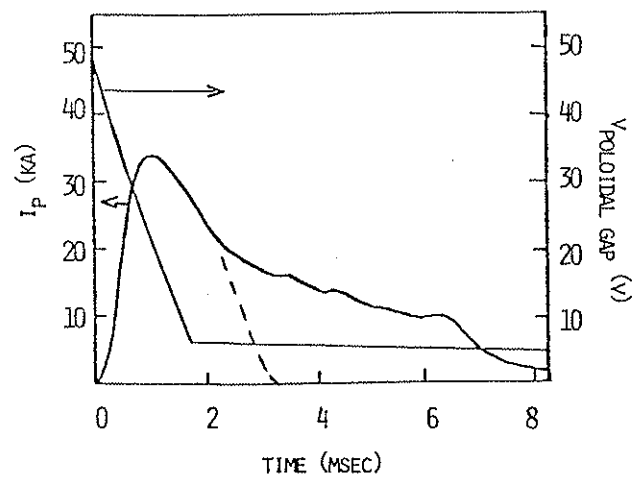
figure 3-7b
Plasma current and line-averaged density for a
typical low current shot

TOKAPOLE II TYPICAL PARAMETERS

Major radius	50 cm
Minor radius of plasma	6-10 cm
Toroidal magnetic field	5 kG
Plasma current	30 kA
Line-averaged density	$2-10 \times 10^{12}$ cm^{-3}
Electron temperature	100 eV
Ion temperature	20 eV
Energy confinement time	0.5-1.0 msec
Discharge length	3-10 msec
Base vacuum	2×10^{-7} torr

table 3-1

REFERENCES

1. A.P. Biddle, R.N. Dexter, R.J. Groebner, D.T. Holly, B. Lipschultz, M.W. Phillips, S.C. Prager, and J.C. Sprott, Nucl. Fusion 9 , 1509 (1979).

2. J.C. Sprott and T.W. Lovell, University of Wisconsin PLP 744 (1978)

3. R.J. Groebner, Ph.D. Thesis, University of Wisconsin (1979)

4. L.A. Artsimovich, Nucl. Fusion 2, 215 (1972)

5. H..P. Furth, Nucl. Fusion 15, 487 (1975)

6. J. Sheffield, Proc. IEEE 69, 885 (1981)

7. N.S. Brickhouse, Ph.D. Thesis, University of Wisconsin (1984)

8. T.H. Osborne, Ph.D. Thesis, University of Wisconsin (1984)

Chapter 4
R.F. Apparatus

4-A   Antennas

There have been several families of antennas used for Alfvén wave studies on the Tokapole. The basic characteristics of these are summarized in Table 4-1. The divertor rings were used initially since they allowed the experiment to commence immediately and were intended as only an intermediate step prior to construction of a proper launching structure. They were used primarily in earlier experiments[1] and are mentioned here only for completeness. The Alfant was designed as these early experiments were starting and had little flexibility built in. Two of these were constructed and used. The Roto-Alfant was designed after initial disappointing results with the Alfants. It shared the feedthrough design with the Alfant but had much greater flexibility. Both were designed with high-power, pulsed service in mind and were manufactured in the Physics department instrument shop at significant cost. After some further disappointing or anomalous results the attention was shifted to low power, cw operation and much less expensive antenna designs. The Large Single Turn Loop antennas were constructed by graduate students for quick turn-around. The results yielded were somewhat more encouraging. Each of these designs will be described in some detail. For detail information concerning construction the reader is referred to the full set of blueprints on file with the

University of Wisconsin Plasma Physics group.

Antenna Specifications

	Internal rings	Alfant	Roto-Alfant	Large Single Turn Loop
Faraday shield	none	yes	removable	removable
Particle shield	none	yes	yes	removable
End limiters	N.A.	yes	removable	no
Rotation range	0	±45°	360°	360°
Radial insertion range	0	6 cm.	6 cm.	22 cm.
Feed	single end	coax	coax	balanced (floating)
Maximum power (design)	100 kW	250 kW	250 kW	50 kW

Table 4-1

4-A 1 High-Power Feedthrough Design

The vacuum feedthrough used for the Alfant and Roto-Alfant has proven quite successful. It has been tested to 15 kV peak voltage insulation at 2 MHz and has handled 1.5 kA of circulating current. After an initial design modification, it has given no problems with vacuum leaks. It is shown in figure 4-1.

The feedthrough is a low inductance coax. This allows the antennas to be rotated and radially inserted. It was necessary to construct the feedthrough in two sections since the largest port in the Tokapole is 19 cm in diameter. The sliding vacuum seal on the outer conductor is accomplished with two Quad-Rings® which are significantly better than O-rings for this type of dynamic seal since they are less prone to twisting. Pumpout is provided between the two seals to eliminate vacuum bubbles when moving the antenna. The outer conductor is made from copper to minimize losses and is then plated with 1 mm of hard chrome to allow it to slide more easily and to protect the soft copper from scratches. The assembly slides in Delrin guides, also to prevent scratching of the sealing surface. In order to use a standard size of tubing for the outer conductor it was necessary to ream out the holes in the Tokapole wall from 1.5" to 1.563" to accept the oversized Delrin sleeves. This was done to four "1½" ports located at TOP 180°, BOTTOM 180°, TOP 330° and BOTTOM 330°(see figures 3-4,5). The vacuum seal between the center and outer conductors is also made with Quad-Rings® to
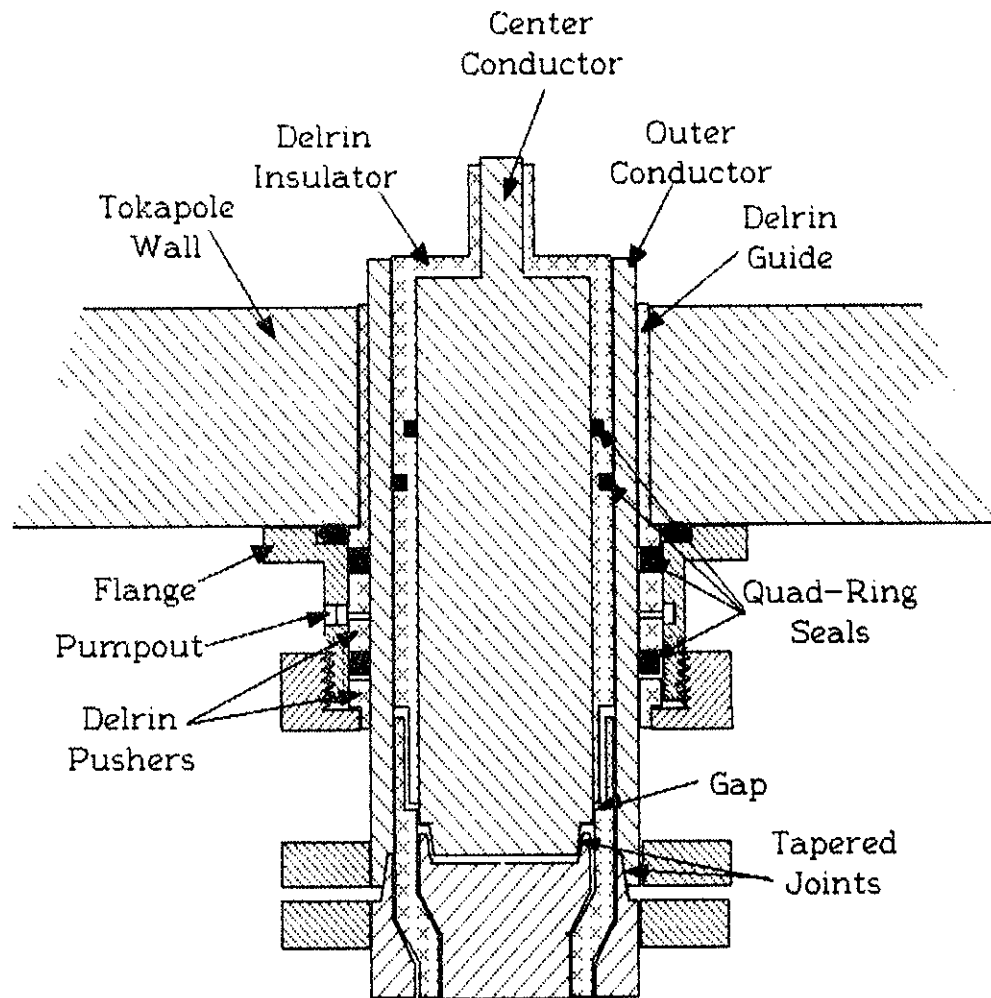
High Power Feedthrough

figure 4-1

eliminate twisting during assembly. The Delrin insulator is first shrink fit onto the center conductor. The Quad-Ring is then compressed on the outside of the insulator. This assembly is then pressed into the outer conductor. Originally this seal was made at the gap between the upper and lower insulators but this had two

problems. The thermal expansion of the insulator from the heating of the Tokapole walls would pinch the O-rings into the corners. If the walls and thus the antenna cooled off, the O-rings remained captured, and a leak would be opened. The other problem was with voltage standoff. It is apparently standard practice in the manufacture of O-rings to finish them in a tumbler with an abrasive dust of metal filings to remove flash from the molding process. This lowers the standoff voltage of the O-rings. Also, the natural O-rings are superior to the ones with carbon black added. In the modified design, this gap is outside of the vacuum and could thus be packed in dielectric grease. The mechanical joints in the current path were made with tapered fit pieces and plated with Cool-Amp® to minimize losses. In the Roto-Alfant, the connection to the antenna coil from the center conductor was made with a Spira-Lock® self locking thread. This technique was apparently successful since the measured resistance of the first Alfant was 0.063 Ω as compared to the resistance of 0.043 Ω which would be calculated for the antenna just from losses in the copper. This loss is dominated by losses in the coil itself and the calculation neglects proximity of the ground plane on the lower portion of the coils. This means that the combined resistance of the 7 mechanical joints is less than half of the loss in the antenna element.

4-A 2 Alfant

The Alfant was constructed as an improvement over the internal divertor rings. It was believed that the large spurious loading of the divertor rings was due primarily to the presence of plasma in the private flux region around them. It was expected

Alfant Specifications

2 Series loops with a coaxial feed

Copper Faraday shield

Macor optical blind

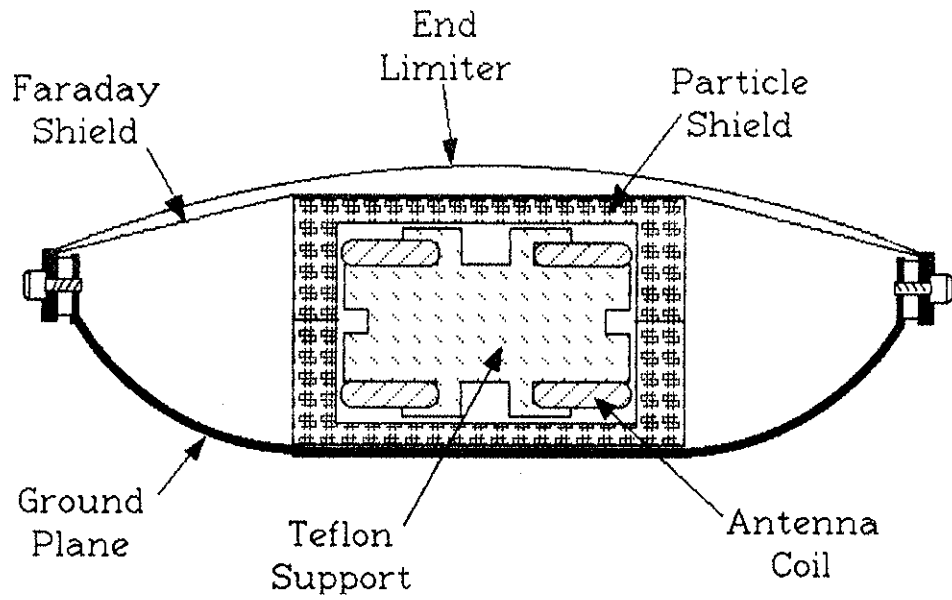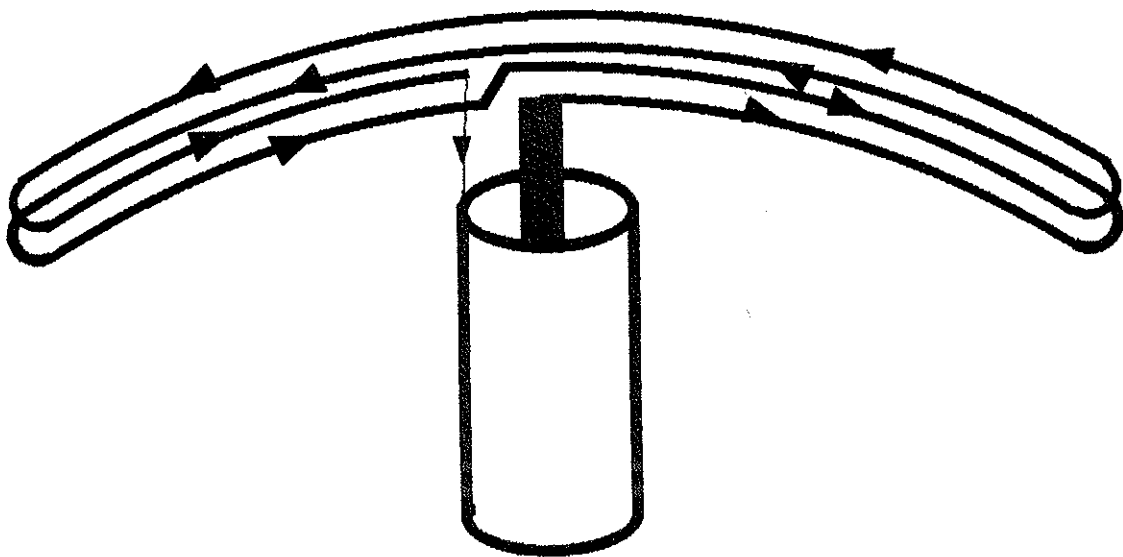|	
Antenna inductance	0.75 μH
Unloaded Q (with shield installed)	100 @ 2MHz
r_{vac} (vacuum resistance)	0.097 Ω @ 2MHz
Maximum current	2 kA
Maximum voltage (breakdown limit)	20 kV
Radial insertion range	6 cm.
Rotation range (on the floor)	± 45°
Rotation range (at full insertion)	± 15°
Toroidal extent	54°

table 4-2

figure 4-2a

Alfant cross section

figure 4-2b

Alfant current path that driving currents in a shielded antenna

parallel to the equilibrium field, directly driving the Shear Alfvén Wave, would yield the best coupling. To test this theory, some rotation range was designed into the antenna, but only very little (see table 4-2).

The antenna is shown in figure 4-2a in cross section. The current path is indicated in figure 4-2b. Since the lower conductors are so close to the ground plane, the field near the top of the antenna falls off as $1/r$ but beyond 2.5 cm the field drops off much faster (see figure 4-3). This is why it was so important to make the antennas radially moveable. The antennas had to retract out to the wall so as not to interfere with other experiments.
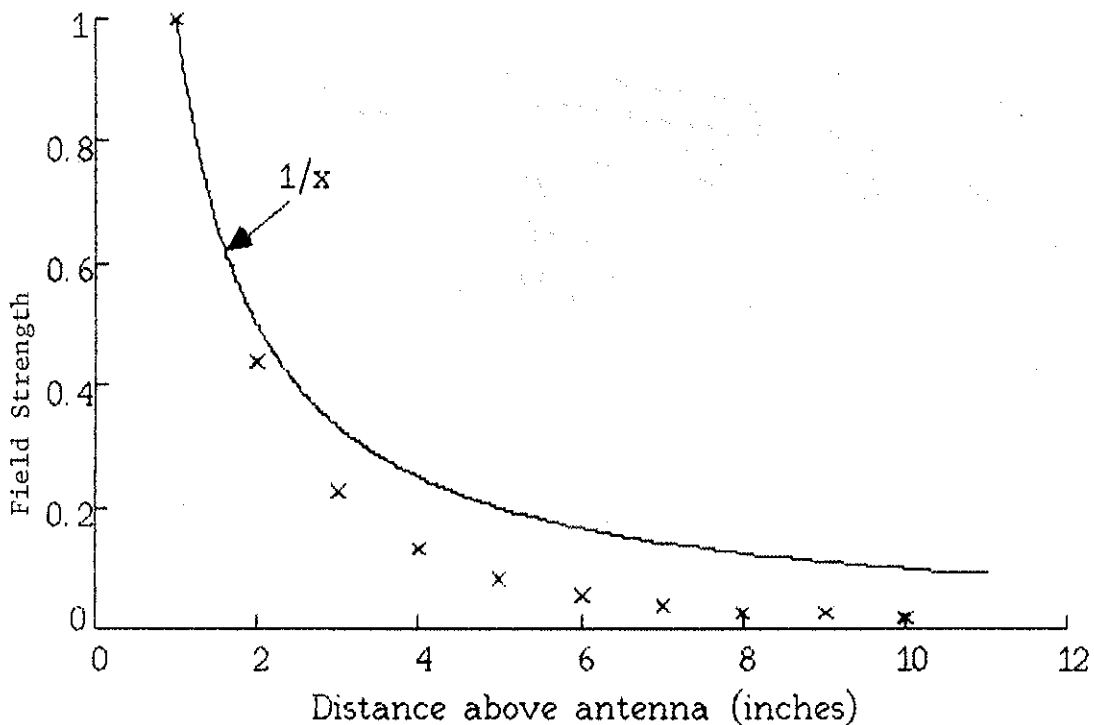

figure 4-3

The antenna was curved to match the major radius of the machine. Its length helps eliminate high toroidal mode numbers. There were two Alfants made. They were located at TOP 180° and BOTTOM 180°. These two could be driven in or out of phase with respect to each other to drive either even or odd poloidal mode numbers. They were grounded individually at the tank wall and transformer coupled at the source to eliminate ground loops.

4-A 3 Roto-Alfant

The next antennas used were designed with much greater flexibility in mind. The primary reason for construction of these antennas was to rotate the driving currents fully to the poloidal direction. They shared the feedthrough design with the Alfant and were very similar electrically. Their characteristics are summarized in table 4-3. A cross section is shown in figure 4-4a and the relative field strength vs radius is plotted in 4-4b. Since the feed currents had to be fed off to one end from the center conductor of the coax feed, there was a significant non-uniformity in the field strength very near the antenna. This is shown in figure 4-5a. This non-uniformity is not very noticeable at 6 cm. above the antenna, as indicated in figure 4-5b.

These antennas were located at TOP 330° and BOTTOM 330° and were operated in the same manner as the Alfants. They were operated with and without Faraday shields, with and without end

Roto-Alfant Specifications

5 Series loops with a coaxial feed

Removable Copper Faraday shield

Macor optical blind

Removable stainless steel end limiters

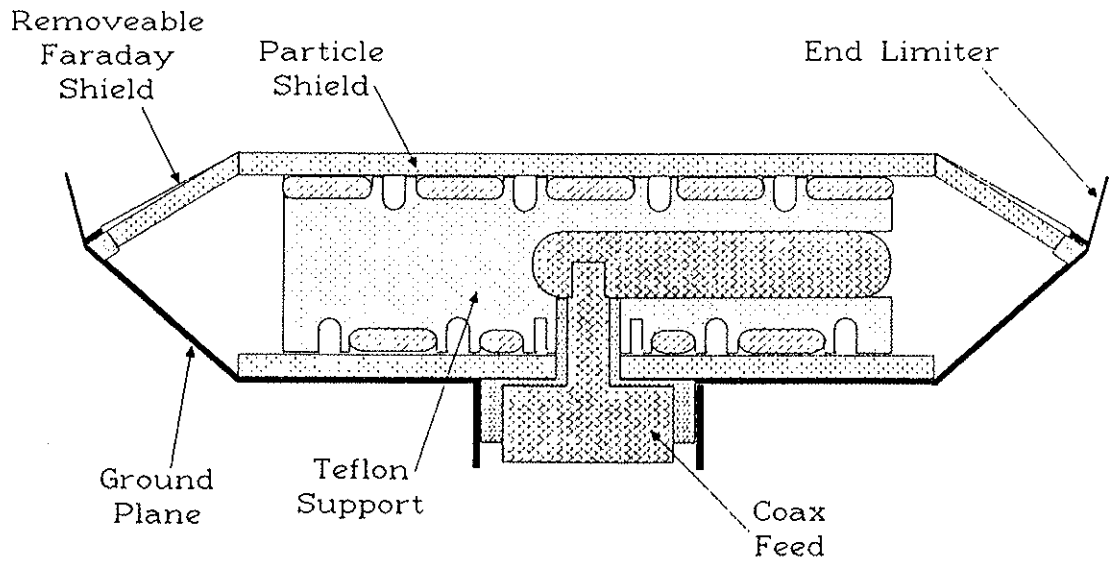|	
Antenna inductance	0.79 μH
Unloaded Q (with shield installed)	89 @ 2MHz
r_{vac}	0.112 Ω @ 2MHz
Maximum current	2 kA
Maximum voltage (breakdown limit)	20 kV
Radial insertion range	6 cm.
Rotation range (on the floor)	360°
Physical dimensions	15.25 x 17.75 x 3.25 cm

table 4-3

figure 4-4a
Alfant cross section

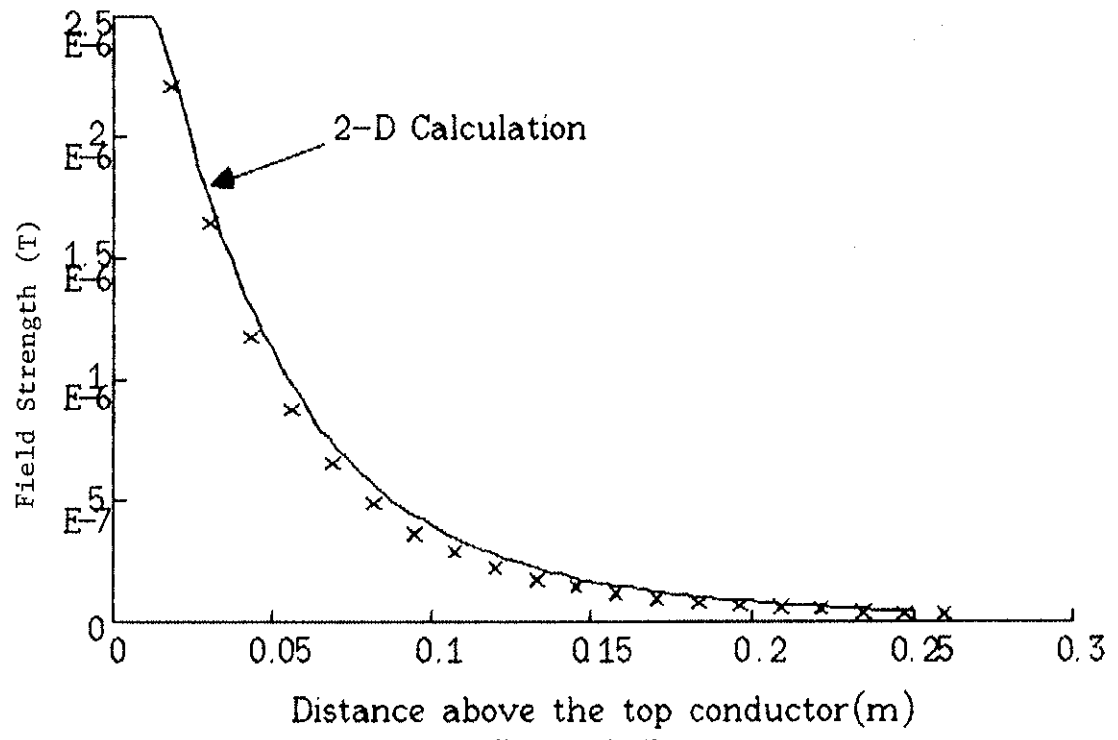Distance above the top conductor(m)
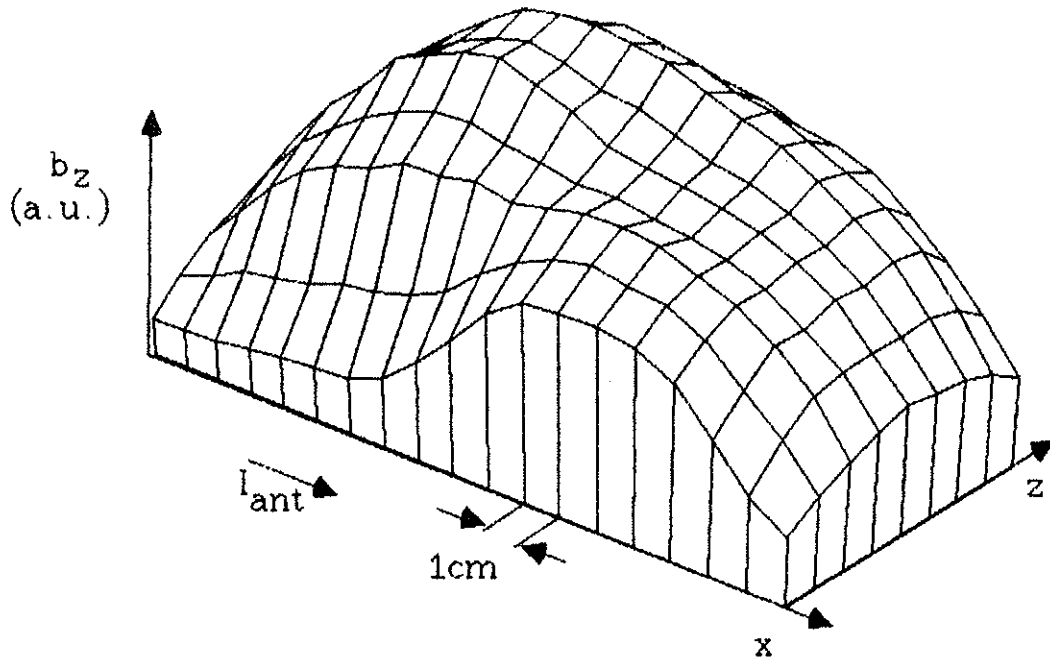figure 4-4b
Field drop off above the Roto-Alfant

figure 4-5a
Surface plot of the field above the Roto-Alfant at 1.2 cm.
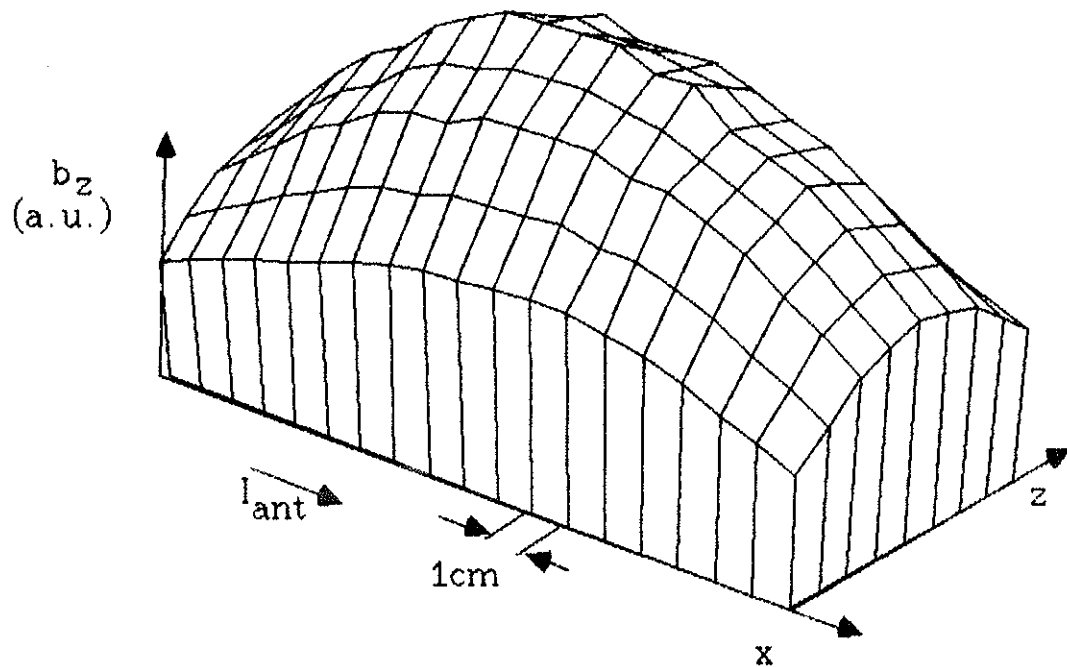

figure 4-5b
Surface plot of the fields 6 cm. above the Roto-Alfant

limiters, and throughout most of the available range of insertion and rotation. Originally the Roto-Alfants were constructed with 2 sides of copper and 2 of stainless. The copper sides were later covered by stainless steel shim stock since the discharges were somewhat more degraded when the copper sides faced the plasma current directly than when the stainless sides faced the plasma current.

4-A 4 Large Single Turn Loop Antenna

This antenna was a significant departure from the Alfants. The primary motivation was to use a much larger physical loop so that with the top of the antenna at the same insertion into the scrape-off region, the field would be larger at the same location above the antenna for the same amp-turns.(see figure 4-6).

The Large Single Turn Loop was constructed of all stainless steel and ceramic components so that it could be cleaned vigorously before insertion into the vacuum, and would clean up in plasma as quickly as possible. Since the feed was balanced, a new feedthrough had to be used. The main vacuum seal for the feedthrough was similar in design to the high-power feed used for the Alfant and Roto-Alfant, but slightly smaller. The shield for the balanced feed and the Faraday shield were connected to machine ground at the tank wall, but the antenna element had no DC reference to ground. This antenna was inserted through a gate valve located at BOTTOM 240° and could be easily removed for modification. It was operated

with and without Faraday shield and particle shield. Its specifications are summarized in table 4-4, and it is sketched in figures 4-7a&b.
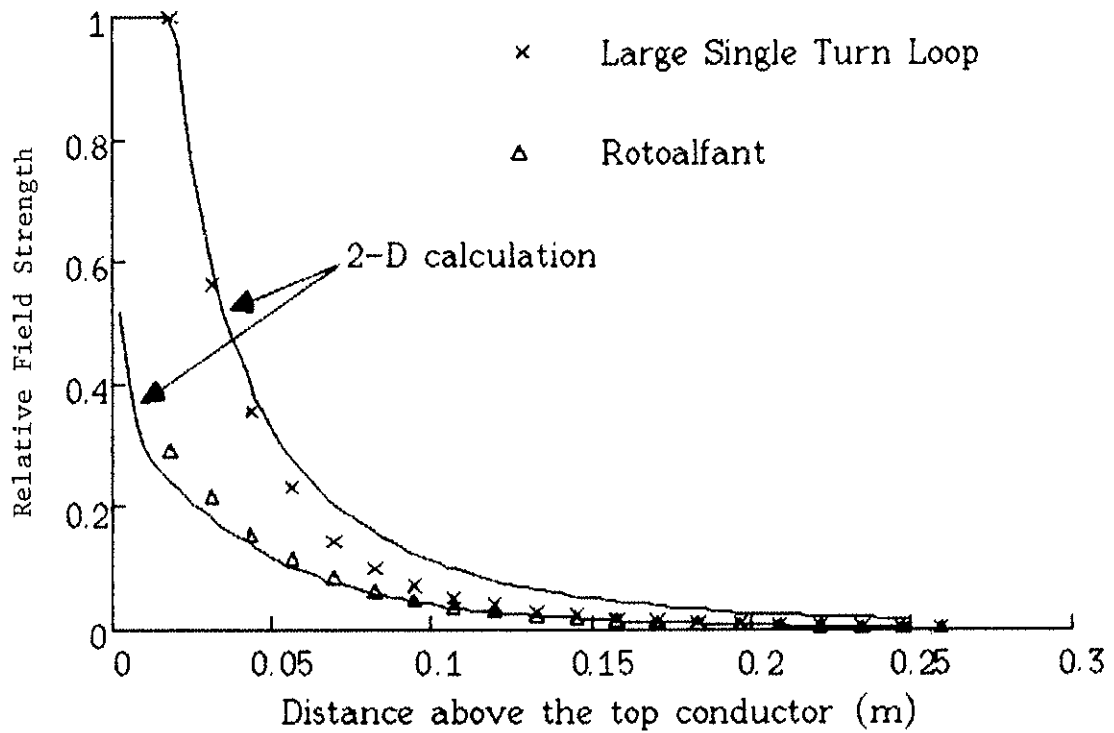
figure 4-6
Comparison of the Large Single Turn Loop to the Roto-Alfant

Large Single Turn Loop Specifications

Removable stainless steel Faraday shield

Macor and ceramic optical blind

Antenna inductance	.4 µH
Unloaded Q (with shield installed)	15 @ 2MHz
r_{vac}	.335 Ω @ 2MHz
Maximum current	200 A
Maximum voltage (breakdown limit)	1 kV
Radial insertion range	24 cm.
Rotation range (on the floor)	360°

table 4-3

figure 4-7a
Cut-away sketch of the Large Single Turn Loop antenna
(side view)

figure 4-7b
Cut-away view of the Large Single Turn Loop antenna
(top view)

4-B RF Sources

There were two different sources used for this research. A one-kilowatt linear amplifier operated cw and a 150-kilowatt amplifier operated pulsed.

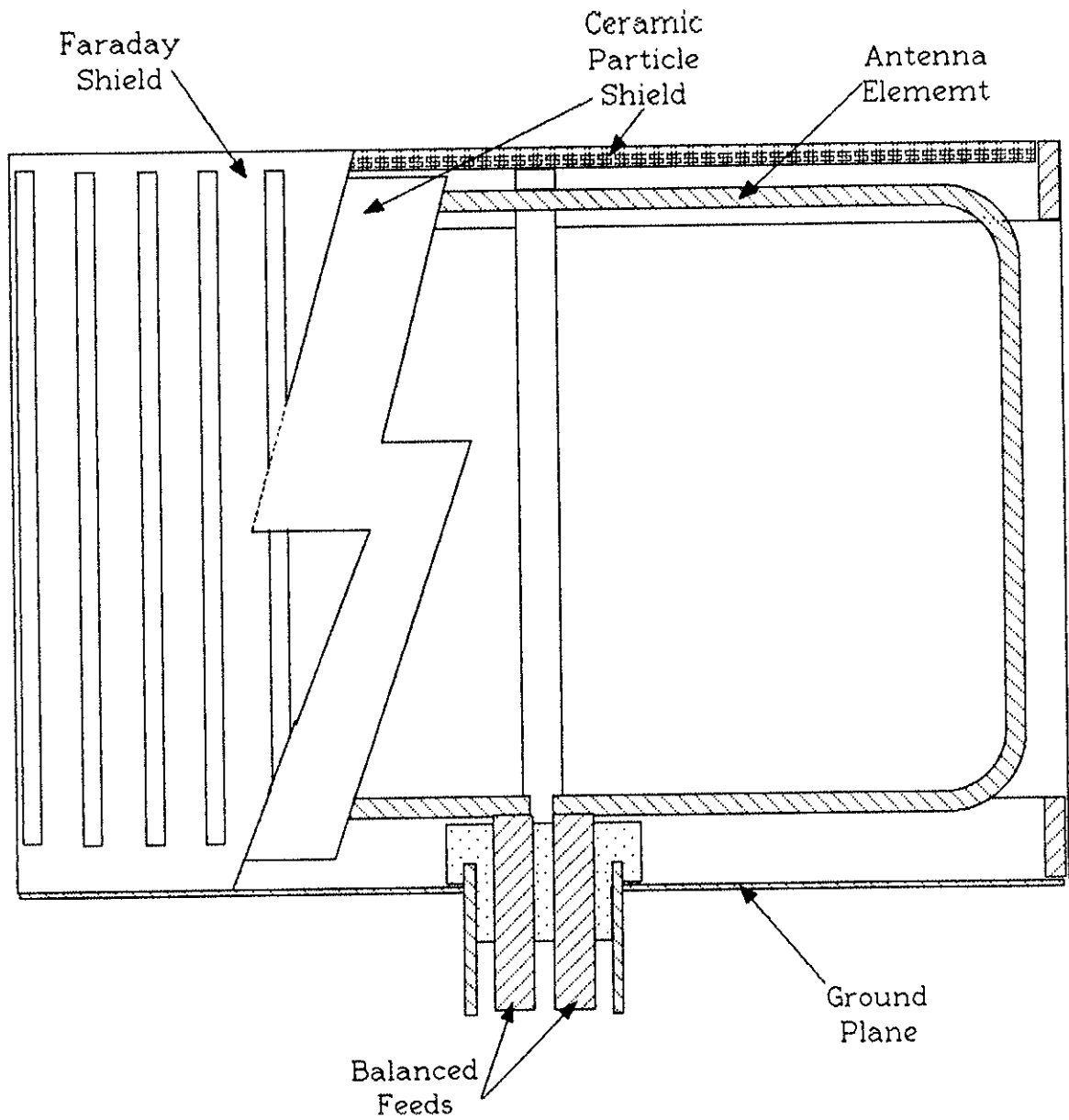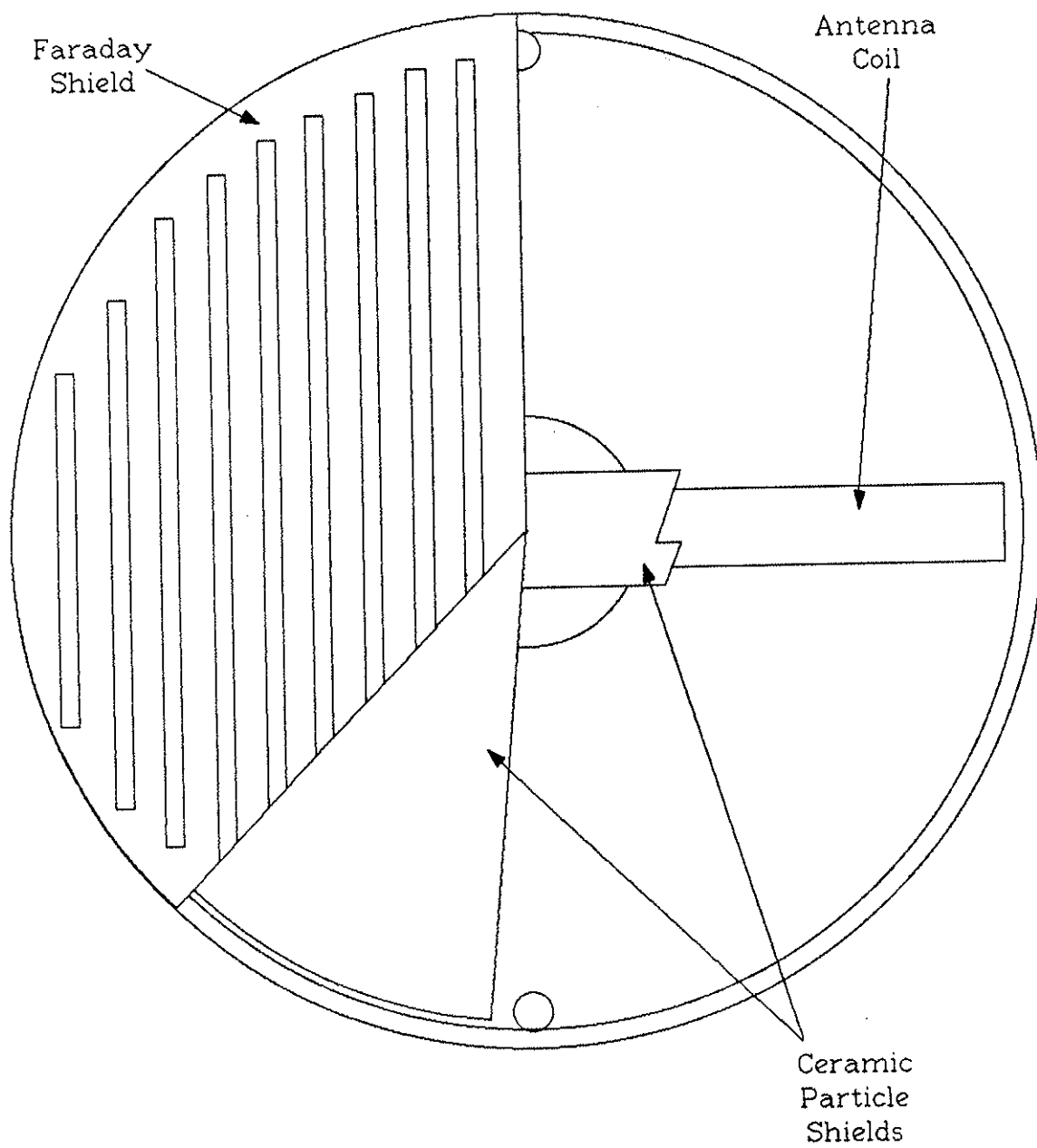The 1kW source was a Dentron MLA 2500 amateur radio set driven by a Johnson Viking II 30-W source which was driven by a General Radio Type 1330-A bridge oscillator. A Dentron 160-10 Monitor Tuner was used for impedance matching. If more than one antenna was being driven, the output was transformer coupled to avoid ground loops.

This system could deliver 600 watts and was typically operated in a "long pulse" mode rather than cw to avoid overheating the output transformers. The RF was switched on 250 μsec after the digitizers were triggered, which was 500 μsec before the poloidal field banks were fired, and remained on for ~15 msec. This allowed any dc offset in the electronics to be stored and subtracted later. The switching was done with a Hewlett-Packard model 10514A double balanced mixer at the output of the oscillator.

The pulsed RF system is sketched in figure 4-8. The tubes used were pulse modulator tetrodes (JAN-CDR-715C) which were perverted into RF service. There were two separate amplifiers driven by a common oscillator. The transformer coupling permitted ±180 degree phasing of the two amplifiers. The output of the amps was transformer coupled to avoid ground loops. The amplifiers could

be driven out of phase into a single center-tapped transformer to have one full power output. The system was driven by a pulse forming network which had a maximum pulse length of 1.2 msec and a maximum power output of 2 MW into 200 Ω. A 1 MW oscillator using ML 8772 triodes was built and tested but not used extensively due to problems with stability when trying to inductively couple to high Q resonant circuits such as the antennas.
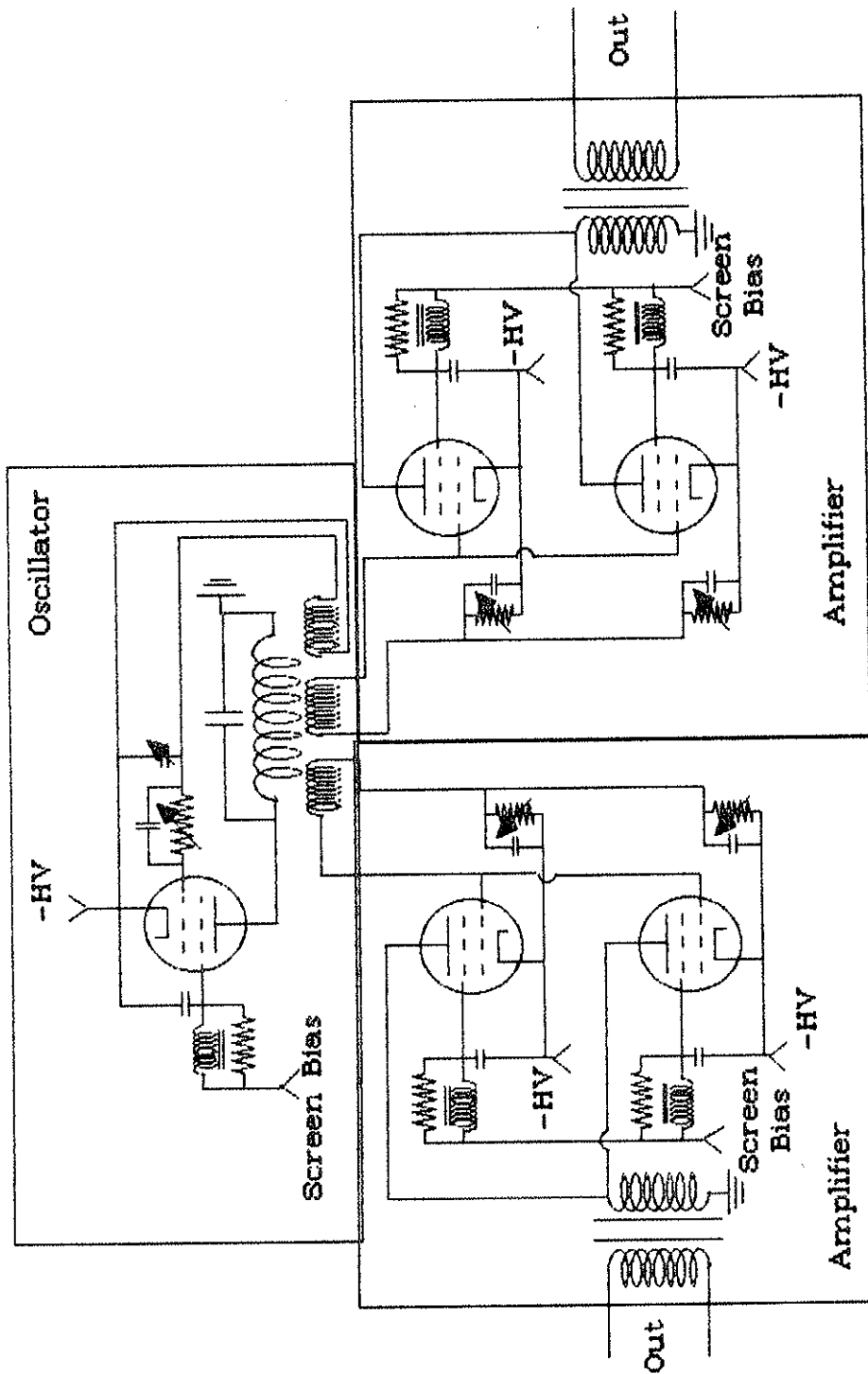
figure 4-8
150 kW oscillator/amplifier system

4-C   Alfvétronics

Alfvétronics is the name given to the large collection of RF electronics developed for this experiment. The prime diagnostics used were magnetic coils for direct measurement of the internal fields and phase detectors for measurement of the antenna loading. The raw magnetic probe signals ranged from 10 µV to 10 mV, and so significant amplification was necessary. The operating frequencies were expected to be in the range from 0.5-5 MHz, and since the majority of the digitizers available had a maximum digitizing rate of 1 MHz it was necessary to detect the amplitude and phase of the signals. Since the signals were quite noisy in certain parameter ranges, the signals were narrow-bandpassed before amplification, and synchronous detection was used to simplify later processing. This system is outlined in figure 4-9. To calibrate the probe-amplifier-detector system, Helmholtz coils were used, and control circuitry was constructed which would hold the current, and hence the field, constant as the frequency was swept. This allowed the entire system to be calibrated as a unit. The calibration curves could then be digitized and stored. To measure resistive loading of the antennas by the plasma, it was easiest to simply measure the phase between the current through and voltage across the antennas. The difference from 90° is, to a very good approximation, proportional to the loading. Phase detectors were constructed which would operate over a wide range of input amplitudes and frequencies.
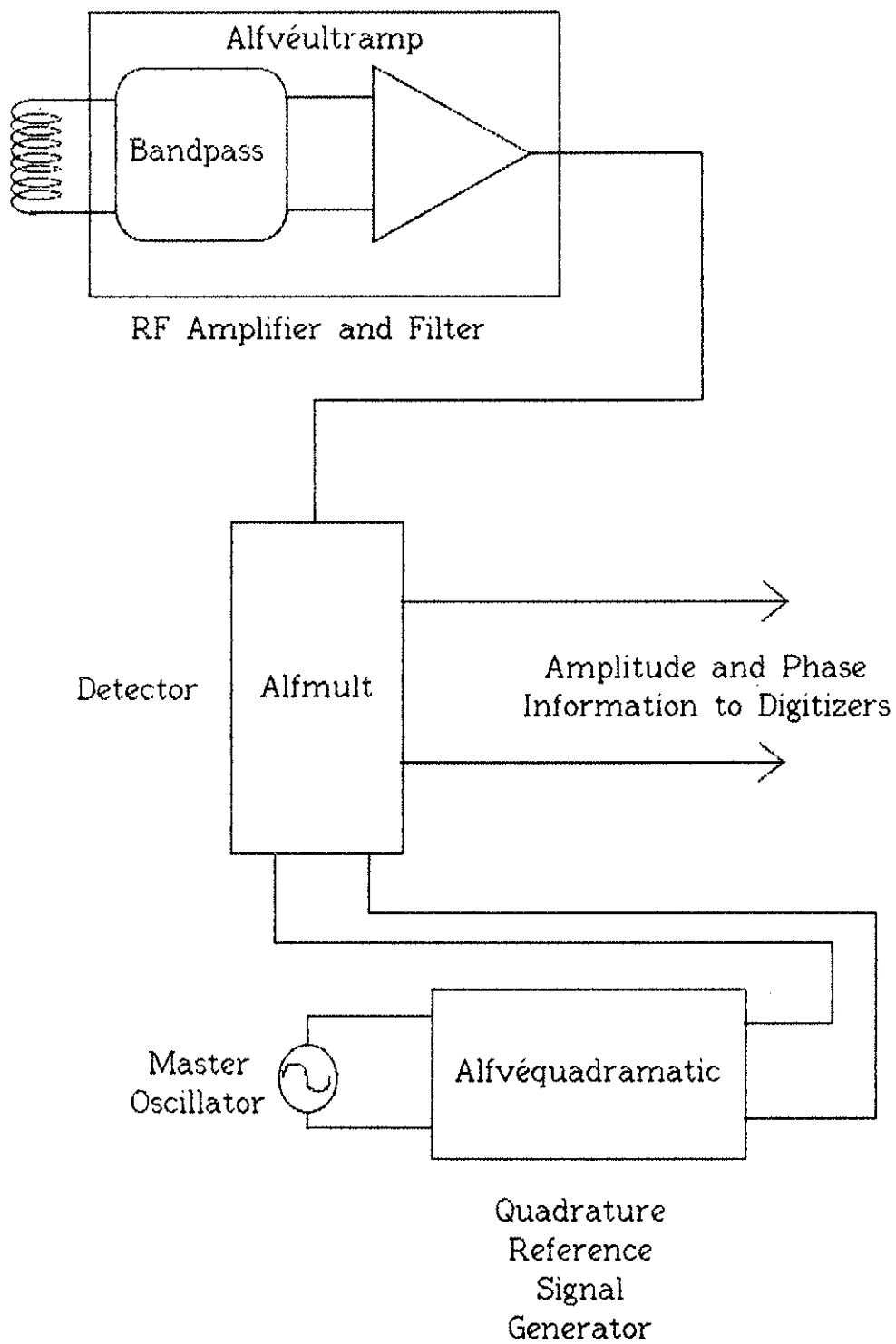
figure 4-9
System diagram for the amplification and detection of magnetic coil
signals indicating the names for the various circuits.

4-C 1 Magnetic pickup coils

The internal magnetic fields were measured directly by means of coils in a stainless steel vacuum envelope which also served as an electrostatic shield. To minimize the attenuation of the high frequency signal a 0.13 mm wall stainless steel tube was used. Since this was much too thin to expose to the plasma directly, it was protected by a boron nitride sheath, which was glued over it. This assembly is sketched in figure 4-10.

figure 4-10
Boron-Nitride-clad probe envelope assembly

The probe assemblies were interchangeable. Two main types were used. Most were single coil probes which could be easily produced in large quantities and were used at several different locations around the machine to try and identify mode structure. Several multicoil probes were used to make radial profile measurements on a single shot. These were much more difficult to

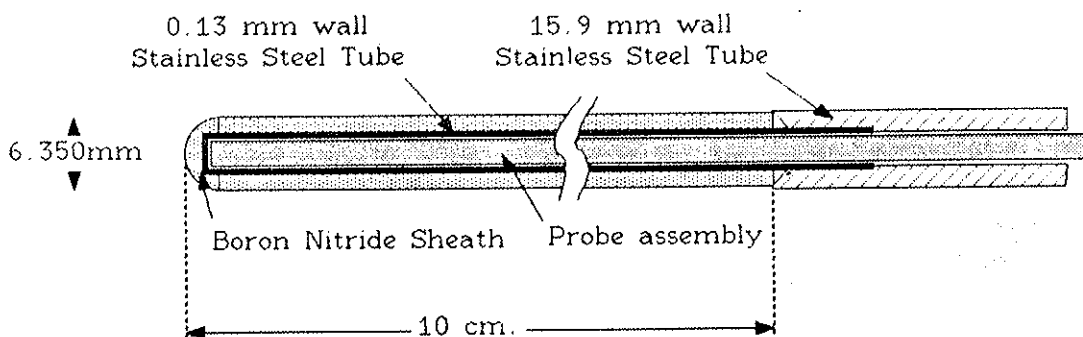manufacture, especially to maintain adequate alignment among the 8 coils. One of the primary difficulties was that temperatures could easily reach 200° C in the probe envelopes when they were inserted to within 4 cm of the geometric axis, well into the current channel. The 8-coil probe assembly is shown in figure 4-11.
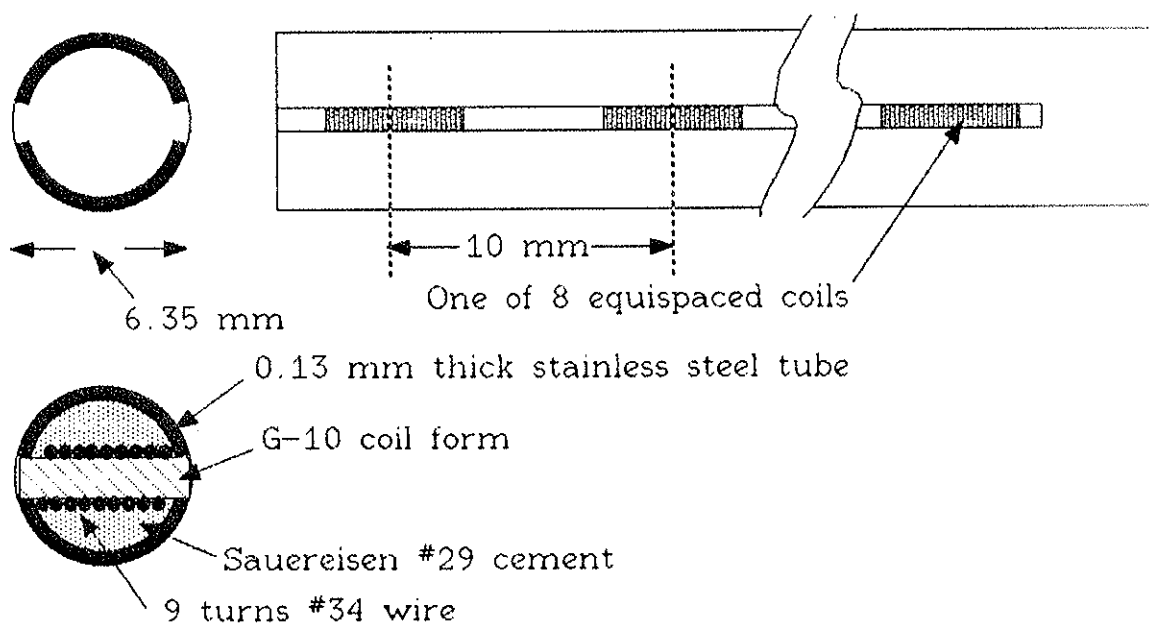
figure 4-11
8-coil transverse probe assembly used for radial profiles

The individual coils were wound on a form of G-10 (high temperature phenolic) which had protruding ends to allow them to be clamped for further assembly. Then the 8 coils were clamped in a jig which held them at the spacing that they would have in the final assembly, and the leads were braided together. This assembly was then fed into a stainless steel tube which had been

slit both to allow for the protruding ends, and to minimize attenuation. This assembly was then placed into a jig which clamped the protruding ends of the coils to align them. Sauereisen #29 high temperature cement was then injected down the length of the assembly and allowed to harden. Once it had hardened, the protruding ends could be machined off. The probe body was then sprayed with a teflon coating to allow easy insertion into the vacuum envelope.

The alignment of the probes was quite good. The few that were made were aligned to better than 3-4° maximum deviation of all 8 coils. The temperatures reached during pulsing had no noticeable effect on the alignment.

The coils had 9 turns of #34 magnet wire with Poly-Thermaleze insulation. The cross sectional area of each turn was 0.04 cm^2.

There was some concern that the crosstalk might be significant among the 8 coils since the leads were not shielded from one another. This proved not to be a problem. The only precaution taken was a tight twisting of the leads of each coil before braiding with the others. The crosstalk was down at least 50 dB, which was the noise level, as measured by having one of the coils shielded by a thick wall stainless tube while the other seven were driven in the calibrating Helmholtz coils near maximum output for the amplifiers.

4-C 2 Alfvéultramp

The Alfvéultramp is a rf signal amplifier having a fairly flat frequency response from 0.5-5 MHz. The maximum gain of the amp is 68 dB. This can be adjusted in 1-dB increments by a variable attenuator at the input down to 37 dB. It has narrow bandpass filters which can be quickly removed to change operating frequencies. Typically, the passband of the filters is ±10% of the center frequency. However, the ultimate bandwidth of the system is set by this passband and the lowpass of the detected signal. The input is differential into a center-tapped transformer. The input impedance is set at 150 Ω to yield reasonable values for the inductors in the input filter, but could be almost arbitrary since the first gain stage is a FET. The input impedance is limited in practice by the leakage inductance of the input transformer on the low end and by its magnetizing inductance on the high end. It can drive 50 ohm loads and clips at ±3V output. The circuit is sketched in figure 4-12.

The drawing also indicates the grounding arrangement found to be most successful at eliminating noise from both plasma and pickup on cabling in the external system. The vacuum envelope was always grounded at the machine wall. Since it was a conductor inserted into a plasma it could draw current (as a Langmuir probe does). By grounding it at the machine wall, these currents were returned directly rather than through the ground path for the rest of the system. The shield ground was isolated all the way back to the computer racks where the ground was made for both it and the

Alfvèultramp
Block Diagram

.005" Wall Stainless Steel Tube

Coil

"Machine Ground"

Variable Attenuator

Band Pass Filter

+26 dB

"Circuit Common"

0 dB

+20 dB

Band Pass Filter

+20 dB

"Shield Ground"

$$A(t)\cos(\omega t + \Phi(t))$$
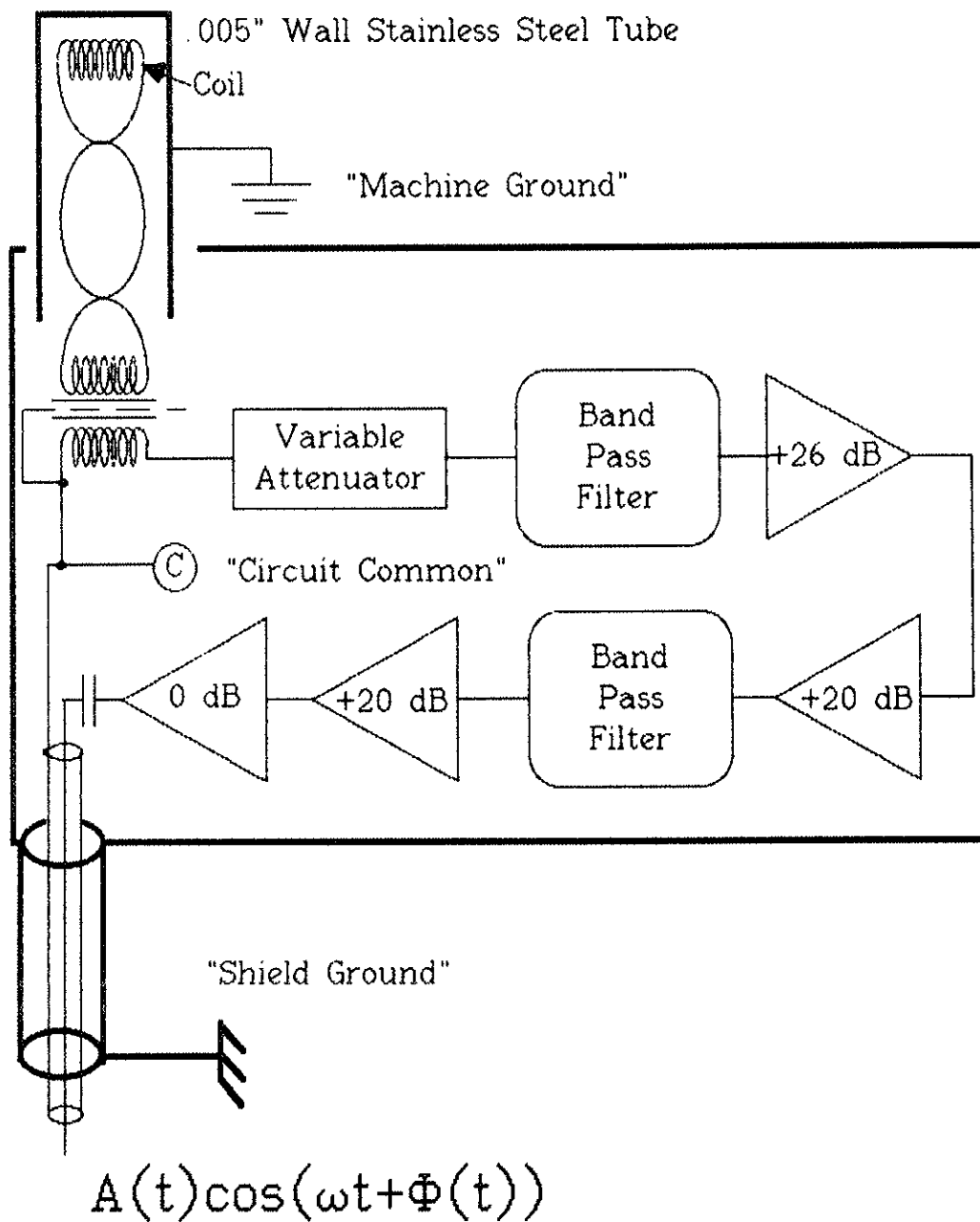
figure 4-12
Alfvéultramp schematic

signal/circuit common. This left the possibility of large ground loops, so care had to be taken since no isolator was used at the computer end. It was also important to have the connections from the coils to the amplifier inputs as short as possible and well shielded.

The broadband frequency response with filters having a center frequency of 2 MHz is shown in figure 4-13 a. The noise floor is quite good at more than 40 dB down, it is actually somewhat better than this plot indicates owing to harmonic content of the signal generator. The filters used are third-order Cauer-Eliptic[2] to get sharp corners. Figure 4-13 b is a plot of the passband. Response is quite flat, the glitch at 1.8 MHz arises from a change of scale on the
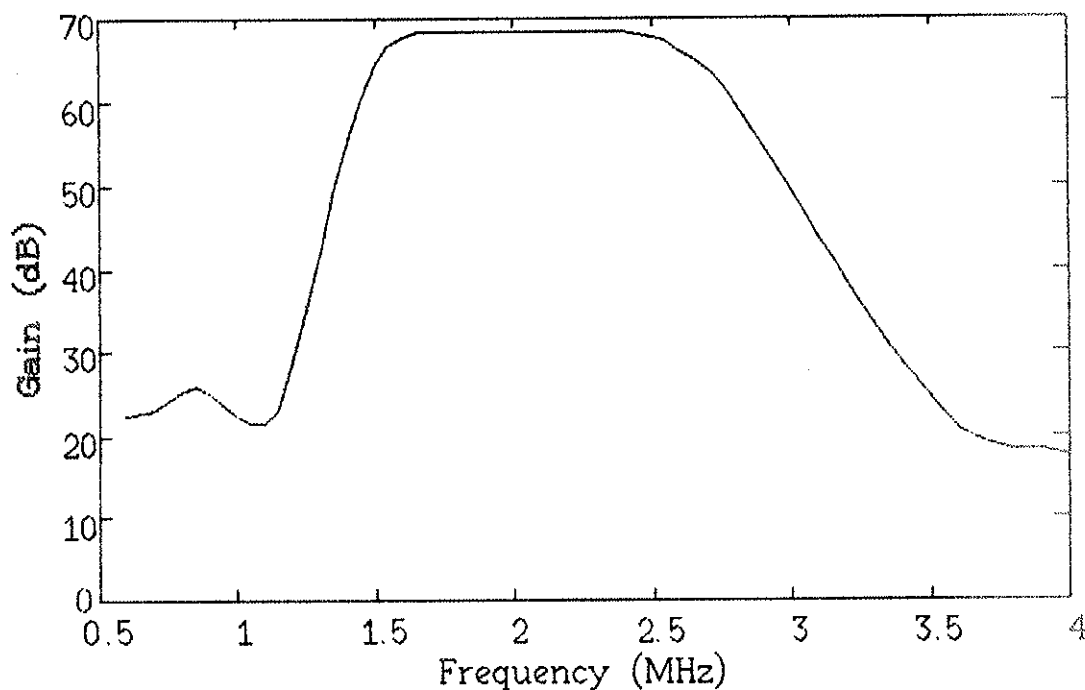
figure 4-13 a
Broadband frequency of the Alfvéultramp with filters installed
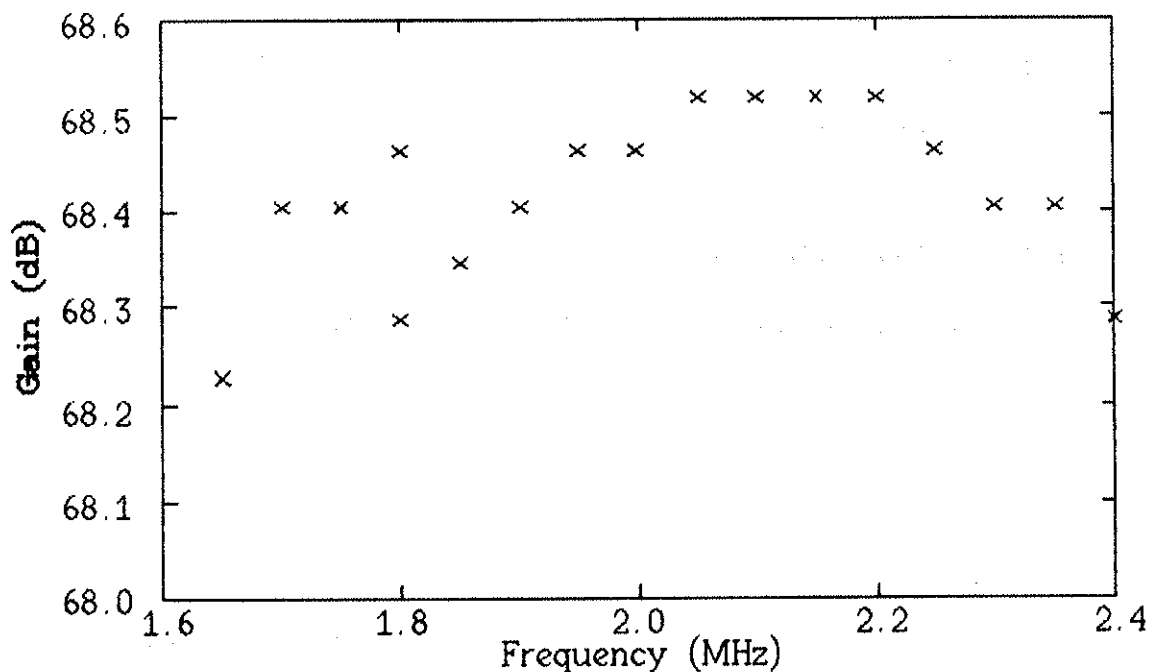
figure 4-13 b
Passband of Alfvéultramp with filters installed.

signal generator. These curves were obtained by driving the input of the amplifier directly rather than using a pickup coil.

The signal out of the amplifier is assumed to be of the form $A(t)\cos(\omega_c t + \Phi(t))$ where ω_c is the frequency of the master oscillator for the driving system, $A(t)$ and $\Phi(t)$ are the amplitude and phase modulation of the signal caused by the plasma.

A potential problem arises if the signals are phase modulated at frequencies nearing the bandwidth of the system since the sidebands for phase modulation contain all harmonics of the modulating frequency[3], $\omega_c \pm \Omega_m$, $\omega_c \pm 2\Omega_m, \ldots$ $\omega_c \pm n\Omega_m$ with amplitudes going as $J_n(m)$ where J_n is the Bessel function of order n and m is the modulation index. Thus, the signal can be distorted,

appearing as additional amplitude modulation. This was not a problem in practice since the driven signals measured, except for background noise, were quite narrowband.

4-C 3 Alfvéquadramatic

The Alfvéquadramatic is a circuit that takes an input signal from the master oscillator for the RF drive system and generates two reference signals of constant amplitude in quadrature with each other. The circuit is sketched in fig 4-14, and the timing diagram is sketched in figure 4-15.

The input signal can range from ~1.2 MHz to 3 MHz. This limit is determined primarily by the corner frequencies of the lowpass filters. The electronics should handle a very broad frequency range from 0.5 MHz < f <100 MHz since the chips are from the ECL logic family. The input signal level can range from ~0.02-0.5 V.

There are a few subtle points about this circuit. The frequency doubler requires reasonably clean sine waves in order to produce a significant amount of power in the second harmonic. This is the reason for the first lowpass filter. The second lowpass is to clean up the second harmonic signal so that the output of the second limiting amplifier will have a 50% duty cycle. This determines the accuracy to which the frequency-divided-square waves out of the flip-flops are in quadrature. The final lowpass filters are to give a sinusoidal output since using fast risetime square waves into the multiplier circuit caused problems with feedthrough of the reference
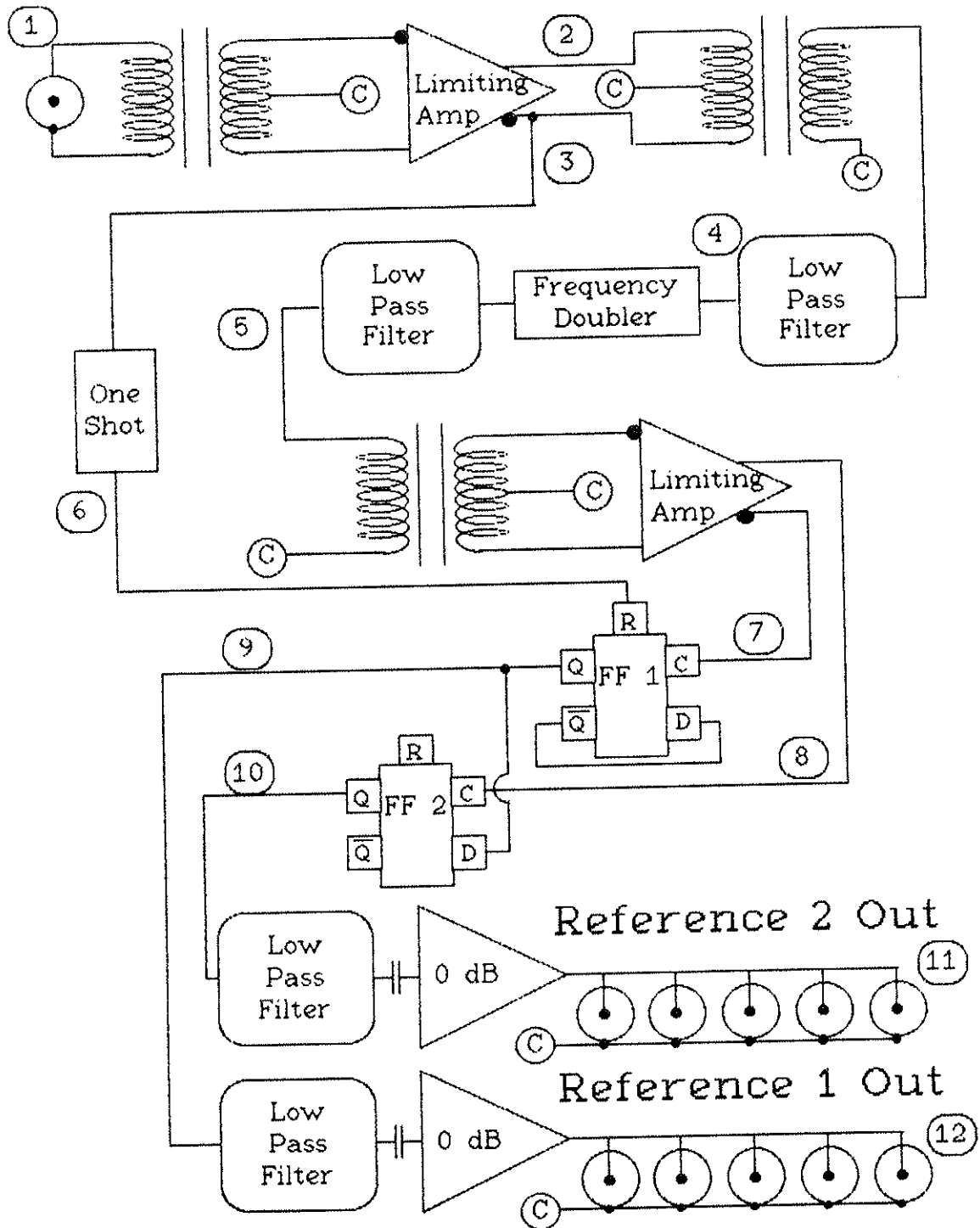
Alfvéquadramatic
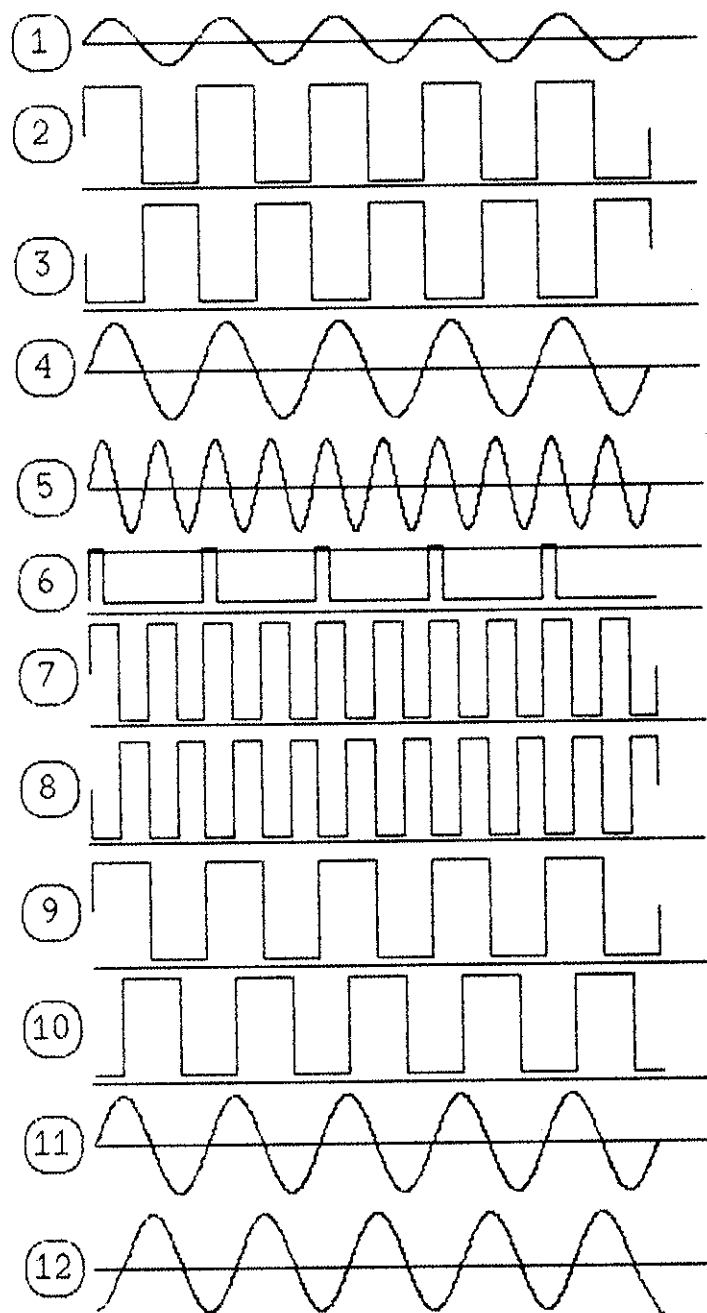

figure 4-14
Alfvéquadramatic schematic

figure 4-15
Timing Diagram for the Alfvéquadramatic

signal. The final stage driver is a LH0063 Damn Fast Buffer Amplifier. Since it is capable of driving 5-Ω loads at the signal levels used, up to 10, 50-Ω loads can be driven in parallel. Since one signal of each phase is needed for every two signals to be demodulated, the output is adequate for up to 20 channels of data. The signals out are 0.5 volt sine waves and are in quadrature to typically less than one degree error, which is approximately the accuracy limit of the oscilloscopes on which they are measured.

4-C 4 Alfmult

The Alfmult is the circuit which does the actual demodulating of the signals. Each board handles two input signals and generates four outputs. The circuit is sketched in figure 4-16 The input signal is linearly multiplied (analog) with the reference signals which are amplified and given a dc offset by the driver (the control channel on the multiplier needs signals from 0 to +3 V). The result is amplified, lowpassed and further amplified. If the reference and input signals are taken to be

$$\text{Ref 1} = 1 + \cos(\omega_0 t)$$

$$\text{Ref 2} = 1 + \sin(\omega_0 t)$$

$$\text{Signal} = A(t)\sin(\omega_0 t + \Phi(t))$$

then after multiplying and lowpassing there are two signals,

$$\text{Ref 1} * \text{Signal} = \tfrac{1}{2}A(t)\sin(\Phi(t))$$

$$\text{Ref 2} * \text{Signal} = \tfrac{1}{2}A(t)\cos(\Phi(t)).$$

These are then amplified and digitized. The phase measured in this way is a phase shift between the reference signal coming from the

Alfmult

Ref 1 In — Reference Driver

Sig 1 In — Power Splitter — Linear Multiplier (AD 539) — LH 0032 — Low Pass Filter — 8-14.5dB — 0 dB — (Ref 1)*(Sig 1) out

— LH 0032 — Low Pass Filter — 8-14.5dB — 0 dB — (Ref 1)*(Sig 2) out

Sig 2 In — Power Splitter — Linear Multiplier (AD 539) — LH 0032 — Low Pass Filter — 8-14.5dB — 0 dB — (Ref 2)*(Sig 1) out

— LH 0032 — Low Pass Filter — 8-14.5dB — 0 dB — (Ref 2)*(Sig 2) out
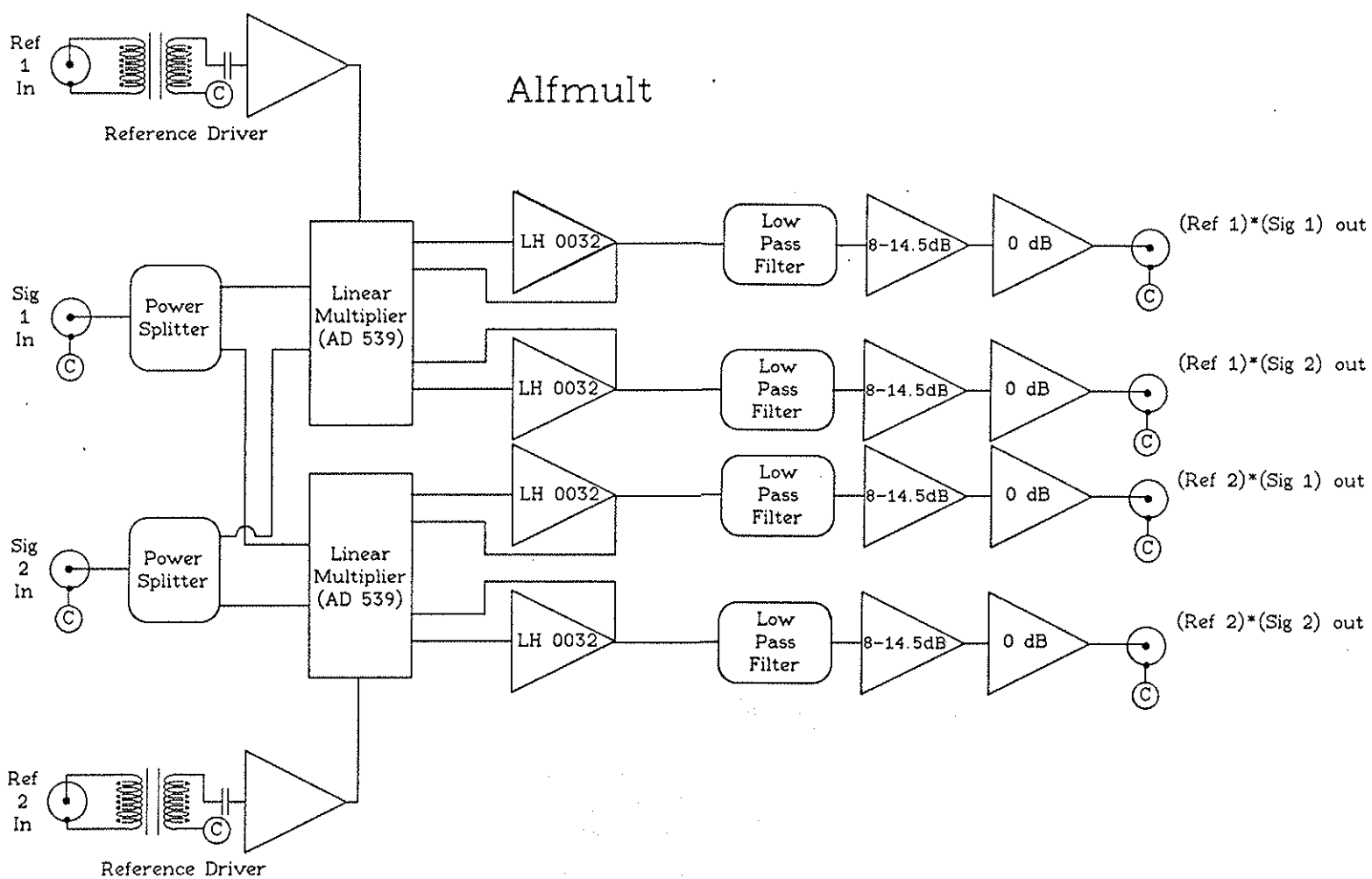
Ref 2 In — Reference Driver

figure 4-16
Alfmult schematic

master oscillator. This reference signal should have a constant phase relationship with the antenna current, and so the phase shift can be interpreted as the phase shift between the magnetic field measured at the position of the coil and the antenna current which drives it. This raw data can be difficult to interpret if the phase is changing rapidly or if there is a great deal of noise. It is, however, not a good idea to process the data to give amplitude and phase without looking at the raw signal since one channel may be saturating, while the other is in range. This is not always obvious when looking at the processed data. Another advantage of having the signals in this form is that they can be filtered digitally as is. If the signal were reduced to amplitude and phase before filtering, the filtered signal would be wrong. This lowpass after multiplying is equivalent to having a narrower passband originally.

The final stage lowpass is what sets the ultimate passband of the system in most frequency ranges. The ultimate gain is also given fine adjustments to equalize the calibration of the various channels. Also, the reference drivers contain a small phase adjustment so that each signal's phase is the same and in true quadrature to high accuracy. There is, however, a small adjustment for phase and gain on each of the Alfvéultramp boards.

4-C 5 Constant Current Calibrator

Once assembled, it was necessary to calibrate the entire system, probe, amplifiers and detectors, also, to check the reference

circuit. Since the multicoil probe was 7.5 cm long, a large region of constant field was needed. This was easily accomplished with a set of Helmholtz coils. A broad frequency range was to be used, and so a control circuit and amplifier was needed to drive the inductive load at a constant current as the frequency was swept. This circuit is sketched in figure 4-17. Even though the calibration curves and the current can be digitized and stored, holding the field constant as frequency is swept allows the aligning of the system to proceed much more quickly and minimizes the correction to the signals later, since they can all be easily adjusted to the same phase and gain.

The driver is a power MOSFET, and some feedback is used to "guess" what the frequency response should be. A Pearson current monitor is used to measure the current and provide a reference signal for the Alfvéquadramatic. This signal is then amplified (0.5 A is run through the coils and the current monitor puts out 0.1V/A) and rectified. The RC time constant of this section determines how fast the frequency can be swept and how low a frequency can be usefully controlled. This signal is then compared to a reference voltage and the difference amplified to generate an error signal. The chip used for the AGC is the same chip used in the Alfmult, a linear multiplier, and so the control signal must be kept in the range of 0-3V. This can cause some problems at the start of a sweep or if the sweep range is too large. The error signal amplifier tries to exceed this voltage range initially since there is no current and

Constant Current Calibrator

Single Turn Helmholtz Coils
Radius=10.5 cm.

Pearson Current Monitor

Power
Amp

+20 dB

V_{error}
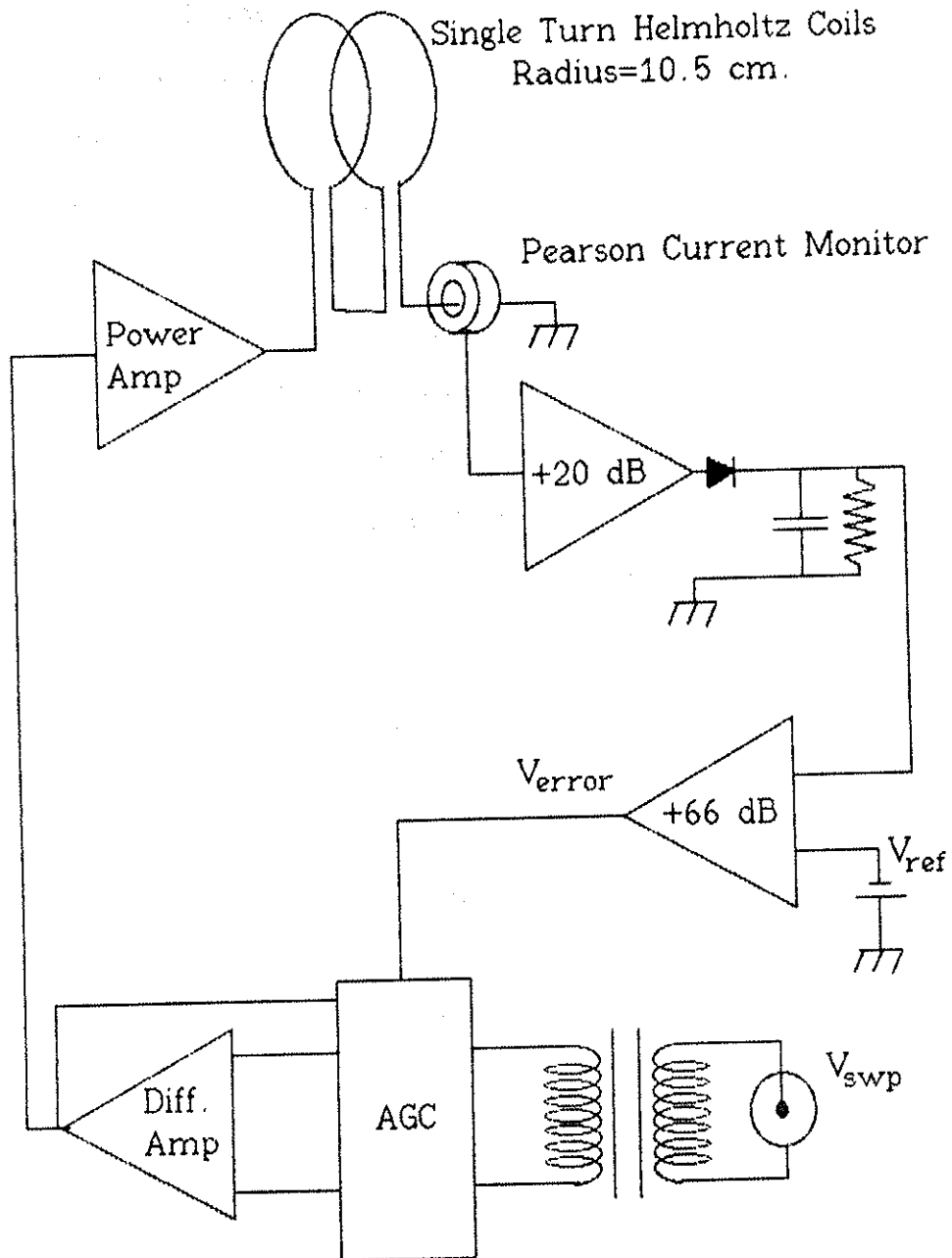
+66 dB

V_{ref}

Diff.
Amp

AGC

V_{swp}

figure 4-17
Constant Current Calibrator schematic

hence no rectified signal (or insufficient current if the sweep range is excessive), and must be limited by diodes. This puts the error amplifier into current saturation, and then it will lash when the current starts and it tries to come down. The feedback circuit in the driver helps by minimizing the dynamic range necessary in the AGC section. The sweep voltage is provided by a sweeping function generator such as a Tektronix FG-504. The field could be maintained constant to within 1% over a sweep from 0.5 to 4 MHz in 10 msec.

The field produced by the 21 cm diameter Helmholtz coils is 0.091 Gauss/amp. This was calculated and checked with a single turn B-dot coil of carefully measured area. The uniformity can be checked by moving a small coil about in the coils and is quite good. The coils are constructed of a single turn each of RG-8 coax with the braid split at the top of each coil, serving as a Faraday shield.

4-C 6 System Alignment and Calibration

The system can be assembled and then adjusted throughout and calibrated as a unit. The multicoil probe is connected to the Alfvéultramps and inserted into the vacuum envelope. This is then placed in the calibrating coils. At 2 MHz, the frequency at which most of the data was taken, the response of the coils in the stainless tube is fairly flat with frequency. The tube integrates the signal. The gain and phase of each of the Alfvéultramps is then adjusted so that the output signals are all the same. The Alfvéultramps are

then connected to the Alfmults. The current sample from the calibrator is then run through an adjustable delay line to the Alfvéquadramatic. The delay is adjusted to minimize either the sine or cosine outputs of all the signals. The phase of each board is then adjusted to null all of the channels. The delay is then increased by one quarter of a period, and the other channel on each of the boards is nulled. Finally, the gain of each channel is adjusted to equalize the calibrations. The final calibration of the system at maximum gain is greater than 100 volts/gauss.

4-C 7 Phase Detectors

To a very good approximation, the loading of an inductive antenna is directly proportional the difference of the phase angle between the current through and the voltage across the antenna, Θ, from 90°. From Ohm's law one has $\tan\Theta = \omega L/r$. Where L is the antenna inductance and r is the total loss. If $\tan\Theta$ is then expanded in a Taylor series about $\pi/2$ with $\Theta=\pi/2-\epsilon$ then, $\tan\Theta = \omega L/r \simeq 1/\epsilon$ to first order, thus $r \simeq \epsilon\omega L$. The error is less than 1% for $Q = \omega L/r$ as low as 6 and less than 5% for Q as low as 2.5.

The phase is measured by using a double balanced mixer, which functions as a multiplier, and running the two signals into the RF and LO ports. The IF signal then contains Fourier components at the sum and difference frequencies. The signal is lowpassed and since the signals are at the same frequency, the difference component is just the phase. To remove any amplitude

dependence, the signals are first run through limiting amplifiers. The circuit is sketched in figure 4-19. The limiting amplifiers consist of three stages of amplifier, each with a gain of +17 dB followed by a Schmidt trigger. The amplifiers used are ECL line receivers and so are designed to saturate. The separate channels are run through separate amplifiers on the same chip in each stage to minimize any change in delay with temperature.

The signal out of a mixer is zero (except for DC offset) at 90° phase difference and is linear in the phase so the loading is approximately proportional to the output of the phase detector.
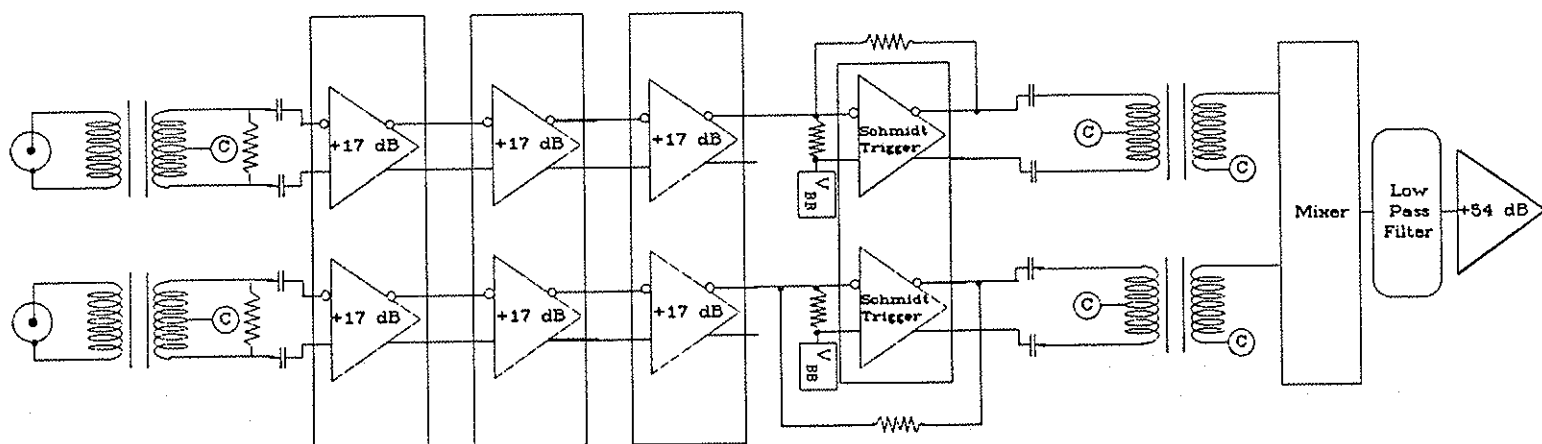
Phase Detector Schematic

figure 4-19
Phase Detector schematic

References

1.) F.D. Witherspoon, Ph.D. Thesis, University of Wisconsin (1984)

2.) A.B. Williams, Electronic Filter Design Handbook, (McGraw-Hill New York 1981) pg. 2-70

3.) I. Gonorovsky, Radio Circuits and Signals, (Mir Publishers, Moscow 1981) pg. 115

Chapter 5
Experimental Results and Discussion

The goal at the outset of this experiment was plasma heating with Alfvén waves. Experiments to determine the optimum antenna configuration were undertaken. Many antenna designs were tested. Magnetic probes were used to characterize the waves driven in the plasma, and to try and measure the energy deposition. As is often the case, the results were not entirely as was expected.

This chapter is a compilation of the data obtained over a several-year period on Tokapole II. It should be said at the outset that there has been no solid indication of successful bulk plasma heating; but much has been learned about antennas and their design, and the nature of waves in the Alfvén range of frequencies. The data are separated into two main topics; antenna coupling which is covered in section 5-A, and internal magnetic field measurements which are covered in section 5-B. Comparisons are made to theory when possible. The key results will be summarized in the next chapter, and suggestions for future work will be presented.

5-A Antenna Coupling

The word antenna is used quite loosely in the plasma community. In general, "antennas" are dominated by the far fields.

In this experiment, the vacuum wavelength exceeds the dimensions of the experimental device by two orders of magnitude. Also, all of the antennas have been "magnetic antennas", which is to say, they couple to the plasma by the magnetic field they generate. The situation here is more like that of a coupling loop in a dielectric loaded resonant cavity, the plasma being a fairly complicated dielectric medium.
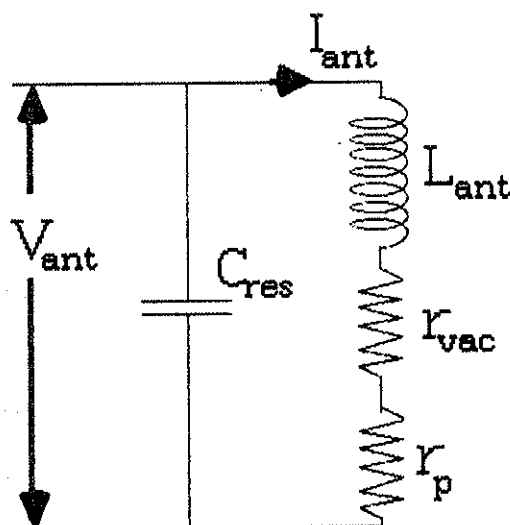

Figure 5-1
Circuit used to describe the antenna with plasma

"Coupling" is any effect on the antenna's impedance by the plasma. Figure 5-1 defines some of the terms which will be used throughout the chapter. L_{ant} is the inductance of the antenna. C_{res} is the external capacitor used to resonate the antenna to maximize the current through it. r_{vac} represents the losses in the antenna, feed, shield, or external circuitry. r_p is the additional loss in the circuit when there is plasma. V_{ant} is the voltage across the

antenna circuit. I_{ant} is the circulating current through the antenna element. Notice that L_{ant} includes any reactive component of the impedance added by the plasma. In practice, this was always quite small, and will not be discussed. The word "loading" will be used to describe the increase of resistance in the circuit from plasma. All data presented are r_p, the vacuum losses having been subtracted off. Unless otherwise indicated, all data were taken at an operating frequency of 2 MHz.

5–A 1 Alfant

Alfant (the antenna with the large toroidal extent) was the first antenna built specifically for this experiment and installed in the Tokapole. It was used before the phase detectors (described in chapter 4) were built. The loading data were obtained by measurement of oscilloscope traces of the voltage and current. It was operated mostly pulsed at high powers.

Figure 5–2 is a plot of r_p vs. angle of antenna currents with respect to the toroidal direction for the Alfant at full insertion (y=–13.5 cm) and full out (–18.5 cm). The loading peaks between –5° and –10° when the antenna is full out. (The angle of the field lines in the scrape off layer above the antenna was in the range of –4° to –7°.) With the antenna full in, the limited range of rotation precludes a conclusion, but it looks to be peaked in the same direction. This is what was initially expected since having the currents parallel to the equilibrium field directly drives the
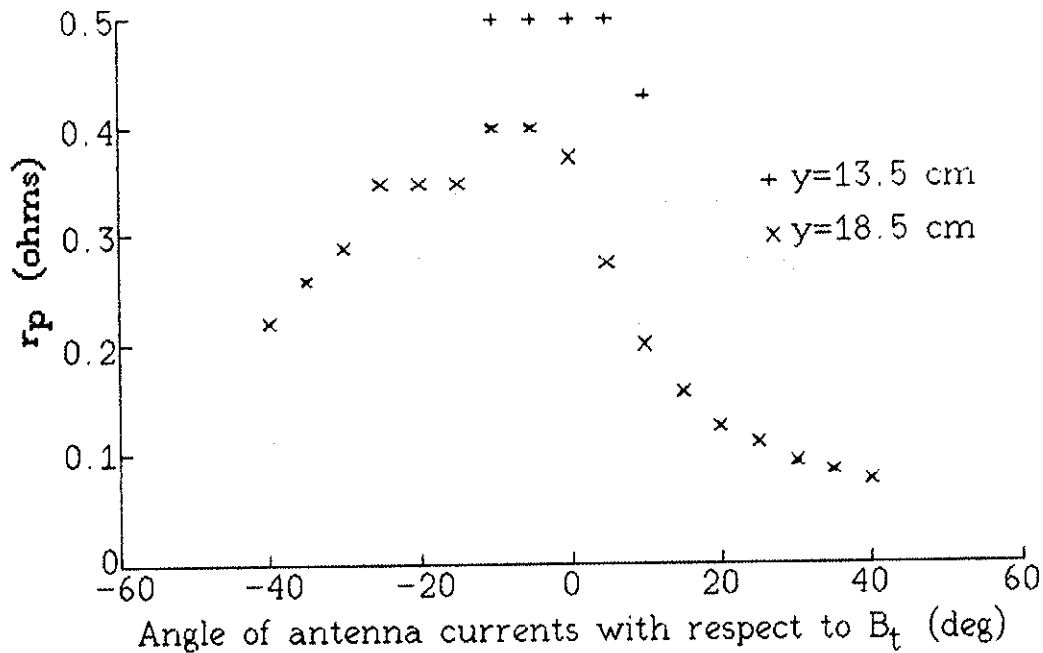
figure 5-2
Plasma loading of Alfant

perpendicular component of the wave magnetic field, which is the most strongly divergent. However, having the current in this direction also generates an electric field from the dA/dt of the magnetic field. This electric field is strongly attenuated by the plasma which is very conductive along the field lines. This shows up at the antenna as loading, but it is not loading from an Alfvén wave. The majority of the loading shown in this plot arises from this "parasitic" loading. (This loading is sometimes referred to as electrostatic loading since it comes from the damping of the electric field. This term is avoided here so as not to confuse this effect with loading seen from the electrostatic coupling of an unshielded antenna.)

There are many other observations to support this conclusion.

The loading measured was fairly insensitive to plasma parameters over an extremely broad range. This is quite unexpected since as the parameters are scanned, resonances would be expected to appear in the machine for different modes, and move radially out. This should have some effect on the loading.

There was no indication of heating of the core plasma (inferred mostly from SXR signals) in spite of a measured 100 kW of power leaving the antenna. (This was approximately equal to the ohmic power.) Most of this energy presumably was dissipated in the edge plasma directly over the antenna. This is difficult to actually verify in practice since the most convenient means to measure the temperature and density in the edge plasma of Tokapole ($T_e \simeq 10$–20 ev, $n_e \simeq 2 \times 10^{12} cm^{-3}$)[1] is by Langmuir probes, which are subject to errors in the presence of the large fields near the antenna.

The most convincing piece of evidence is shown in figure 5-3. This shows the resonant field measured 90° toroidally away from the antenna at three different orientations of the antenna. The peak signal does not change significantly while the loading varies by nearly a factor of 5. This clearly implies that the majority of the loading of the antenna when the currents are parallel to the equilibrium field is parasitic.

The profiles in figure 5-3 were obtained by moving a single coil radially inside a boron-nitride clad probe tube. The probes were not absolutely calibrated, but the fields were of the order of 0.1-0.2 gauss, comparable to the background noise of the plasma. Also, the
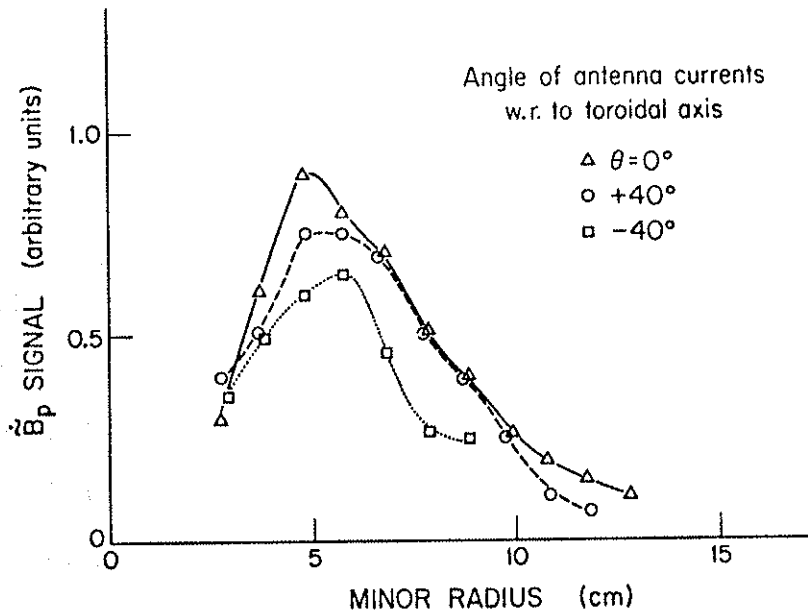
figure 5-3
Poloidal wave magnetic field measured 90° toroidally from the Alfant

amplitudes were determined by measuring the envelope of the signal from oscilloscope traces, the background noise could not be filtered out. This fact and shot to shot variability will combine to make the apparent resonance width broader than those to be presented later which were obtained with the synchronous detection system and the multi-coil probe described in chapter 4. The antenna was operated pulsed; antenna current was $\simeq$ 300 A zero to peak.

5-A 2 Roto-Alfant

The Roto-Alfants were constructed after the disappointing results with the Alfants. The major design changes were the full rotation range even when fully inserted to the extent of the divertor

rings and a removable Faraday shield. The intention was to measure loading as a function of angle of the antenna currents with respect to the toroidal direction. In particular, attempts were made to launch the fast wave, which is coupled to the shear Alfvén wave, with the antenna currents perpendicular to the equilibrium field thus avoiding the large parasitic loading. Any resonant loading would then be much more noticeable. Since the Alfvén wave is resonant, the coupling between the waves should not need to be very strong in order to get significant accumulation of energy at the resonant surface.

Figure 5-4 is a plot of loading vs. angle of antenna currents with respect to the toroidal direction for the Roto-Alfant. This scan

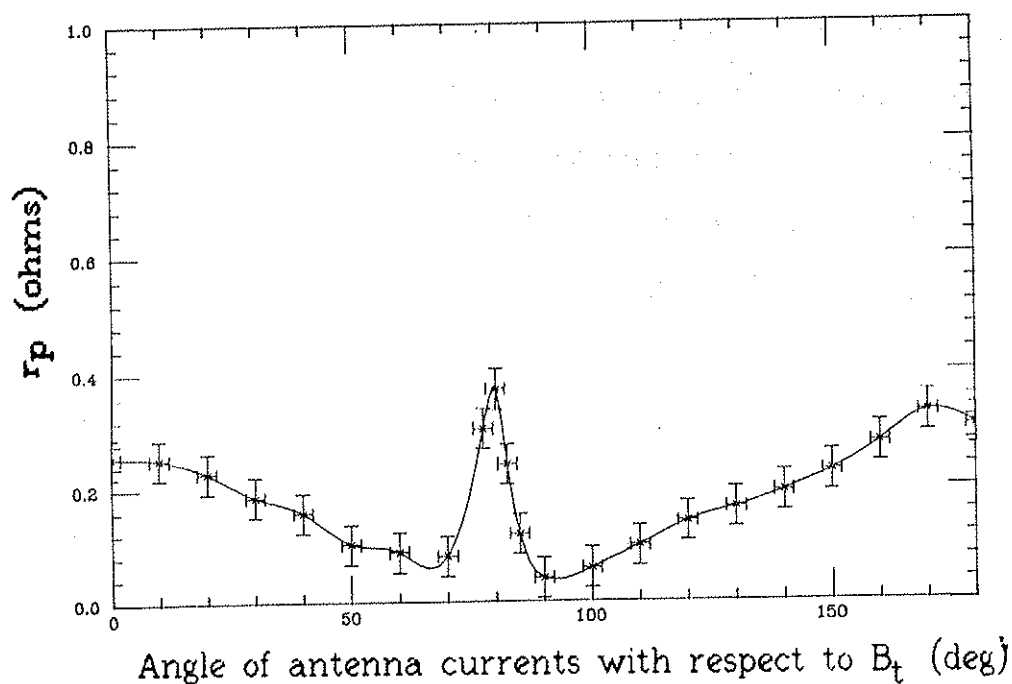Angle of antenna currents with respect to B_t (deg)

figure 5-4
Loading vs angle with respect to the
toroidal direction for the Roto-Alfant

was made at low power (40 W) with the RF on throughout the shot. The loading in the range common to the Alfant is quite similar, and the same explanation applies to it. The other distinct feature in this plot is the spike near 80 degrees. This anomaly was very strange in nature, and is not understood. It appeared on both antennas, but was only seen on the upper antenna near 80° when the toroidal field was "forward", and on the lower antenna near 280° when the toroidal field was "reversed". It was very reproducible day-to-day. There was no correlation with increased probe signal. It went away when end limiters were placed on the antennas. Pictures taken of the antenna as the machine was pulsed showed what appeared to be arcing across the Faraday shield strips, but the traces of loading and antenna voltage and current did not look like other traces when arcing was clearly seen in external circuitry at other times. Also, arcing only over such a narrow range of angles and the dependence on the direction of B_t is not easily explained.

There was still no indication that any significant fraction of the loading seen on these antennas was due to an Alfvén wave. The loading when the antenna currents were poloidal was small and quite insensitive to plasma parameters, never showing clear indications of "resonant" loading. It was also quite independent of the relative phasing of the two antennas (figure 5-5). The figure shows the loading for the antennas driven out of phase (M=0), in phase (M=1), and the lower antenna alone (M=all).
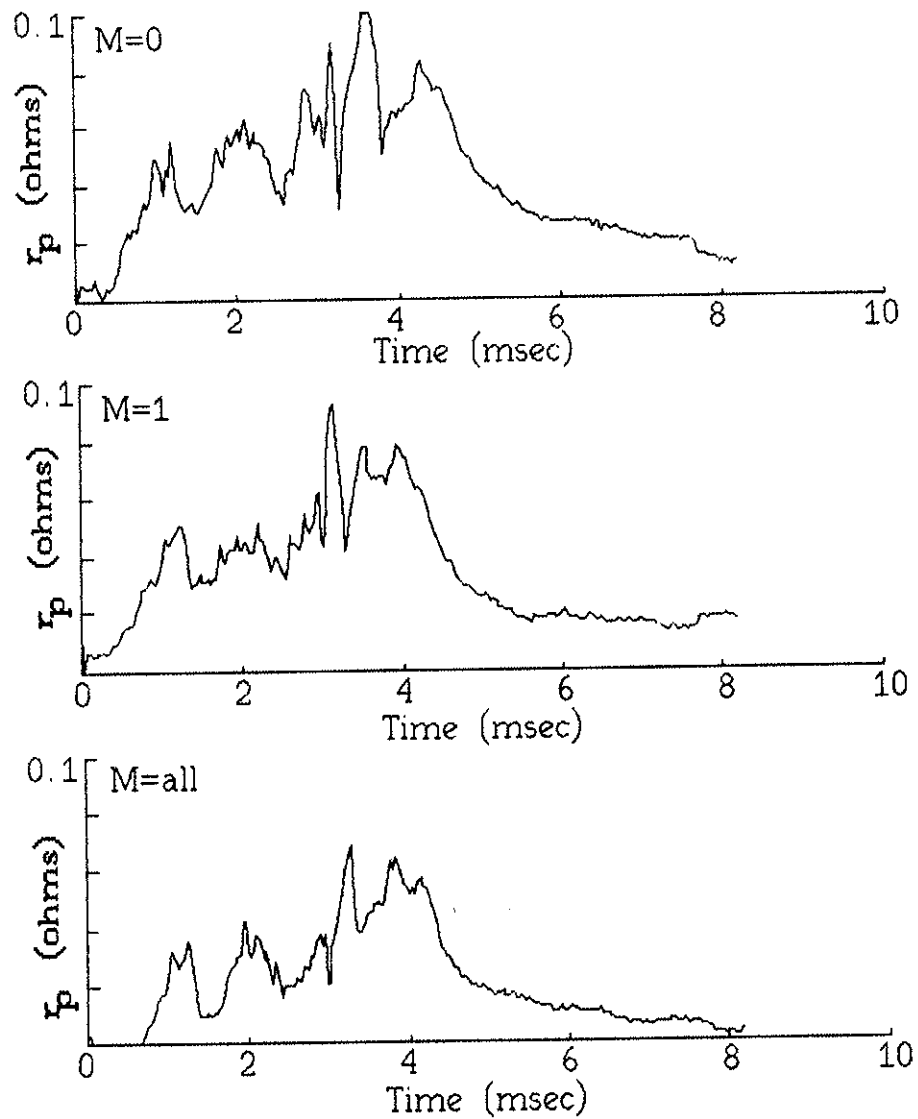
figure 5-5

Loading of the lower Roto-Alfant at three different relative phasings

The upper Roto-Alfant was also operated without a Faraday shield, but with end limiters and the particle shield. (figure 5-6). The small quantitative difference in the loading can be explained by the fact that the data with and without the Faraday shield were taken several months apart and global plasma parameters and

machine conditions were somewhat different. The general similarity of the two cases indicates that a Faraday shield is not essential as long as the plasma is not in direct contact with the antenna element.
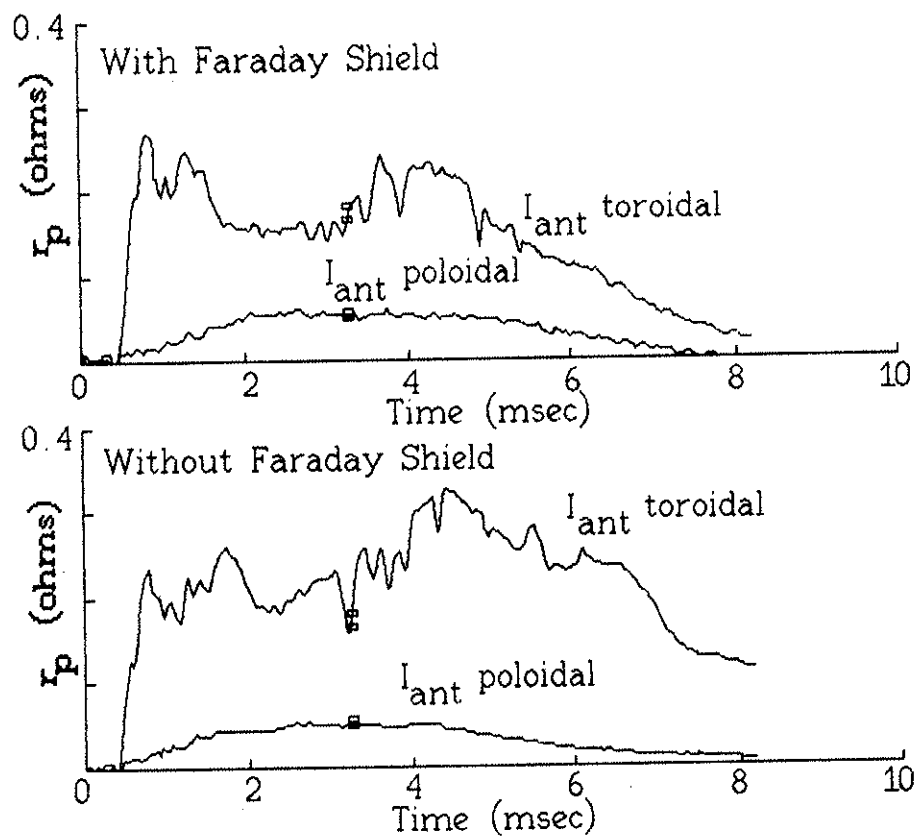

figure 5-6
Loading of the upper Roto-Alfant with
and without a Faraday shield

5-A 3 Large Single Turn Loop Antennas

The Large Single Turn Loop Antenna was operated bare in the plasma. The loading was very large and quite insensitive to most everything including angle of the antenna current with respect to
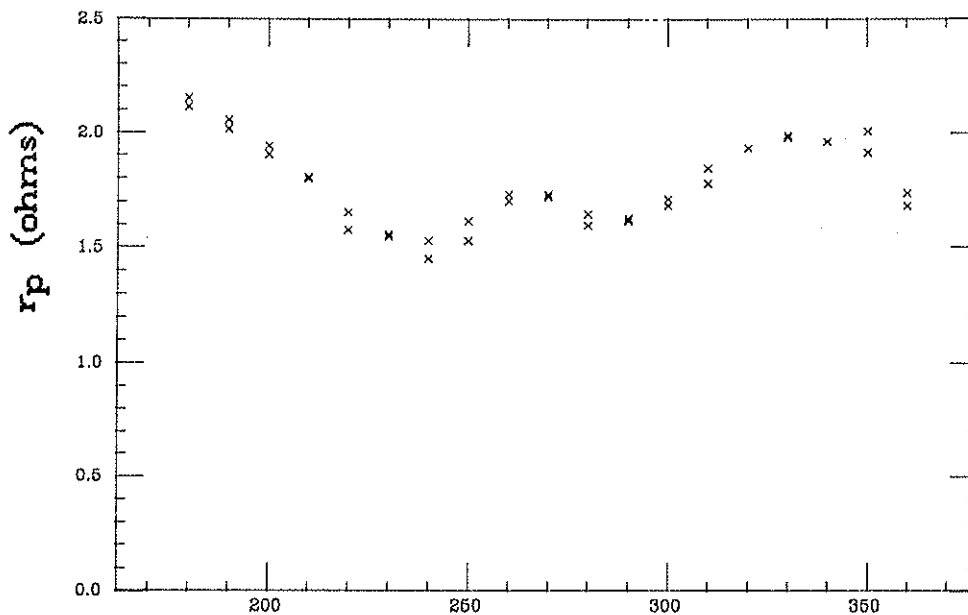
figure 5-7
Loading vs angle with respect to the toroidal
direction of a bare Large Single Turn Loop

the toroidal direction (figure 5-7). This was not very surprising. The antenna was only operated in this configuration for the sake of completeness. Bare antennas have been operated successfully elsewhere[2], but in the sharp shadow of a limiter. On Tokapole there is a significant amount of plasma in the scrape off region even with the limiter plates inserted. This plasma is in contact with the antenna element and appears as a resistive load across it. Currents could readily be measured flowing from the antenna element through the scrape-off plasma to ground. This loading was entirely spurious.

The Large Single Turn Loop was also operated with a Faraday shield and a partial particle shield. The loading of this antenna was

small at all angles, but was qualitatively like that of the two previously discussed antennas, (without the anomalous spike near 90°) and is shown in figure 5-8. (Notice that full scale is 50 mΩ.)
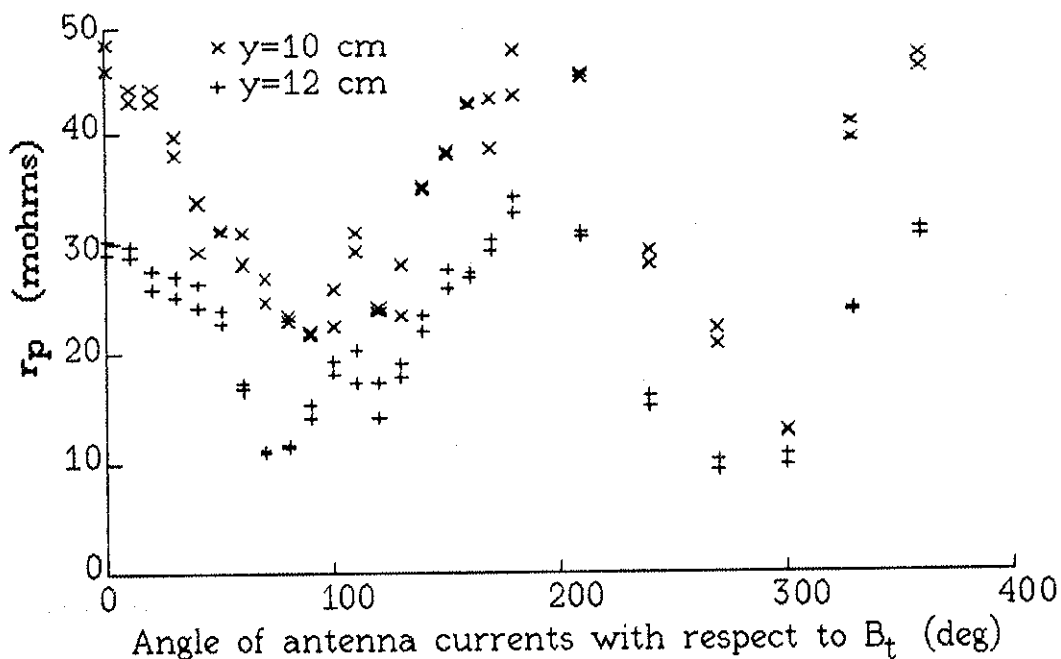

figure 5-8
Loading vs angle with respect to the toroidal
direction of the Large Single Turn Loop with
Faraday shield and partial particle shield

The loading of the Large Single Turn Loop with Faraday shield and full particle shield was very similar but smaller still. It is plotted vs. angle in figure 5-9. In both cases, the loading when the antenna current is parallel to the equilibrium field is believed to be parasitic like that described in connection with the Alfant.

The major design change in these antennas from the Alfant and Roto-Alfant was the significant increase in the size of the current carrying loop with the intention of giving larger fields per amp-turn in the antenna at some distance above it. Indeed these
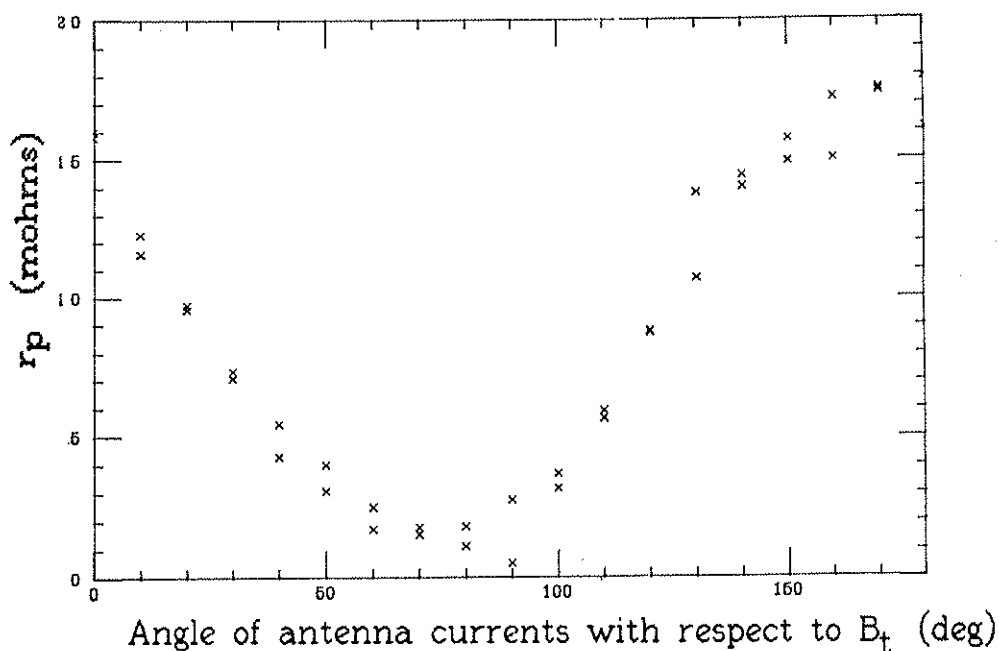
figure 5-9
Loading vs angle with respect to the toroidal
direction of the Large Single Turn Loop with
Faraday shield and full particle shield

two configurations gave the largest measured field in the plasma per amp-turn of antenna current with the antenna currents poloidal, while having the lowest loading. Even then, there still was little indication that what loading there was could be attributed to the presence of an Alfvén resonance in the plasma.

Figure 5-10 shows loading and the amplitude of the wave magnetic field measured directly above the antenna. The probe signal changes significantly while the loading remains relatively unaffected. The loading goes negative in this plot. This is merely an indication of the limitations of this measurement technique. At these small levels it is subject to significant errors from noise pickup of the antenna, and a 60 Hz variation arising from frequency
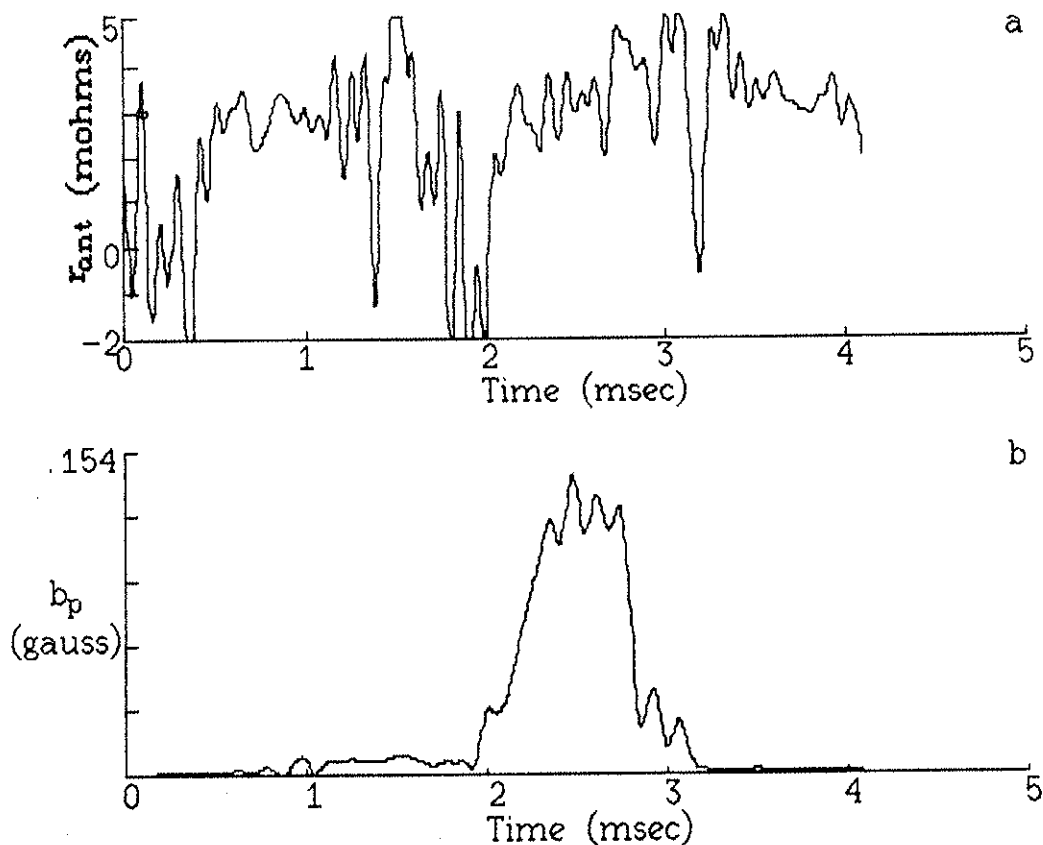
figure 5-10
Loading and wave field amplitude vs. time

modulation of the amplifier had to be subtracted off.

The current through the antenna for this case was 33 amps zero-to-peak which gives a power dissipation of 1.6 watts taking $3\,m\Omega$ for an average value in the time range which has significant probe signal. The loading is somewhat greater when a full particle shield is not used, but there is no increase in probe signal. In a later section this value will be compared to an estimate of the total power dissipated in the plasma.

5-B Internal Magnetic Field Measurements

The shear Alfvén wave in a tokamak should be readily identifiable by the spatial structure and temporal behavior of the wave magnetic fields. The component perpendicular to the equilibrium field and minor radius should show a spatial resonance localized to a magnetic surface, and the component parallel to it should be smaller and relatively flat across the resonance zone. The location of this resonance should have some dependence on the magnitude of the equilibrium field and the mass density profile. In this section, data are presented which clearly indicate that there is a driven Alfvén wave present in the device. Unless otherwise indicated, the following conditions apply. Most of the data presented in this section were taken at 2 MHz with the Large Single Turn Loop with Faraday shield and either a full or partial particle shield, since, as stated above, these two configurations gave the largest values of measured field in the plasma per amp-turn of antenna current. (The probe signal showed no noticeable difference between these two configurations, and they will not be distinguished here.) In section 5-B 3 a direct comparison between results from the Large Single Turn Loop antenna and the Roto-Alfant is made. All of the magnetic probe data have been digitally filtered to an effective passband of ±5 kHz about the driving frequency. (This will be justified in a later section.) Signals have been smoothed freely to allow clear presentation of the points to be made. All attempts have been made to keep the scale of the plots the same when direct

comparisons are to be made.

5-B 1 Spatial Structure of the Wave Fields

There are three topics which will be discussed separately; radial structure, poloidal and toroidal structure, and polarization. Comparison of these results with theoretical predictions will be given in an overall view in section 5-B 2.

5-B 1 a Radial Structure

The time evolution of the radial structure of the poloidal wave magnetic field measured by an 8-coil probe inserted to x=4cm at Side 240° (directly above the antenna) is shown in figure 5-11.

This plot was obtained by averaging 5 shots with the probe fully inserted in the vacuum envelope and 5 shots with the probe withdrawn 0.5 cm to give 16 radial points. A radial peak clearly evolves in time. The peak is at x=6 cm which is equivalent to a minor radius of approximately 4 cm when the usual 2 cm outward shift of the Tokapole discharges is factored in. (The bump at 9-9.5 cm is an instrumentation problem.) The radial profile of the field near the peak amplitude of this "averaged" shot is plotted in figure 5-12.

The half width to half maximum (measured going out radially) is 0.9 cm, although it appears to drop off more slowly going in radially. This could not be further investigated as inserting the probe any further in degraded discharges to the point that a resonance was not clearly seen. The shot-to-shot reproducibility was quite good, and so the uncertainty in this width should be less
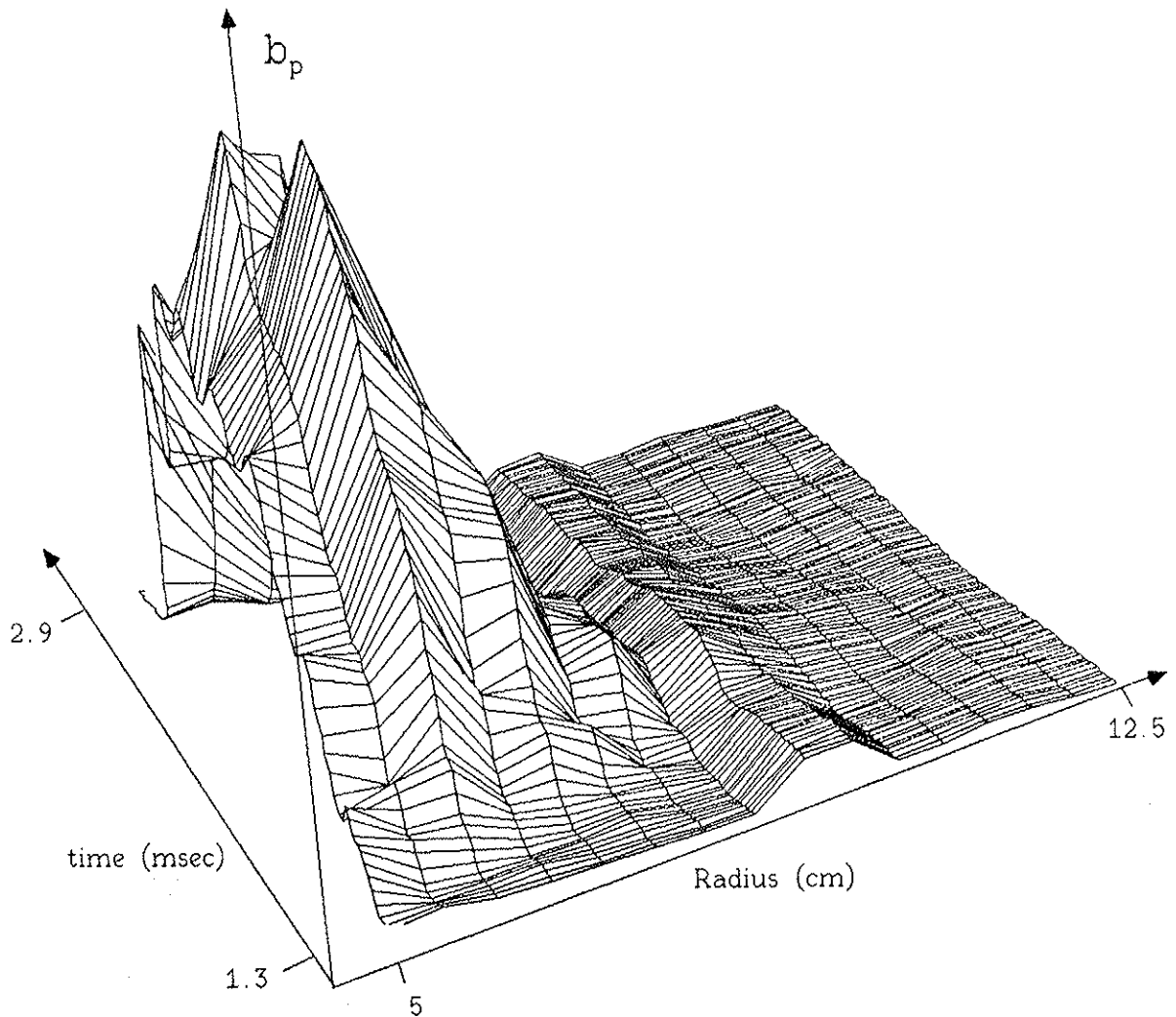
figure 5-11
Surface plot of the poloidal wave magnetic field

than the coil width of 0.5 cm. This number was reasonably consistent from day to day as well. The absolute calibration of the coils should be good to within 5%, and the relative calibration of the coils over this limited range in frequency should be within 1-2%, and so this makes no significant contribution to the uncertainty.
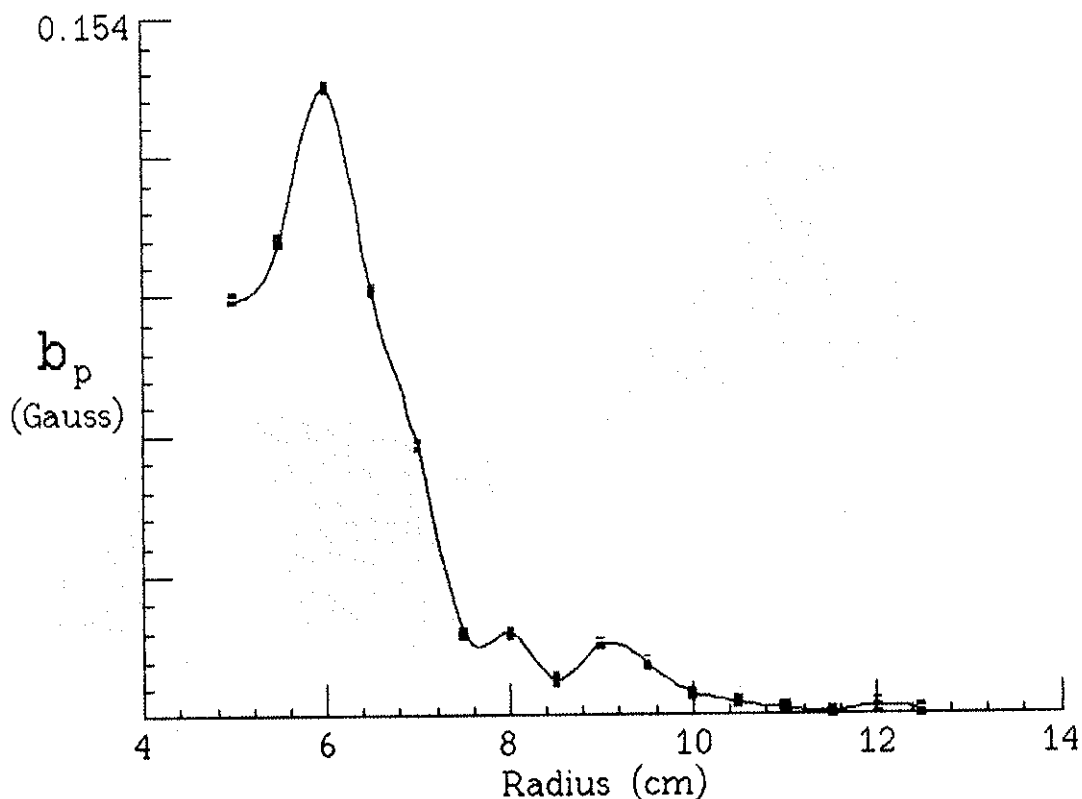
figure 5-12
Radial profile of the poloidal wave magnetic field.

The radial profile of the phase of the poloidal wave magnetic field with respect to the master oscillator is shown in figure 5-13. The slope of the phase indicates an inward radial propagation.

The phase plotted in fig 5-13 is the temporal phase shift of the measured wave magnetic field at the location of the coil with respect to the reference signal generated from the master oscillator for the rf system. This signal has only a constant (in time) phase difference from the current driven in the antenna, thus, this phase can be interpreted as the phase difference between the driving current in the antenna and the wave magnetic field
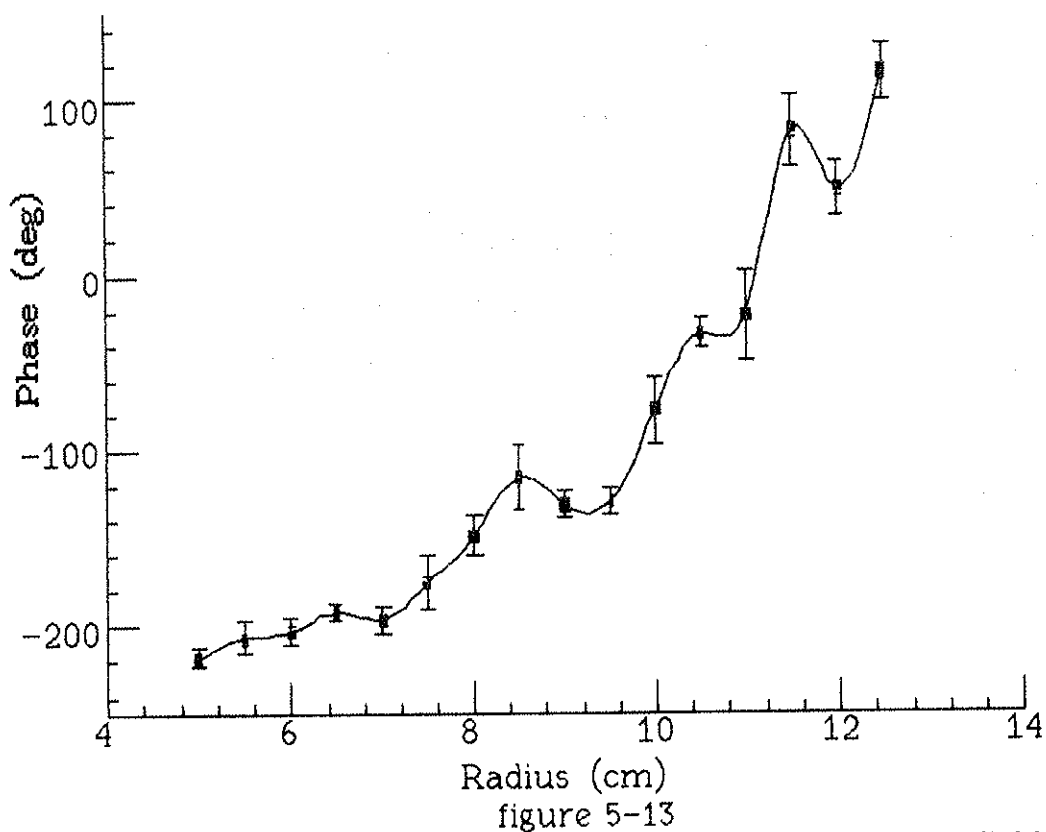
figure 5-13

Profile of the phase of the poloidal wave magnetic field measured by the pickup coil. (The difference in time between the zero crossings of the two signals, times the carrier frequency, ω_0.) In practice, this phase difference can only be measured over a range of $\pm180°$. The data plotted here have been adjusted to account for the jump from $-180°$ to $+180°$ that occurs at r=7.5 to 8 cm. The error bars are the standard deviation measured for the five shots that were averaged for this plot. The advance of this phase with increasing radius indicates a wave propagating radially in from the outer regions of the plasma. This general trend (phase increasing with radius) is constant in time. The exact shape of the plot would vary in time, but the sign of the

slope is the same. The flattening of the phase variation in the vicinity of the resonance is due to the fact that most of the signal measured is not this propagating wave but the shear Alfvén resonance which does not propagate radially. This behavior is consistent with a fast wave propagating radially in to the resonant surface and being mode converted to the shear Alfvén wave.

Figure 5-14 has surface plots of the radial profile at three different values of the toroidal field. The location of the peak seems to move predominantly in as the field is lowered. The variation is not simple and is further complicated by the fact that the profile of mass density is not known to be constant for the three discharges. There were some noticeable differences in the global plasma parameters. (At the time these data were taken, the interferometer was not functioning reliably so it would be difficult to draw any conclusions as to the relative densities.) From the time evolution in a single discharge, one can see the radial position of the peak move about significantly. Since these profiles were obtained on single shots, some of the apparent motion of the peak may be due to noise, however, the signal-to-noise ratio is quite good after filtering of the raw signals, and so a significant fraction of the motion is real.

Figure 5-15 shows the time evolution of the plasma current, amplitude of the poloidal wave magnetic field at a radius of 6 cm, the OIII radiation, NIII radiation, CuI radiation, and a soft X-ray detector which views a chord just below the midplane. Also shown is an expanded time scale plot of the OIII radiation and the
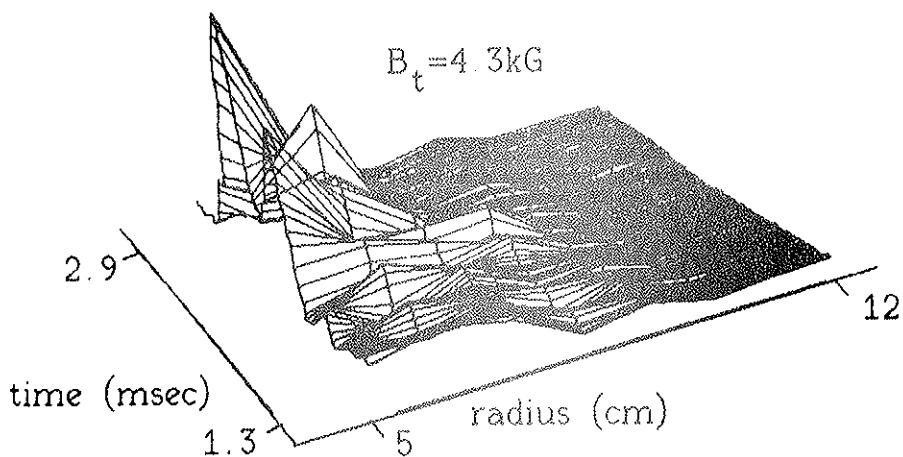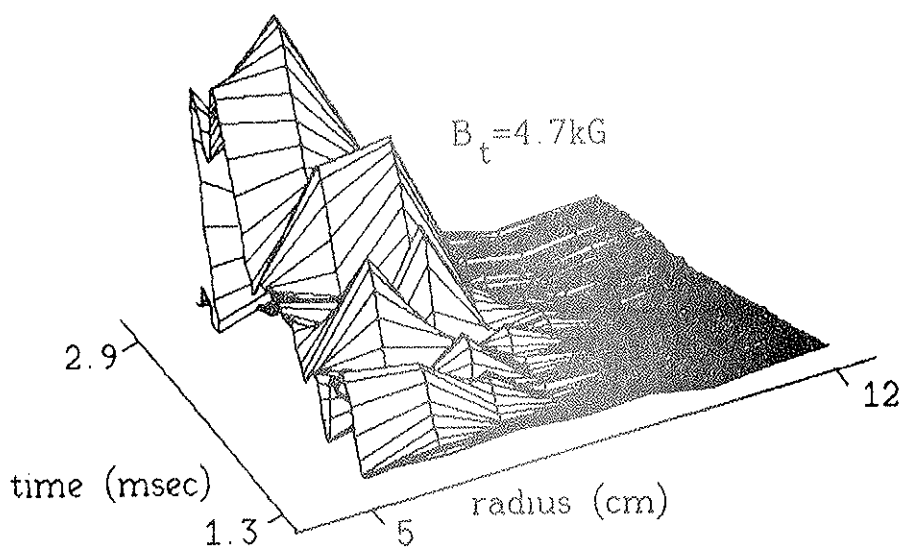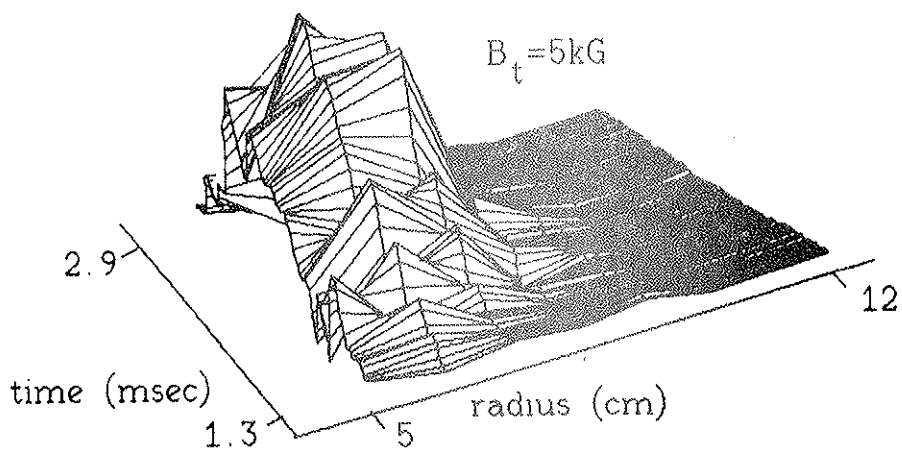
figure 5-14
Time evolution of the radial profile of the wave
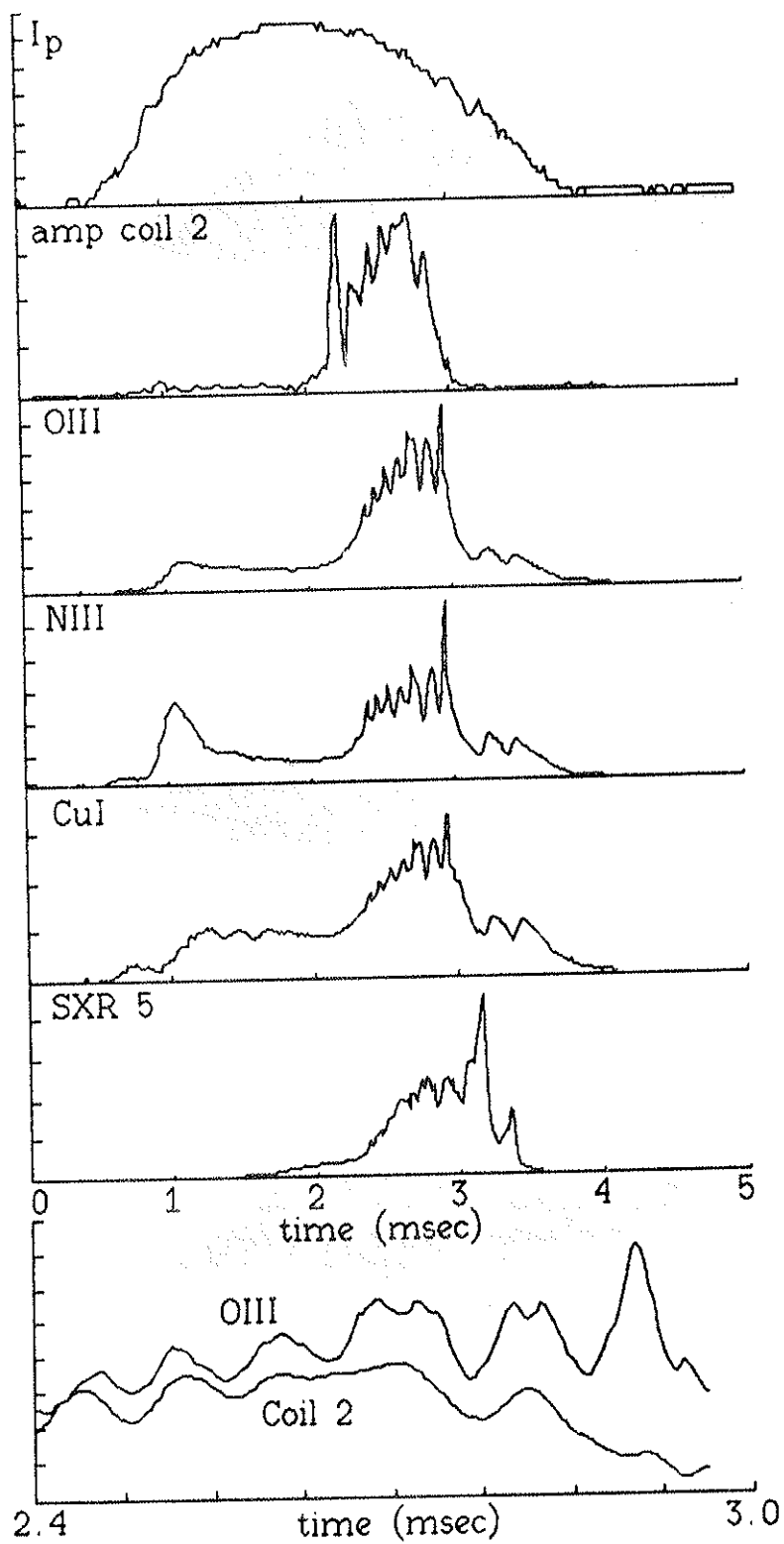magnetic field for three different values of B_t

figure 5-15
Time evolution of a typical discharge

amplitude of coil 2. The rise of the probe signal correlates strongly with the onset of significant soft X-ray activity and impurity radiation. Both of these signals depend on the density of impurities and T_e. The impurity radiation was not routinely monitored to this time resolution, but the soft X-ray signals were, and this strong correlation was always observed. The correlation with the soft X-ray signal is only in overall shape and time dependence, not in detail. The expanded plot shows that the magnetic field and OIII radiation are strongly correlated even in detail. The size of the impurity signals indicates a significant influx of impurities. The correlation of the increase in the impurities with the rise in the probe signal indicates that the resonance is affected by the variation in the mass density, which would be changed by the influx of impurities.

5-B 1 b Poloidal and Toroidal Structure

At the outset of this experiment, it was expected that eigenmodes would be established in the plasma, their mode numbers being determined by the relative phasing of the antennas. There have been only rare occasions during the course of this experiment when a well defined mode structure (a signal distributed over a significant extent in the machine with a distinct m and n) seemed to exist. Witherspoon[3] reported such a case using the internal divertor rings as an antenna, but it could not be reproduced from day to day. As shown in figure 5-3 resonances could be observed at

a toroidal distance of 90° from the Alfant, but only at high power. These resonances were also very elusive.

To attempt to determine the poloidal and toroidal structure of the wave fields, single coils were used in locations distributed around the machine while the 8-coil probe was left at SIDE 240° (directly above the Large Single Turn Loop antenna which was located at BOTTOM 240° for all of these experiments) as a monitor. After extensive conditioning, discharges could be obtained which showed a resonance above the antenna with at least one other Boron-Nitride-clad-probe tube inserted to x=4 cm and several others in as far as x=6 cm. During one extended run period, 10 probe tubes were inserted (SIDE 60°, 90°, 180°, and 330°; TOP 60°, 90°, 150°, 270°, and 300°; BOTTOM 60°) and conditioned such that any one could be put in at the same time as the monitor probe at SIDE 240°. Single coils were used in most of these, and the 8-coil probe was also used in all of the side ports with a single coil left in at SIDE 240° as monitor. With the exception of TOP 270°, no clear, reproducible evidence of a driven signal was found at any of the other locations. There were occasional shots where some signal ,just above the noise level, could be seen on probes located 30° or 60° away from the antenna toroidally, however, there were also occasional shots when the RF was switched off that such signals could be seen. (This will be discussed further in section 5-B 4.) Even then, the probe at TOP 270° had to be swiveled towards the antenna for the signal to be clear above the noise.

The probe at SIDE 240° could be swiveled. Figure 5-16 shows the poloidal magnetic field amplitude with the probe swiveled toward greater toroidal azimuth and inserted such that coil 1 is at x≈6 (where the field peaks above the antenna) and 9.2° away toroidally from the antenna. Two shots are shown, one with and one without RF switched on. The signal with the RF switched on rises above the vacuum signal but not significantly more than the noise level when the RF is not on. The result is similar with the probe swiveled
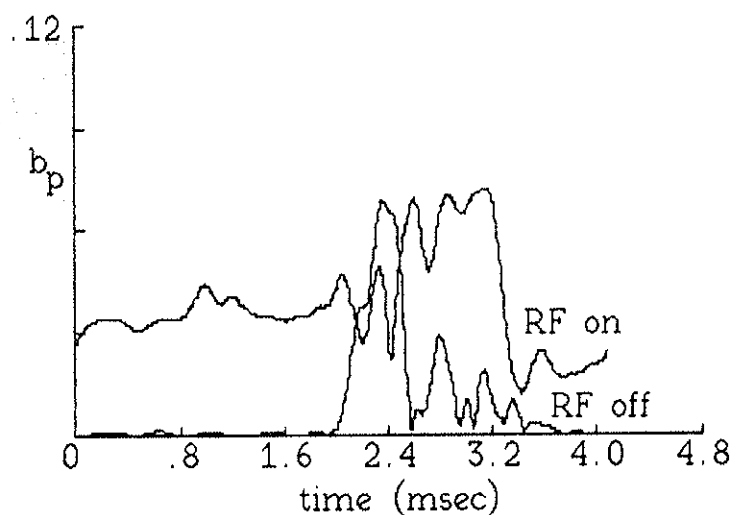
figure 5-16
Poloidal wave magnetic field at x=6cm and
9.2° away toroidally from the antenna

toward smaller toroidal azimuth. The probe is located approximately 9 cm along a toroidal arc from the position above the antenna where a significant enhancement is seen. The extent of the signal in the toroidal direction is quite short.

Figure 5-17 shows the amplitudes of coils 1(figure a), 2(figure b), 3(figure c), 4(figure d) vs. time with the 8-coil probe swiveled
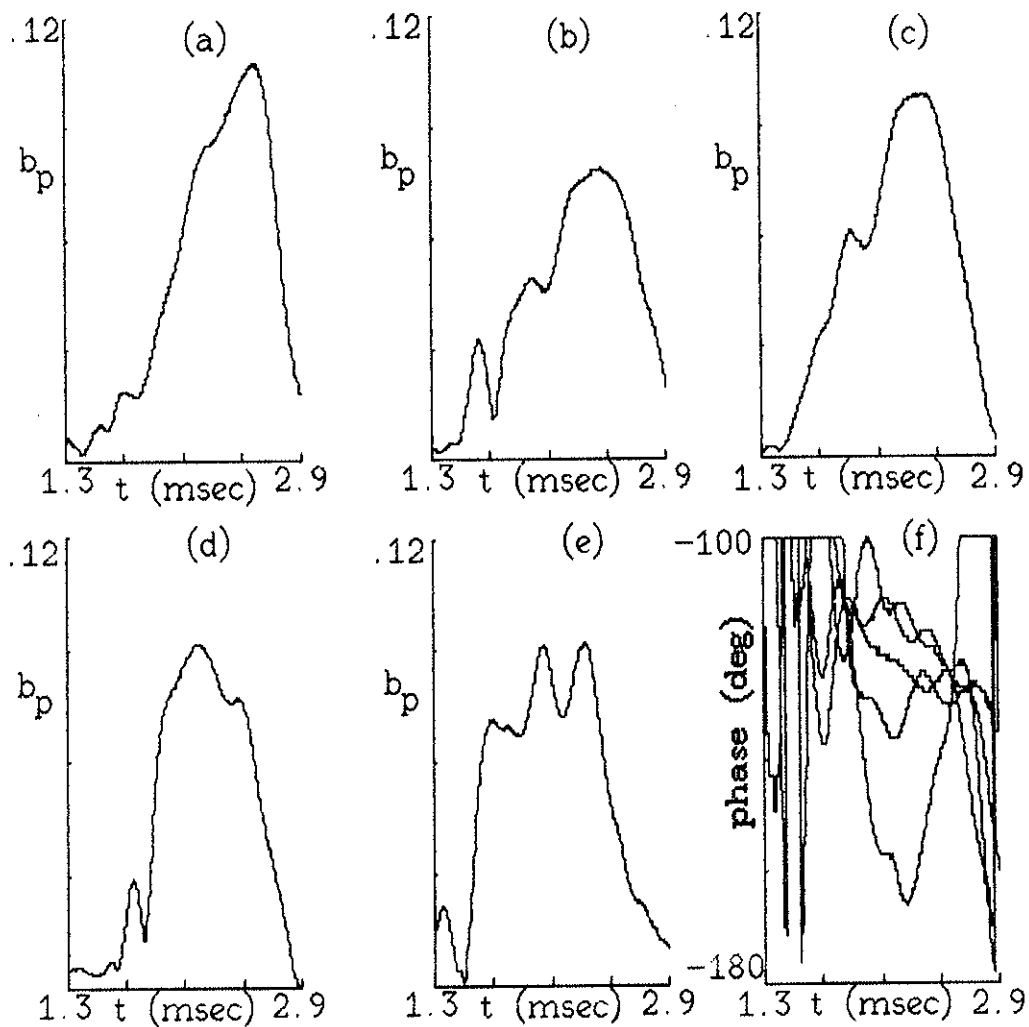
figure 5-17
Amplitude and phases for a poloidal scan
(see text for identification of the plots)

down poloidally 15° and inserted in radially such that at 0° swivel it was at x=2.5 cm, coil 1 (figure e) with the probe swiveled back to 0° and pulled out to x=6 cm, and the phases for all five cases(figure f). (The coils are located in the following positions in the x-y coordinate system centered at the geometric axis of the machine: figure a; (4.2,-5.2), figure b; (5.1,-4.9), figure c; (6.1,-4.7), figure

d; (7.1,-4.4), figure e; (6,0).)

With the probe swiveled down poloidally, it is nearly tangent to a magnetic surface (assuming the usual 2 cm outward shift). This explains why coils 1 and 3 give larger signals than does coil 2. The magnetic surfaces this far out radially are starting to be more square with rounded corners. The probe cuts across one of these corners putting coils 1, 3, and 4 nearer to the resonant magnetic surface than coil 2. The results are similar, but signals are smaller with the probe swiveled up poloidally. This, along with figure (e) where the coil is located near the same magnetic surface show that the signal is distributed on a a magnetic surface in a poloidal cross section.

The plot of the phases is somewhat crowded, but one point can be made from it. In the region where they are fairly well separated (which corresponds to the time of maximum amplitude), the traces are from top to bottom coils 1, 2, 3, 4, and 1 without swiveling. The phase varies fairly smoothly over a range of about 50°.

Figure 5-18 shows the amplitudes of coil 1 at SIDE 240° at x=7 (a) and a single coil inserted at TOP 270° (b), and their phases. The coil at TOP 270° was inserted to y≈5 cm when swiveled 25° towards the antenna. This translates to a minor radius of 5-5.5 cm, since plasmas in Tokapole tend to be a bit low (as indicated by soft X-ray signals), and so it is slightly outside of the resonant surface.
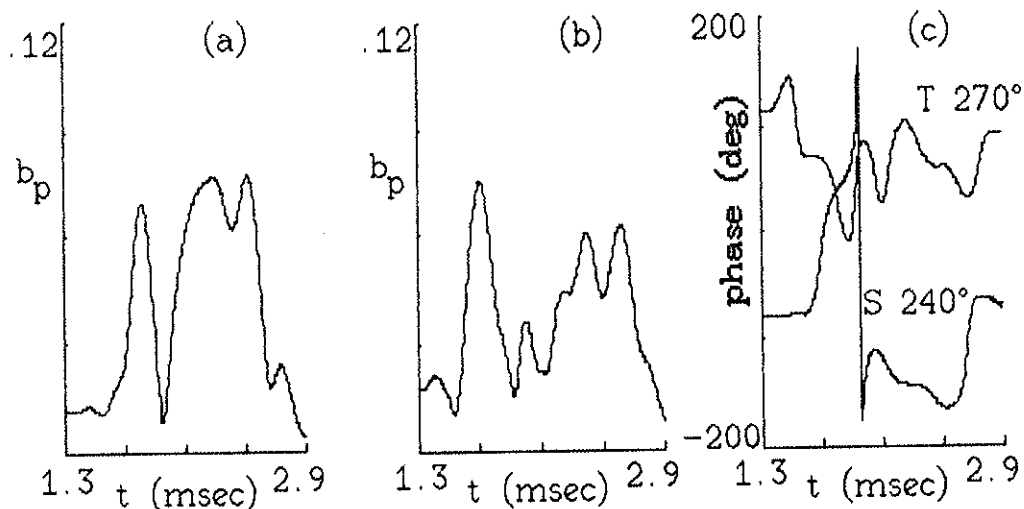
figure 5-18
Amplitudes and phases of coils at SIDE 240° and TOP 270°

The amplitude of the signal from the single coil shows some enhanced signal. The phase is shifted from the coil by approximately 100°. This shift is consistent with the phase shift seen in figure 5-17 which was 50° for about one half the poloidal displacement. These phase differences are not very precise measurements since it can clearly be seen from the plots that the phases and phase differences vary significantly in time. There is also some toroidal separation. They do give a clear indication that the signal is distrubuted poloidally on a magnetic surface with a wavelength on the order of the minor circumference.

5-B 1 c Polarization

By subtracting off the vacuum signal from the measured toroidal wave magnetic field, the angle of the fields in the plasma with respect to the toroidal direction can be calculated. At the time

of peak poloidal wave magnetic field this angle is approximately 75° to 80°. If this were taken as a measure of the direction of the angle of the equilibrium field, it would imply an extremely peaked current profile to generate sufficient poloidal field at this radius ($r \approx 4$ cm). However, since the magnetic coils and amplifiers have no sensitivity to frequencies of the order of the equilibrium fields, they cannot be aligned to the actual field directions as can be done with "equilibrium" coils. The alignment is thus done by iteratively nulling the probe and adjusting the antenna angle. The probe should be nulled simultaneously at all radial locations when the antenna currents are poloidal and the coil axes are all poloidal. The uncertainty is further increased by any shot to shot variation and uncertainty in the probe angle as it is rotated to pick up the toroidal and poloidal signal. Typically this could be off by as much as 5°, but certainly less than 10°. The point to be made is that the wave magnetic field is polarized in the poloidal direction which would be perpendicular to the equilibrium magnetic field. There may be some indication of a peaked current profile.

Shown in figure 5-19 is the amplitude of the field at an angle of 15° from the toroidal direction. It is relatively flat across the resonance zone compared to the poloidal field.
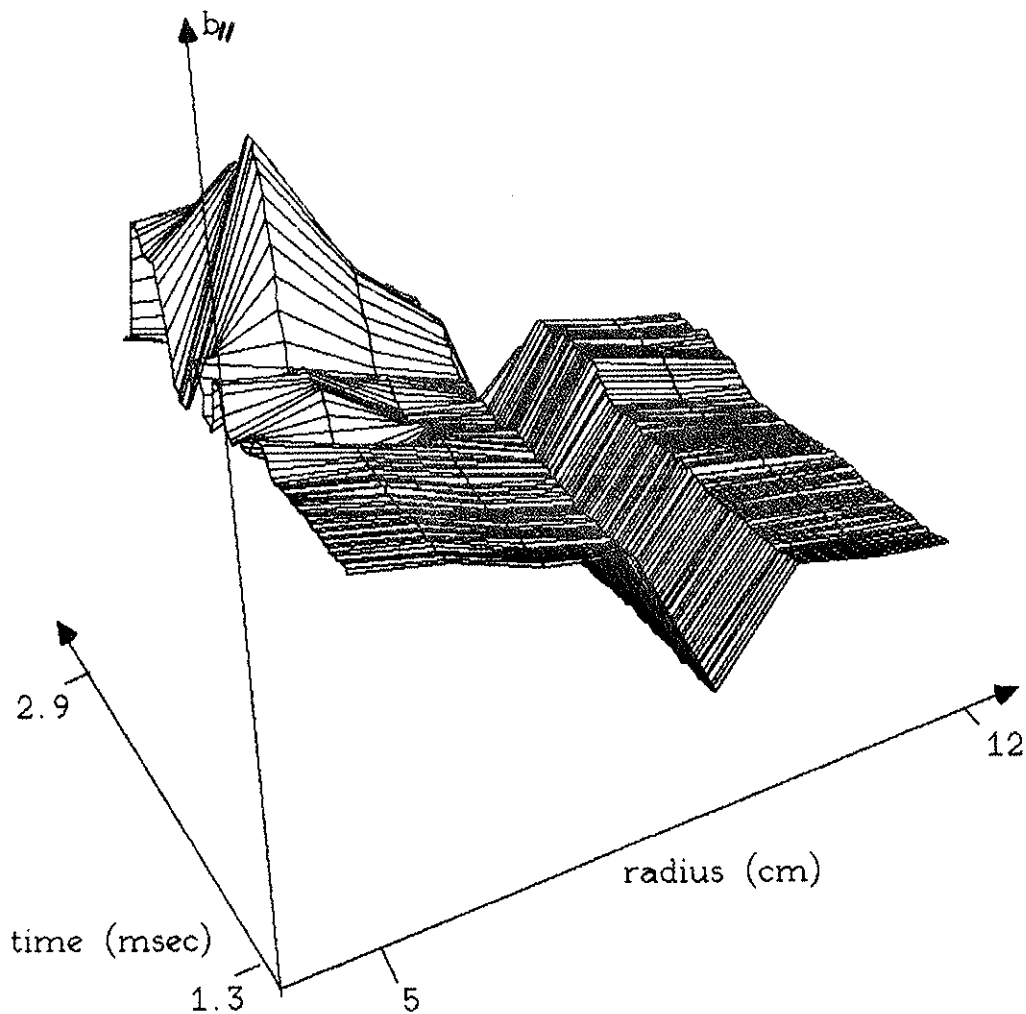
figure 5-19
Amplitude of the wave magnetic field at an
angle of 15° with respect to the toroidal direction

5-B 2 Comparison to Theory of the Spatial Structure

The wave fields observed have much of the spatial structure
expected of a shear Alfvén wave. The perpendicular field is spatially
resonant on a magnetic surface. The position of the resonance is
affected by the value of the equilibrium field, and the mass density.
The parallel field is relatively flat across the resonance zone. The
wavelength in the poloidal direction is on the order of the minor

circumference. The radial phase variation is consistent with the inward propagation of the fast wave to the resonant surface. There is, however, no clear indication of an enhanced signal distributed around the machine toroidally. The toroidal fall-off length is small (less than 1/6 of the major circumference).

Qualitatively, the radial location is seen to behave in a reasonable manner. It is affected by the value of the equilibrium field (figure 5-14). It is also affected by changes in the mass density (figure 5-15). Quantitatively, the radial position is hard to predict.

Since there is no long-scale toroidal structure, the radial location is presumably determined by the $k_\parallel$ spectrum of the single antenna and the frequency. When these match the local Alfvén speed, a resonance can occur. Figure 5-15 clearly indicates that the presence of the resonance is strongly affected by the impurities, presumably by their effect on the mass density. The 2-D code used to calculate the wave fields above the antenna predicts a dominant wavelength of 40 to 60 cm for the spectrum of the antenna. This would imply an Alfvén speed somewhat low for the densities usually encountered in the Tokapole. This may indicate that we are operating at too high a frequency or with a density that is too low for a plasma relatively free of impurities.

There exists a code[4] for predicting the resonance locations for the Tokapole. This code takes as input the current and density profiles of the discharge, and these are not well known empirically for Tokapole. Past experience with the code has shown that it is

fairly sensitive to the details of these profiles and over a range of "reasonable" estimates, the code predictions for the resonance locations can be changed significantly. The code also solves for eigenmodes with a well defined toroidal and poloidal structure. These are not seen in the experiment. For these reasons one would not expect comparisons to the code predictions to be particularly illuminating.

Equation 2-4 gives a prediction for the width of the resonance due to ohmic dissipation, and 2-3 predicts the rise time. Ohmic dissipation is the weakest of the damping mechanisms usually considered for Alfvén wave heating so these numbers are to be taken as a lower limit on the width and an upper limit on the rise time. Assuming a parabolic density profile, a 1/R variation of the equilibrium field, and other typical Tokapole parameters, these give a radial width, Δ, of 6 cm and a rise time of 12 μsec. If the profile of mass density were steeper than assumed, the width would be smaller, and the rise time shorter.

The rise time is shown in figure 5-20 which is a plot of the measured wave amplitude for three cases; one with the RF on throughout the discharge, one where the RF turns on at 2.3 msec, and one with just vacuum rf toroidal field signal. The rise time of the antenna current is long ($\simeq$ 100 μsec). The rise time in plasma is virtually identical to that in vacuum. However, if there were any significant delay due to plasma, the rise time in plasma would not overlay the vacuum rise time so well. The rise time is thus quite

.12

b_p
(Gauss)

RF on at t=0

Vacuum

RF on at t≈2.3

2.1   2.2   2.3   2.4   2.5   2.6
Time (msec)
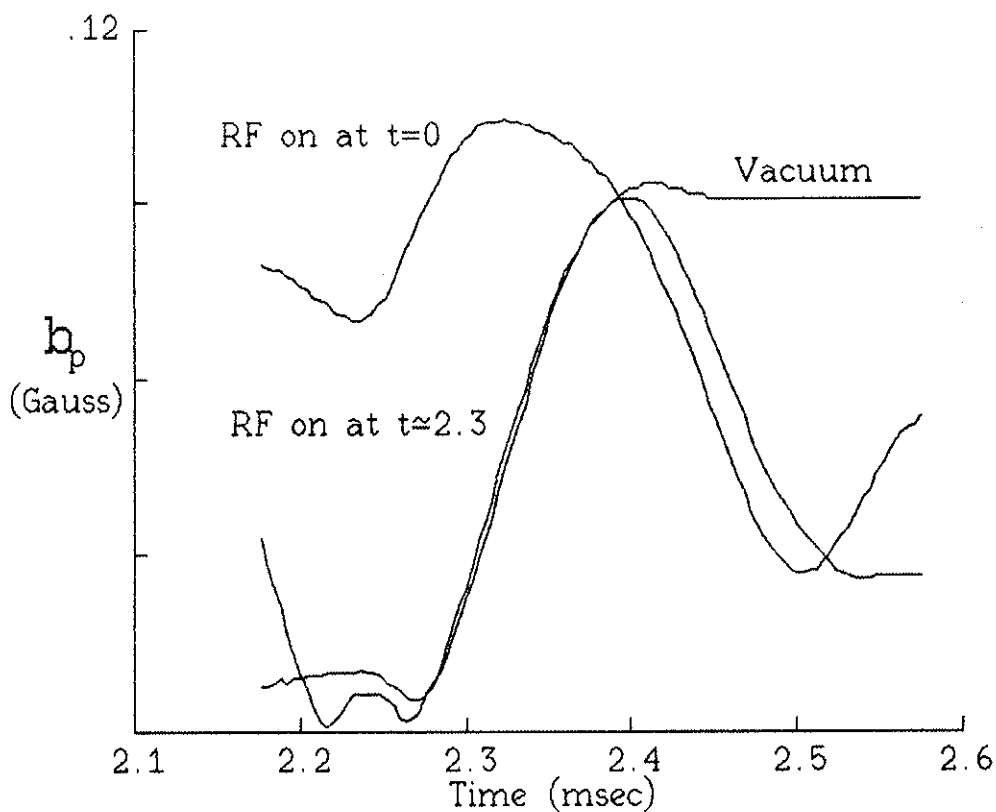
figure 5-20
Plot of the rise of the wave field in plasma and vacuum

short, certainly less than 10 μsec. This indicates a strongly damped wave. This is in agreement with the fact that a wave is not seen to propagate toroidally. It is presumably damped out.

The measured width seems to be quite narrow, $\Delta \simeq 2$ cm. This is significantly narrower than the theoretical estimate. From figure 5-12, one can see that the slope of the amplitude vs. radius is lower on the inward side of the resonance, thus, the radial width may be somewhat broader than this estimate. This could not be detected since inserting the probes any further would degrade the discharge too severely. Another possible explanation for the

discrepancy could be steep gradients in the mass density profile. The angle of the wave magnetic field with respect to the toroidal direction indicates a sharply peaked current distribution, this would presumably also lead to mass density profile which is more peaked than what would normally be expected. Also, the presence of the probe could be producing a local sharpening of the profile, which would peak up the resonance. The relatively sharp width of the resonance is of course somewhat at odds with the claim of strong damping.

Given the magnitude of the wave magnetic magnetic field, one can calculate the power expected to be dissipated by various damping mechanisms and compare this to the power being delivered by the antenna to the plasma. From figure 5-10, the power radiated from the antenna was estimated to be 1.6 watts. This is to be taken as an order of magnitude only, since the error bar on the loading is large. The damping rates for ion viscous damping, ohmic dissipation, and ion and electron Landau damping are given in equations 2-5, 6, 7, and 8. Taking the magnitude of the field to be 0.15 gauss and $k_x \simeq 1/10\text{cm}$, one gets 0.821 W/m^3 for Landau damping which is predicted to be the strongest damping mechanism. If the resonance width is taken as 2 cm and the signal is presumed uniform over the entire magnetic surface for 1/6 of the toroidal extent of the vessel, this gives a total power dissipation of 2 milliwatts. This is much less than the power going away from the antenna as might have been expected since the loading shows no

change, while the probe signal increases significantly. Even this small loading is likely parasitic. The conclusion to be drawn here is that the antennas used couple only loosely to the Alfvén wave. Even if the signal is strongly damped, the energy is not being efficiently delivered to the resonance layer, i.e., the measured wave magnetic field is too small for the amount of power being radiated by the antenna.

Eqn. 2-9 is a prediction for the resonant enhancement of the wave field over the vacuum level. Since $k_x \rho_i \simeq 0.01$, for any reasonable value of T_e/T_i for Tokapole, the second term in the parentheses is negligible, and the resonant enhancement is given by $(\kappa \rho_i)^{-\frac{2}{3}}$. Taking 10 cm for κ, the inhomogeneity scale length, gives a resonant enhancement of 21. This is expected to be the resonant enhancement of the perpendicular field over the vacuum value. In the experiment, using the estimated angle of polarization, we get an enhancement of this order. It is not clear that this is a relevant comparison since the antenna is generating a vacuum field which is mostly toroidal to drive the fast wave which then couples to the shear Alfvén wave at the resonant surface, and the calculation is based on a global helical antenna which would directly drive the shear Alfvén wave. The main point to be made is that the signal is significantly enhanced over any signal present in the absence of plasma.

In summary, the qualitative behavior of the observed signals is consistent with a strongly damped shear Alfvén wave resonance

driven by the coupling to the inwardly propagating fast wave. There is no clear toroidal mode structure, but the signal does seem to have a low poloidal mode number consistent with the significant poloidal extent of the antenna. The measured phase velocity and the frequency are consistent with the expected spatial wavelength of the antenna toroidally. The antennas couple only weakly to the Alfvén wave and energy is not efficiently delivered to the resonant surface.

5-B 3 Variation with Antenna Angle and Comparison with the
        Roto-Alfant

Figure 5-21 shows the time evolution of the radial profile of the poloidal wave magnetic field for two cases. The antenna current is poloidal for the top plot, and toroidal for the lower. A resonance is clearly visible in the top plot, but is not as obvious in the lower plot. When the antenna current is poloidal, it couples to the fast wave which propagates radially with little attenuation, allowing some energy to reach the resonant surface where it can couple to the shear Alfvén wave. When the antenna current is toroidal, the signal is attenuated by the outer layers of plasma, and very little is coupled in to the resonant surface. Even though launching the fast wave is less direct, it couples more efficiently than trying to drive the shear Alfvén wave directly.

The energy in the wave is quite small in either case indicating inefficient coupling. As mentioned in section 5-A the plasma has
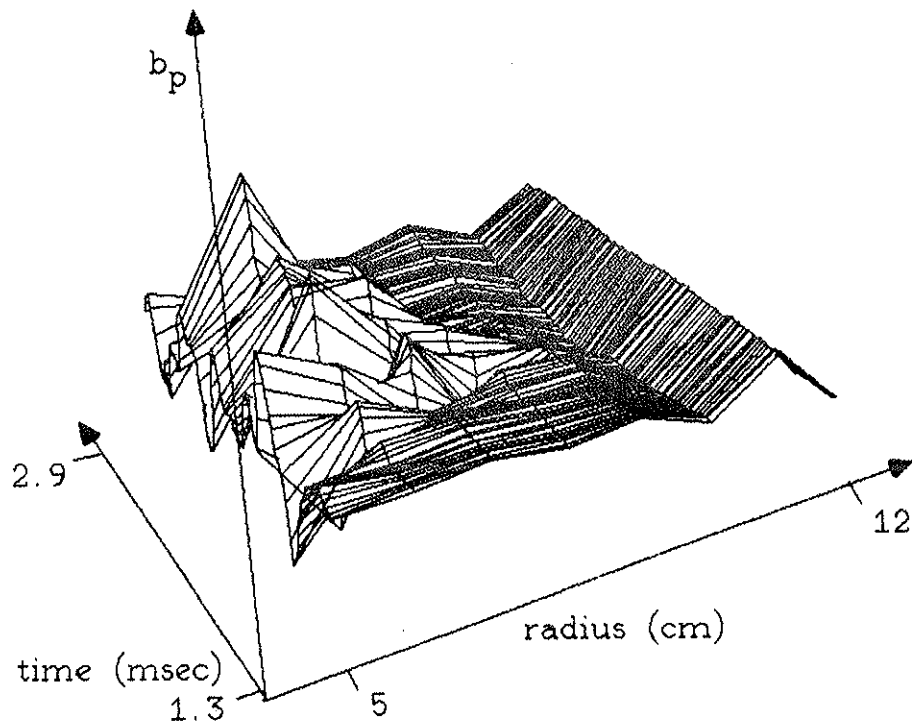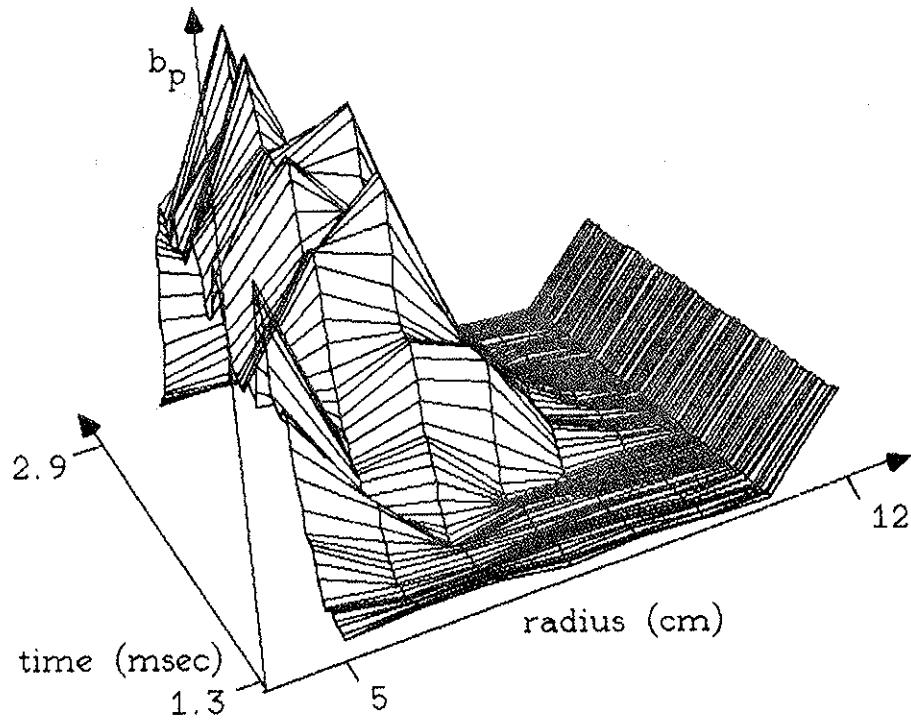
figure 5-21
Time evolution of the radial profile of b_p with
antenna currents poloidal (top) and toroidal (bottom)

little effect on the reactive component of the antenna impedance. This is also indicative of weak coupling to the Alfvén wave since this would be magnetic coupling and should affect the inductance of the antenna if the coupling of the magnetic energy were strong.

Figure 5-22 shows the amplitude and phase of coil 2 of the 8-coil probe with (a and b) and without RF (c and d) when the probe was located directly below the Roto-Alfant at TOP 330°. The total number of amp-turns through the antenna was approximately

figure 5-22
Amplitude and phase above the Roto-Alfant
with (a and b) and without (c and d) RF

equal to that for the Large Single Turn Loop in the previous data ($\simeq$30 amp-turns peak). There is an enhanced signal, but it is not nearly as large as that for the Large Single Turn Loop antenna in the same discharges. (These data were 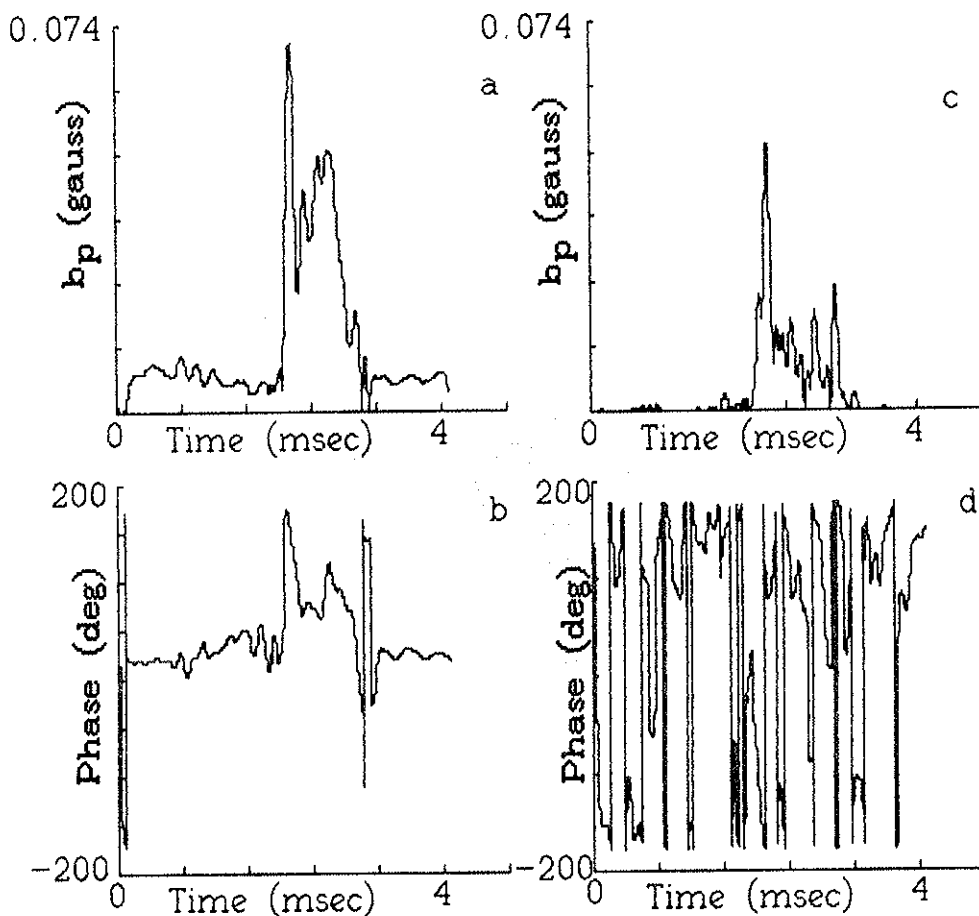taken on the same run day as the "averaged" profile shown in figure 5-12 which has a peak amplitude of 0.15 gauss.) This is primarily due to the smaller size of the loop in the Roto-Alfant which generates a field which falls off faster above the antenna (figure 4-6).

5-B 4 The Undriven Spectrum

The probe signals shown have been filtered to remove a large amount of background noise in the passband of the Alfvéultramps. The power spectrum of the unfiltered signal of coil 2 is shown in figure 5-23 both with and without RF. To make these plots, the original signal had to be recreated including the carrier. The gentle peaking of the undriven signal at 2 MHz in 5-23 b is due to the frequency response of the amplifier-detector system.

The peak at the driving frequency is quite obvious, but beyond 5-10 kHz away from the driving frequency, the signals with RF show no discernible difference from the no-RF case. Some peaks can be seen in the undriven spectrum at various frequencies. Looking at the undriven signals over the course of many run days, occasional shots could be found where the amplitude would be noticeably larger than usual and the phase would have a relatively slow variation indicating a significant amount of noise near the

driving frequency. This noise was always largest on the innermost coil and dropped off rapidly in radius. (Coil 3 was typically down an order of magnitude from coil 1.) If the probe tube was moved out radially 1 cm, the noise on the innermost coil, which is now in the same radial location that the second coil was in, has a signal nearly as large as when the tube was further in. This indicates that at least some of the noise is caused by the presence of the probe. (This was not a significant problem when looking at the driven signal, the peak of the resonance did not move significantly in radius as the prove tube was moved. The plots with 16 radial data points were obtained by moving the coil assembly inside of the probe tube, leaving the probe tube fixed in space.) When the probe is out past $x = 6$ cm, the noise is smaller even on the innermost coil. The noise is also strongly polarized in the poloidal direction.

Figure 5-24 shows the broadband power spectra for several shots. These were obtained using an Alfvéultramp with the bandpass filters replaced by a low pass filter, and a 20 MHz digitizer. The poloidal component is much larger than the toroidal component. The signal does not smoothly decrease as frequency goes up as is seen at lower frequencies[5], but shows a great deal of structure. This structure varies widely from shot to shot for nominally identical discharges. There is some work being done on calculating the spectrum in this range of frequencies[6], but no conclusions have been reached as yet, and no explanation will be offered here.
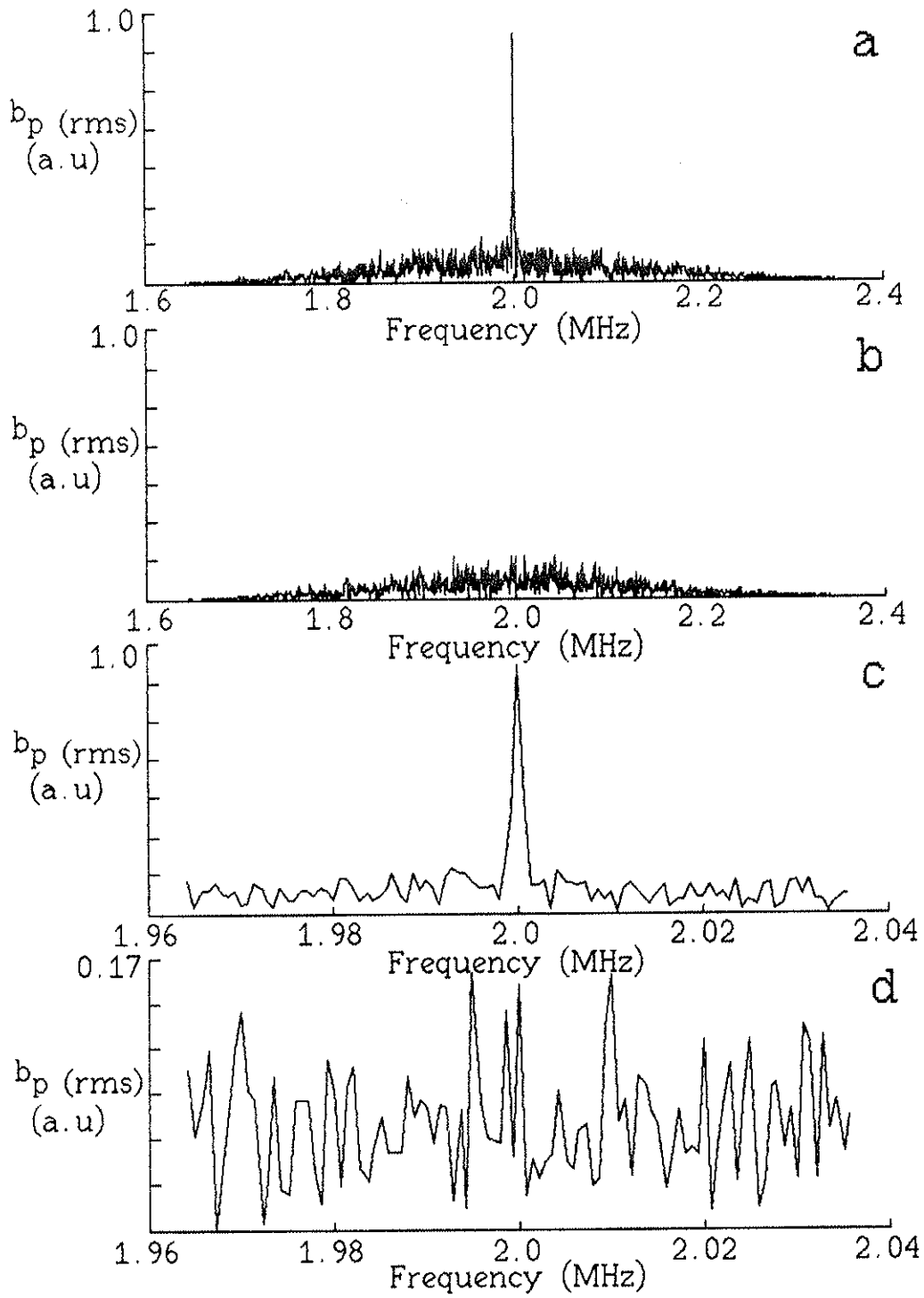
figure 5-23
Power spectra of the rf magnetic field in the passband of the Alfvéultramp
a and c with RF, b and d without RF
Notice the change scale in d.
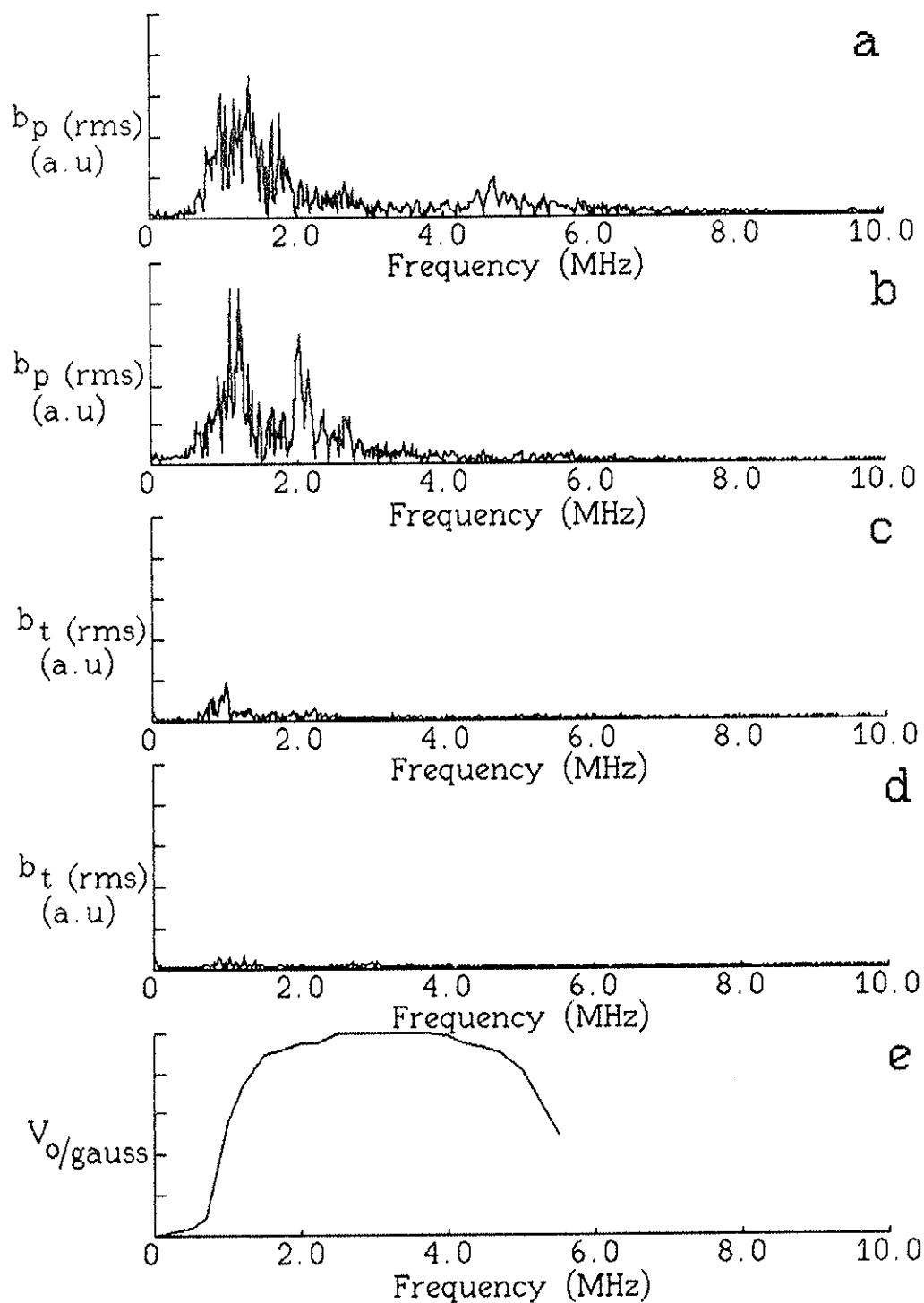
figure 5-24
Broadband power spectra of the undriven rf magnetic field
(a and b are poloidal field, c and d are toroidal field,
and e is a calibration for the probe.)

References

1. T.D. Rempel, G.A. Emmert, PLP 894 (1983)

2. G.A. Collins, F. Hoffman, B. Joye, R. Keller, A. Lietti, J.B. Lister, and A. Pochelon, Phys. Fluids, $\underline{29}$, 2260, (1986)

3. F.D. Witherspoon, Ph.D. Thesis, University of Wisconsin (1984)

4. C.E. Kieras, Ph.D. Thesis, University of Wisconsin (1984)

5. D.E. Graessle, R.N. Dexter, S.C. Prager, To be submitted to Phys. Rev. Lett. (October, 1987)

6. Y.Z. Agim, S.C. Prager, Bull. of American Phys. Soc., $\underline{30}$, 1433 (1986)

Chapter 6
Summary and Suggestions for Future Work

This chapter is a summary of the conclusions reached for this work and some thoughts on the directions of future work.

Antenna Design

Three things stand out as the most important results from the study of various designs:

1.) Orienting the antenna currents parallel to the equilibrium field leads to large parasitic loading and does not seem to couple efficiently to the shear Alfvén wave. Driving the fast wave which will couple to the shear Alfvén wave at the resonant surface leads to some energy deposition at the resonance, but this was still not very efficient for this experiment.

2.) The antenna element must be shielded from the plasma by something. A Faraday shield or a particle shield eliminates much of the parasitic loading.

3.) The physical size of the antenna loop should be as large as possible to maximize the field strength above it.

There has been no indication of strong coupling to the Alfvén wave on any of the antenna designs tried to date, and the measured

field strengths do not indicate that any significant fraction of the power leaving the antenna is going to the Alfvén resonance. In particular, there are no jumps in the antenna loading as a resonance enters the machine, or spikes on the loading from global Alfvén eigenmodes. Unless this situation changes in future designs, there is no point to attempting heating experiments, and no conclusions can be made about the nature of the heating mechanism. A prototype of a new design has been installed on the Tokapole and will be tested soon, it is sketched below. For future work, up to 12 may be installed to better determine an N spectrum.

Tokapole wall

Ceramic shield
(antenna element inside)

Coaxial feed
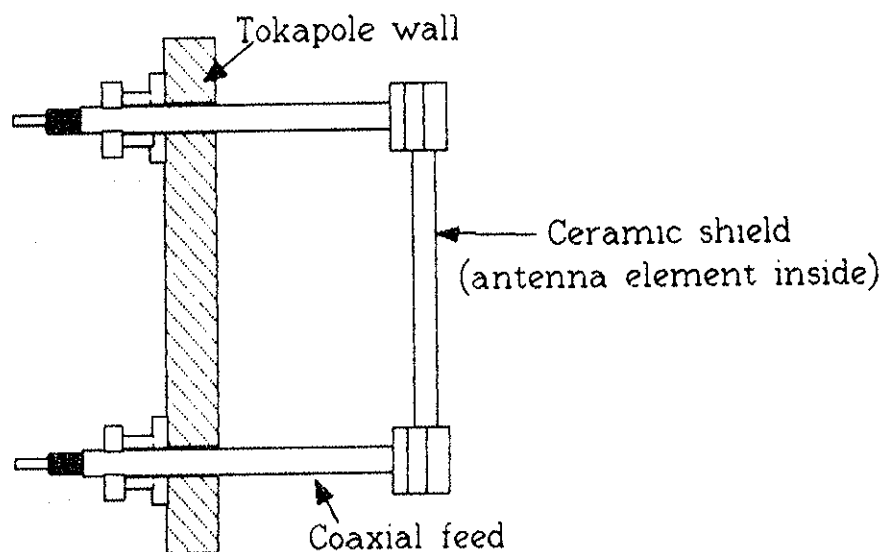
It mounts on the side of the device and can be inserted up to the separatrix. It can be driven either balanced or single ended. This antenna is similar in principle to the Large Single Turn Loop antenna which produced the largest measured fields per amp-turn of antenna current. Ports do not yet exist for mounting these

antennas (the prototype borrows two ports from a future project), but the mounting holes and surfaces that formerly held heating busses on the device would be an ideal location to mount up to 12 such antennas. If the prototype produces results comparable to those of the Large Single Turn Loop antenna, more will be constructed in an attempt to establish a global mode structure. Results from the TCA[1] tokamak indicate that only one antenna per toroidal azimuth should be needed.

Internal Magnetic Field Measurements

The rf magnetic fields measured in the plasma have the following characteristics:

1.) The signal is spatially resonant, and distributed on a magnetic surface in the poloidal plane near the antenna.

2.) The location of the resonant surface is affected by variations of the equilibrium field and the mass density.

3.) The rf magnetic field is polarized nearly perpendicular to the equilibrium field.

4.) The signal propagates radially in to the resonant surface.

5.) The signal appears to be strongly damped and does not propagate far toroidally.

These characteristics are all consistent with a strongly damped shear Alfvén wave, which is driven by coupling to the fast wave

launched by the antenna. There is not much else it could be. The operating frequency of the rf system is nearly a factor of four below the ion cyclotron frequency, and is too high for drift waves. The narrow radial structure fairly well rules out the global Alfvén eignemode. For typical Tokapole parameters, the criterion of $\beta >$ m_e/m_i is very marginal. There is however no indication of a significant fraction of the power being reflected back out from the resonant surface.

Another possibility has been suggested to account for the absence of signal distributed toroidally around the machine. The broad spectrum of the antenna could be coupling to a large number of modes which phase mix to give small fields far from the antenna. This would require many modes to be resonant on or near the same magnetic surface. Since $k_\parallel \sim (n+m/q)$, and the data indicate a relatively low value for m, this would require a large variation in q over a small range of radius to have the large number of modes with different n numbers (necessary to account for the relatively short toroidal extent) all resonant in the narrow region over which an enhanced signal is seen. Near the separatrix, q has a large gradient, but the resonance is located significantly inside of the radius usually taken as the separatrix.

A further possibility is that it is not actual damping of the shear Alfvén wave, but rather the energy is coupled off to other waves which are subsequently damped[2]. This would be very difficult to distinguish from damping of the shear Alfvén wave

directly. Since none of the dissipation mechanisms usually considered for Alfvén waves would give as large a damping rate as would be needed to account for the short toroidal extent of the signal, this alternative explanation is plausible.

Quantitative agreement with theoretical predictions is not as good as might be hoped, however. Comparison is difficult due to a lack of detailed knowledge of the current and mass density profiles. The most glaring contradiction is the sharpness of the resonance which indicates weak damping. This is in contrast with the short rise time and the lack of toroidal propagation, both of which imply strong damping. TCA[3] recently reported a measurement of driven density fluctuations localized near the resonant surface. The measured width of the resonance (when normalized to the minor radius) is approximately equal to that seen on Tokapole. They attribute this relatively narrow width to strong damping of the mode converted kinetic Alfvén wave.

Future work should concentrate on scanning the driving frequency. The correlation of the rise of the resonant signal with the impurity radiation may indicate that the frequency used in this experiment is too high for the prevailing plasma conditions in many "standard" discharges (which have lower impurity radiation signals and are presumably much cleaner). The predicted gaps in the continuum should be looked for. However, to make a detailed comparison of any such structure of the spectrum to theory would require better measurements of the equilibrium field and density

profiles for the device. Of course, if such a structure can be found, the global Alfvén eigenmodes should be sought. More filters and an improved low-power source are being made to allow the range from 0.5 to 5 MHz to be covered.

The undriven spectrum should be investigated in greater detail. It shows a great deal of structure which may be indicative of the presence of Alfvén resonances, and it could be used as a guide to the frequencies at which the antennas should be operated.

There are many questions left unanswered by the work presented here, not the least of which is why there is no strong coupling to the Alfvén wave in the Tokapole when excellent results have been obtained at TCA[1,4] (R=61cm, a=18cm, B_t=0.71-1.5T, $I_p \leq$170kA, $<n_e> < 10^{14}$cm^{-3}, $T_e(0) \simeq$500eV). First, it should be said that the results obtained on Tokapole are similar in many ways to those seen on TORTUS[5] (R=44cm, a=10cm, B_t=0.8T, I_p=16kA, $n_e(0) \simeq 10^{13}$cm^{-3}, $T_e(0) \simeq$100eV) and PRETEXT[6] (R=53cm, a=14cm, B_t=0.75-1.0T, I_p=20-50kA, $<n_e>$=(4-20)x10^{12}cm^{-3}, $T_e(0)$=200-400eV).

TORTUS[5] has recently operated with antennas with currents in both the poloidal and toroidal directions and found, similar to the results presented here, that antenna currents parallel to the equilibrium field can couple to waves in the edge plasma, which can lead to parasitic loading. They do in fact see propagating Alfvén waves in the edge region. (There have been no real attempts to look for such signals with any of the antennas described in this thesis, but significant edge signals were seen when the internal divertor

rings were used as a launching structure on Tokapole[7].) When they operate a shielded antenna with its currents poloidal, they see peaks in the radial profiles of b_p and b_r at certain frequencies which are consistent with an Alfvén wave. (The profiles are poloidally asymmetric, with most of the energy in the regions close to the antenna, thus, the signal does not appear to be resonant on a magnetic surface.) They do observe the signals at a toroidal location 180° away from the antenna, but the values of b_p/I_{ant} are down an order of magnitude from those seen on Tokapole near the Large Single Turn Loop Antenna. The background noise level on Tokapole would make signals of that level very difficult to detect reliably. The loading of the poloidally oriented antenna on TORTUS is also seen to rise smoothly from near zero at $\omega \simeq 0.1\omega_{ci}$ to about 0.35 ohms at $1.6\omega_{ci}$. They do not explain the origin of this loading. However, it is implied that it can not be attributed to the Alfvén wave. (Experiments on Tokapole have operated almost exclusively at 2 MHz. As mentioned above, the frequency should be scanned.)

The PRETEXT[6] group has reported direct observation of the structure of the global Alfvén eigenmode by measurement of the driven density fluctuations with a CO_2 laser interferometer. They drive this mode with two unshielded (but insulated) antennas carrying toroidal currents. Each antenna covers a 90° toroidal arc. The loading of the antennas shows a small peak (0.2Ω) on a large background parasitic loading (1.16Ω) which correlates strongly with the peak in the measured density fluctuation amplitude. The

background loading is quite insensitive to plasma parameters and is not attributed to continua loading by an Alfvén wave[8].

TCA has a total of 8 groups of antennas. A group is located at the top and bottom of the torus at 4 equispaced toroidal locations. The results of their experiments have been recently summarized[1,3,4]. The key results are listed below:

    a.) They observe clear evidence of loading due both to global Alfvén eigenmodes and the continuum with toroidal coupling of modes of different poloidal mode numbers. Loading is largest when all antennas are used in an N=2, M=1 configuration. On Tokapole, the loading observed cannot be correlated with either continuum resonances or global Alfvén eigenmodes.

    b.) They observe efficient heating with most of the power going into the electrons, however, a noticeable fraction is seen to go to the ions. The power does not appear to be absorbed completely at the resonance surface, and measurements of the driven density fluctuations indicate inward propagation of the kinetic Alfvén wave. The measured width of the resonance is comparable to that seen on Tokapole.

    c.) There have been noticeable effects on the profiles with the application of rf power at particular locations in the excited spectrum.

There may be several reasons to account for the significant

discrepancies between the favorable results seen on TCA and those seen elsewhere. When only a subset of the antenna system on TCA is driven, the loading per antenna is seen to decrease. In particular, the coupling to the global Alfvén eigenmode is nearly eliminated and the jumps in loading at the onset of new continuum ranges are significantly reduced when only one pair of antennas at one toroidal location is used. In this configuration, the loading also scales linearly with frequency and is relatively insensitive to other parameters[9]. Loading is also seen to be quite small for the higher toroidal mode numbers even when the full set of antennas is used. Loading is also seen to decrease as the distance from the plasma to the antenna is increased, and the loading is predicted to decrease as the antenna-wall spacing decreases (due to the nearness of the image currents). Their cylindrical model for the antenna loading predicts that the loading will decrease as the plasma current decreases (holding q(0) constant). This is observed experimentally for both the global Alfvén eigenmodes and the continuum. In particular, if the RF is applied at a time when the sawtooth activity disappears and the soft X-ray emission profile flattens (indicating a flattening of the current profile) the loading increases. The interpretation of this effect is the subject of debate within the TCA group. In the numerical calculations, the coupling to the fast wave increases when current is added to the model. Changes in the profiles of the current density and mass density both have significant effects on the code predictions[10]. The problem is clearly

not a trivial one.

Many of these observations can be compared to what is seen on Tokapole. The lack of loading which can be attributed to an Alfvén wave for the Alfant and the Roto-Alfant is probably due to the relative proximity of the return currents and the ground plane, and their limited insertion range. The loading that remains when the Roto-Alfant (with end limiters installed) is perpendicular to the equilibrium field is probably due to dissipation in the edge plasma that the wave would have to propagate through before getting into the current channel. The lack of significant loading of the Large Single Turn Loop Antenna may be attributable to the relatively high toroidal mode numbers that dominate its spectrum (even higher than those of a single antenna group of the TCA type which have a toroidal extent of 26° as compared to 1.5° for the Large Single Turn Loop Antenna). Another significant difference may be the current and density profiles, which are not known for Tokapole. The measured angle of the wave field with respect to the toroidal direction implies a relatively peaked profile. The absence of the global Alfvén eigenmodes may again be due to the use of a single antenna or the inefficient coupling of the multiple antennas tested due to their construction.

Clear explanations of the discrepancies amongst the different experiments are not easy to offer. There are, however, many hints. In order to study further this problem on Tokapole, several things are clear. The operating frequency (and other plasma

parameters) should be scanned over a broad range. The recent upgrade of the Tokapole with its expanded parameter range should facilitate this. More antennas should be installed to try to establish a global mode structure. The results on the toroidal coupling from TCA imply that only one antenna per toroidal azimuth should be needed (at some cost of loading per antenna). Before this is tried it may be wise to try an antenna with a significantly greater toroidal extent. Multiple antennas would not make a significant difference if the signal from one antenna were completely damped out before it reached a region where another antenna is generating significant signal. Antennas of the size of the Large Single Turn Loop antenna would have to be placed very near each other toroidally to accomplish this. It would be wise to test antennas of a larger toroidal extent in an attempt to couple to lower toroidal mode numbers before installing many antennas of a small size.

It is expected that these experiments will continue for at least several years on the Tokapole. There is clearly still a great deal to investigate.

References

1. G.A. Collins, F. Hofman, B. Joye, R. Keller, A. Lietti, J.B. Lister, and A. Pochelon, Phys. Fluids 29, 2260 (1986)

2. J.A. Tataronis, Private Communication

3. R. Behn, G.A. Collins, J.B. Lister, and H. Weisen, Plasma Phys. Contr. Fusion 29, 75 (1987)

4. G. Besson, A. de Charbrier, G.A. Collins, B. Joye, A. Lietti, J.B. Lister, J.M. Moret, S. Nowak, C. Simm, H. Weisen, 13th European Conference on Controlled Fusion and Plasma Physics, Schliersee, Germany (1986)

5. G.G. Borg, M.H. Brennan, R.C. Cross, J.A. Lehane, and A.B. Murphy, 13th European Conference on Controlled Fusion and Plasma Physics, Schliersee, Germany (1986)

6. T.E. Evans, P.M. Valanju, J.F. Benesch, Roger D. Bengtson, Y.-M. Li, S.M. Mahajan, M.E. Oakes, D.W. Ross, X.-Z. Wang, and J.G. Watkins, and C.M. Surko, Phys. Rev. Lett. 53, 1743 (1984)

7. F.D. Witherspoon, Ph.D. Thesis, University of Wisconsin (1984)

8. M.E. Oakes, P.M. Valanju, Jay F. Benesch, Roger D. Bengtson, X-Z. Wang, and J.G. Watkins, Proceedings of the Fifth Topical Conference on Radio Frequency Heating (Madison, WI 1983)

9. A. de Chambrier, A.D. Cheetham, A. Heym, F. Hofmann, B. Joye, R. Keller, A. Lietti, J.B. Lister, and A. Pochelon, Plasma Physics 24, 893 (1982)

10. J.B. Lister, Private Communication